NONLINEAR FINITE ELEMENT-BASED INVESTIGATION OF THE EFFECT OF BEDDING THICKNESS ON UNDERGROUND PIPE

by

ANUPONG KARARAM

Presented to the Faculty of the Graduate School of

The University of Texas at Arlington in Partial Fulfillment

of the Requirements

for the Degree of

MASTER OF SCIENCE IN CIVIL ENGINEERING

THE UNIVERSITY OF TEXAS AT ARLINGTON

August 2006

ACKNOWLEDGEMENTS

I wish to express my sincere thanks to Dr. Ali Abolmaali for his guidance and remarkable patience throughout the supervision of this research. I am also grateful to Dr. Ali Abolmaali for providing a great deal of suggestions and corrections during the preparation and completion of my thesis.

I would like to extend my appreciation to Professor Sahadat Hossain and Professor J. H. Matthys in the Department of Civil Engineering for their comments and suggestions for this study.

My gratitude goes to Joe Lundy, Joe Zicaro, Josh Beakley, and Kim Spahn for providing invaluable input in understanding the pipe behavior, in general.

I especially wish to thank the American Concrete Pipe Association, National Science Foundation, and Department of Civil and Environmental Engineering of the University of Texas at Arlington for their financial assistance throughout the careers of this study.

Finally, I thank my mother, father, and brothers for their support from my country, Thailand. I also extend my appreciation to my friends here, in USA, without whom the completion of this thesis was not possible.

June 1, 2006

ABSTRACT

NONLINEAR FINITE ELEMENT-BASED INVESTIGATION
OF THE EFFECT OF BEDDING THICKNESS
ON UNDERGROUND PIPE

Publication No. _____

Anupong Kararam, M.S.

The University of Texas at Arlington, 2006

Supervising Professor: Ali Abolmaali

The pipe-soil interaction is studied by using the finite element software, ABAQUS/CAE Version 6.5-1 as a symmetric model of embankment installation to study the effect of bedding property and thickness on pipe-soil interaction with increase in the height of fill. A three-dimensional finite element model (FEM) of the concrete pipe and surrounding soil is developed. The FEM is capable of simulating material, geometric, and contact nonlinearities which employs a nonlinear incremental solution algorithm. Several different element types and mesh size were tested to obtain the optimum converged mesh. These elements were eight-noded linear brick (C3D8R) and six-noded linear triangular prism (C3D6) for modeling of the concrete pipe and surrounding soil. The behavior of the 3-D model is investigated by varying the pipe

diameter, backfill height, bedding thickness, and bedding material. Three material constitutive relationships of soil involving in the model are gravelly sand (Sn), sandy silt (Si), and silty clay (CL).

To study the effect of bedding thickness on the pipe wall, due to the increment of backfill soil depth, contact elements were employed in the interface between each two regions. The lateral boundaries and model length were also studied for the converged solution. A parametric study was conducted to study the effects of bedding thicknesses 3 in (7.5 cm), 5 in (12.5 cm), 7 in (17.5 cm), and 9 in (22.5 cm) with backfill heights 20 ft (6 m), 40 ft (12 m), 60 ft (18 m), 80 ft (24 m), and 100 ft (30 m). The different types of material used for the inside bedding zone are as follows: Si70; Si90; Sn85; and Sn90. The results show the increase in bedding thickness reduces tensile stress at crown, springline, and especially invert of the pipe wall depending on the material property. This means the change in material property and compaction level has a greater effect on the reduction of tensile stresses than the effect from the variation of bedding thicknesses. Also, materials with lower bedding stiffness (high deformability characteristics) cause greater reduction in induced stresses. This study shows that for commonly used bedding material (Sn90), the effect of the increase in bedding thickness has a minimal effect on stress reduction of the pipes studied.

TABLE OF CONTENTS

Appendix

LIST OF ILLUSTRATIONS

LIST OF TABLES

CHAPTER 1

INTRODUCTION

1.1 History of Concrete Pipe

Historical records include many references to engineering feats undertaken by ancient civilizations to collect and convey water. Archaeological explorations indicate an understanding of drainage principles existing very early in human history. For example, a sewer arch constructed about 3750 B.C. was unearthed in an excavation at Nippur, India. Another excavation in Tell Asmar, near Baghdad, exposed a sewer constructed in 2600 B.C. The Minoans, who lived in Crete about 1700 B.C., were master builders and installed elaborate systems of stone drains which carried sewage and drainage. Most renowned of these early construction efforts were the aqueducts of Rome. The water carried by these aqueducts was used primarily as a supply of drinking water and to carry sewage through Rome's main sewer, the Cloacae Maxima. Built in 800 B.C., and constructed mainly of stone masonry and natural cement, the Cloacae Maxima was the first known man-made waterborne method of sewage disposal. After more than 2000 years, sections of this concrete sewer are still being utilized.

As the great cities grew and people built permanent homes, increasingly greater amounts of sewage, garbage and refuse were deposited in the streets. When the piles became high, and the odor nuisance great enough, the filth was removed using picks, shovels and carts. This condition existed until the early part of the 19th century when

water distribution systems made it possible to use water to carry off the sewage. Many cities like Paris, London and Baltimore tried cesspools with disastrous results. The cesspools became breeding areas for disease. It took the waterborne sewage disposal system to clean up the large cities from health and aesthetic standpoints.

Very little theoretical pipeline technology existed prior to the 19th century. In 1775, however, the precursor of the modern formula for relation velocity of flow and head loss due to friction in open channel flow was developed by Antoine Chezy, a French engineer and mathematician. It was over 50 years before significant improvements to his concept were recorded.

During the first 5000 years of recorded history, the need for sewers, water supply, and drainage was recognized and practical methods for handling the flow of water were developed. From the remains of ancient structures, it is apparent that the building materials progressed from relatively simple applications of natural materials to cast concrete. In many applications, permanency was a major requirement, and concrete was one of the earliest substitutes for natural stone. While not all stone and concrete structures were able to survive the ravages of time, weather and warfare, concrete has an ancient and notable heritage.

The 19th century brought a period of political consolidation and industrial expansion, and the push toward the American West began. Three areas of expansion during this period produced the beginnings of the concrete pipe industry; public health requirements of water and sewage treatment, transportation, and agricultural needs for irrigation and drainage.

Concrete sewer pipe was developed during the 19th century after the public became conscious of the needs for sanitation. Many installations of concrete pipe had been made prior to 1880, and its durability characteristics soon because apparent. The large sewers constructed in Paris during the middle of the 19th century were built of rough stone heavily plastered with cement on the interior. Dr. Rudolph Hering, a well-known sanitary engineer, reported in 1915 that his examination of the interior surfaces of these sewers found them to be "quite good." He attributed this to the density and the smoothness of the plaster. In 1881, he had examined 10 to 20 year old concrete sewers in Vienna and found no deterioration.

In 1868, a concrete pipe sanitary sewer was installed in St. Louis, Missouri. An examination in 1962 showed the line to be in excellent condition, and it remained in service. A concrete pipeline installed as a combined sewer in St. Paul, Minnesota in 1875 is serving satisfactorily a century later. Between 1875 and 1888, this city installed over 94,000 linear feet of concrete pipe for combined sewers. These pipelines, varying in size from 9-in (23-cm) circular to 21-in (53-cm) by 28-in. (70-cm) oval, have provided 100 years of service.

Katona, M.G., & AKL, A.Y. (2004) provided a study of the analysis of long span culverts by the finite element method that would be a foundation for future studies. Two finite element programs were used; ADINA and CANDE. The two programs were used to examine large deformation theory versus small deformation theory. Katona found that the large deformation solution is not significantly different from the small deformation solution; the differences at most were 8 percent at the crown. Katona stated

small deformation theory and infinitesimal stress-strain laws may be used for analyzing long span systems if the percentage of crown deflection remains within practical limits.

Arockiasamy et al. (2002) report on tests conducted for FDOT as part of an overall assessment of culvert pipes. Pipes with 36-in (90-cm) and 48-in (122-cm) inside diameters were buried at depths of 0.5, 1.0, and 1.5 diameters. Two backfills were used, both classifying as poorly graded sands with silt (SP-SM per ASTM D 2487). These materials would both be considered as Si soils per current AASHTO specifications for thermoplastic pipe. Live loads were calculated based on an HS-20 truck with additional load to account for impact per AASHTO LRFD. For the 0.5 diameter burial case, this was an axle load of approximately 40,000 lbs (177,928 N). Changes in vertical diameter were about 0.2 in (5 mm) maximum for the depth of 0.5 diameter, 36-in (90-cm) pipe diameter. Maximum measured longitudinal tensile strains were 0.05% for the same depth. No failures or damage to the pipe were noted.

McGrath et al. (2002) provided an interim report on live load testing of 60-in (150-cm) diameter type pipe under depths of fill of 1 ft (0.30 m) and 2 ft (0.60 m). over a period of two years. A total of 8 HDPE pipes were installed, along with one concrete and one corrugated steel pipe that were used as references. The study used two backfill materials, a coarse-grained material without fines and silty sand with about 25% fines. Both backfill materials were compacted to 90% of maximum. The pipes were installed in the Minnesota Research Road facility, a closed loop road that is subjected to repetitive cycles of truck loads with axle loads of 18,000 lbs (80,068 N) and 24,000 lbs (106,757 N). The peak circumferential tensile strains recorded during live load testing

were approximately 0.12% at 1 ft (0.3 m) of cover. Peak deflections under live load were on the order of 0.12 in (3 mm). The deflections increase slightly during the spring thaw but then return to lower values. The overall pipe deflections have been stable for the 2 year life of the project. The testing work is being used to calibrate full three-dimensional pipe-soil models of the live load condition, and the models are then being extended to evaluate design axle loads with impact. These studies suggest good pipe behavior at a depth of 2 ft (0.6 m).

McGrath, T.J. (2003) also studied the anticipated stress levels on a HDPE pipe installed for 100 years. With several compaction conditions, varying depths of fill and variable support under the pipe haunch, he found that tensile stresses are relatively low when pipe installation meets typical requirements. Long-term tensile strain for the service condition should be less than 1.6%, corresponding to a long-term stress of 300 psi (2,068 kPa), or about 2.5% and 500 psi (3,447 kPa) for the factored load condition. This is significantly reduced from the current AASHTO requirement of 5% long-term tensile strain capacity. Moreover, backfill materials that provide the best performance with minimal controls on construction procedures are well-graded coarse-grained soils (sands and gravels, SW and GW). Uniformly graded coarse-grained soils (SP and GP) also provide good service but are not recommended unless provisions are made to evaluate and control possible migration of fines into open voids. Uniform fine sands should be avoided and criteria were presented for controlling this. Coarse-grained soils with fines (GC, GM, SP, SM or sandy silts and sandy clays) provide good service if placed and compacted properly, but increased inspection during construction is

recommended. Backfill should be compacted to at least 95% of maximum standard Proctor density.

1.2 The Pipe-Soil Installations

The analysis and design procedures for concrete pipe-soil installations are based on a soil-structure interaction analysis of the pipe-soil system that accounts for the combined behavior of the pipe and its surrounding soil considered as a single structural system. The main characteristics of pipe-soil installations are included in this section.

1.2.1. Pipe-Soil Installations

The following three types of structural components are found in all pipe-soil installations.

- Precast reinforced or nonreinforced concrete pipe.
- In-situ soil in the foundation below the pipe and, in some cases, in vertical or sloping trench walls.
- Placed soils (constructed bedding and backfill) in locations below and around the pipe and in locations over the top of the pipe up to the surface.

Pipe-soil installations are called “trench type” (Figure 1.1) when the pipe is located completely below the natural ground surface and the backfill over the pipe is placed between vertical (Figure 1.1a) or sloping walls (Figure 1.1b) of natural (in-situ) soil extending to the surface. Trench installations are made in relatively narrow excavations and the pipeline covered with earth backfill which extends to the original ground surface. Sewers, drains and water mains are usually constructed in trenches.

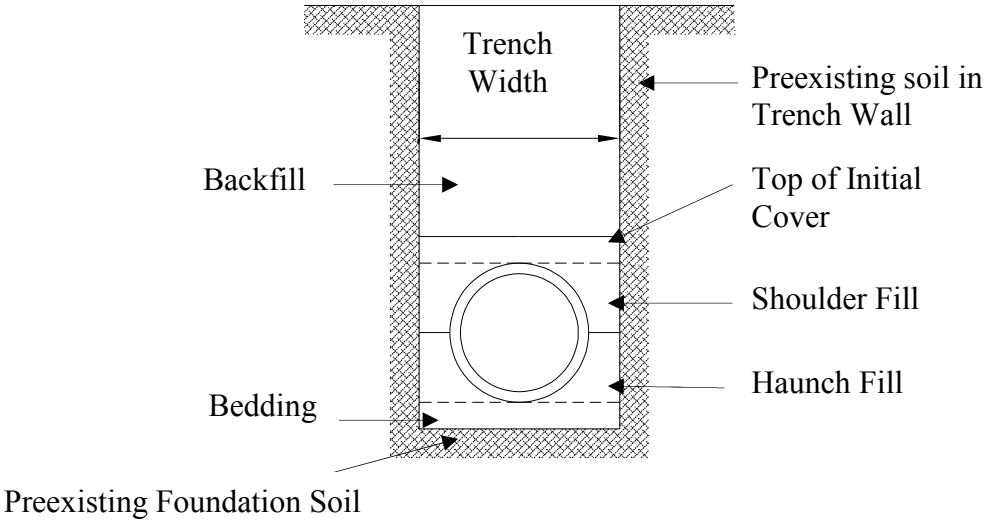

(a)

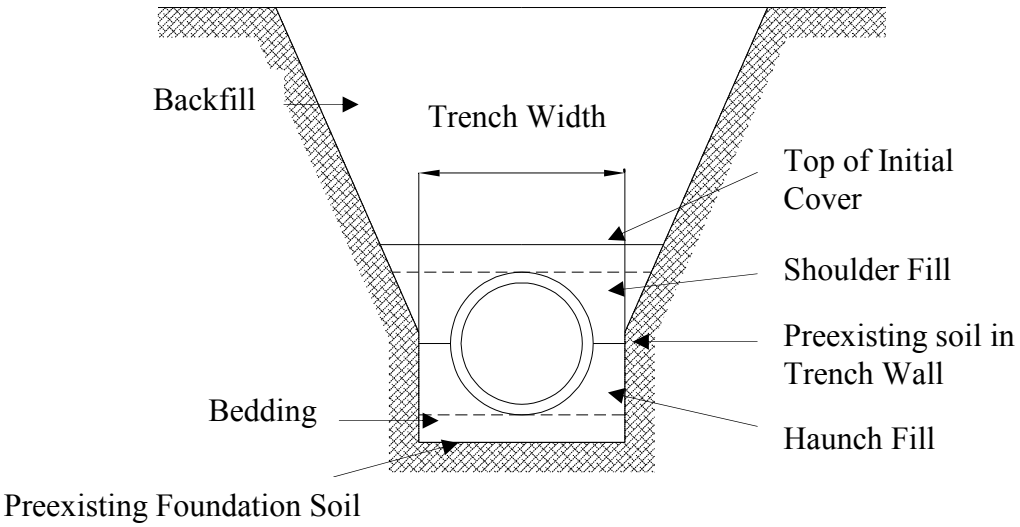

(b)

Figure 1.1 Trench Installation; (a) Vertical wall and (b) Sloping Wall

Pipe-soil installation are called “embankment type” when soil is placed in layers above the natural ground. Highway and railroad culverts are typically installed under fills or embankments. There are three types of embankment installation:

- Positive projection in sub-trench: pipe is initially installed as positive projection. When the embankment fill has been placed to an elevation of at least one pipe diameter over the proposed top of the pipe, a trench is excavated over the pipe and backfilled with a more compressible material, simulating a negative projection installation. (Figure 1.2a)
- Negative projection: pipe is installed in relatively shallow trenches of such depth that the top of the pipe is below the level of the natural ground surface or compacted fill, and the covered with earth backfill to a height appreciably greater than the distance from the natural ground surface or original compacted fill surface to the top of the pipe. (Figure 1.2b)
- Positive projection: pipe is installed with the top of the pipe projecting above the surface of the natural ground, or compacted fill, and then covered with earth backfill soil. This type also includes pipe installed in extremely wide trenches. (Figure 1.3)

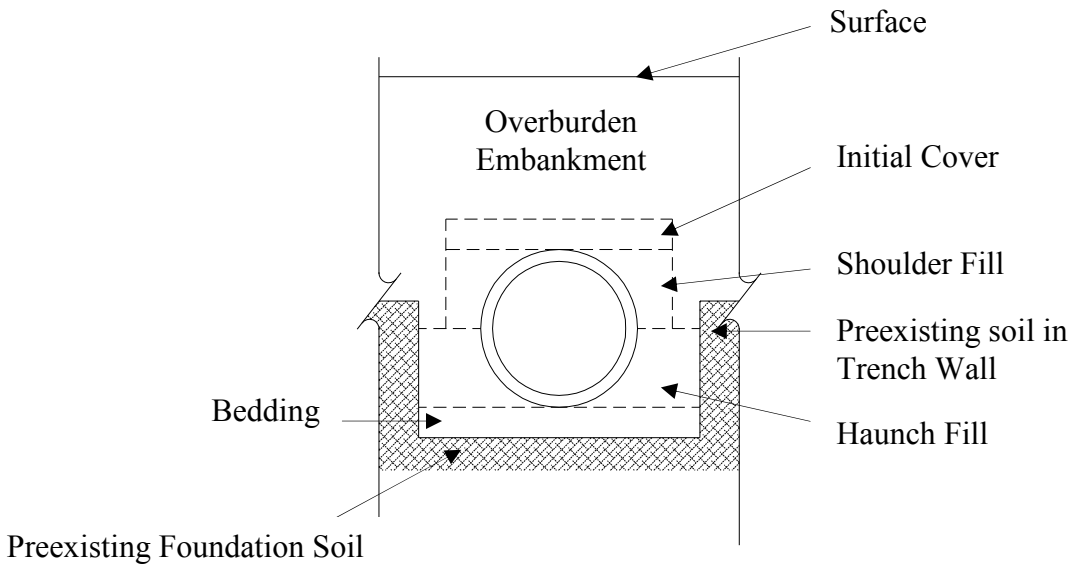

(a)

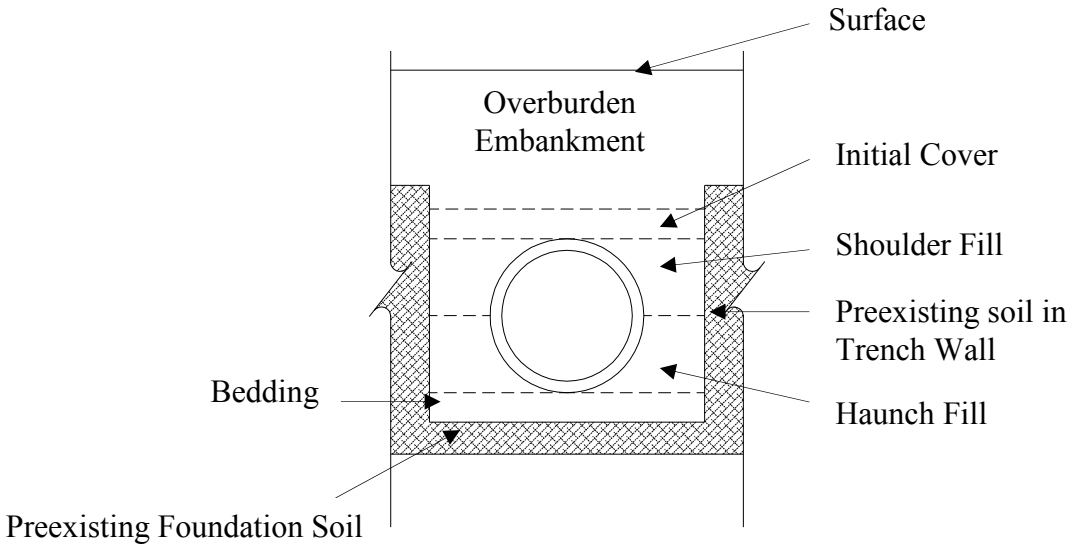

(b)

Figure 1.2 Embankment Installation With Partial Height Trench; (a) Positive Projecting and (b) Negative Projecting

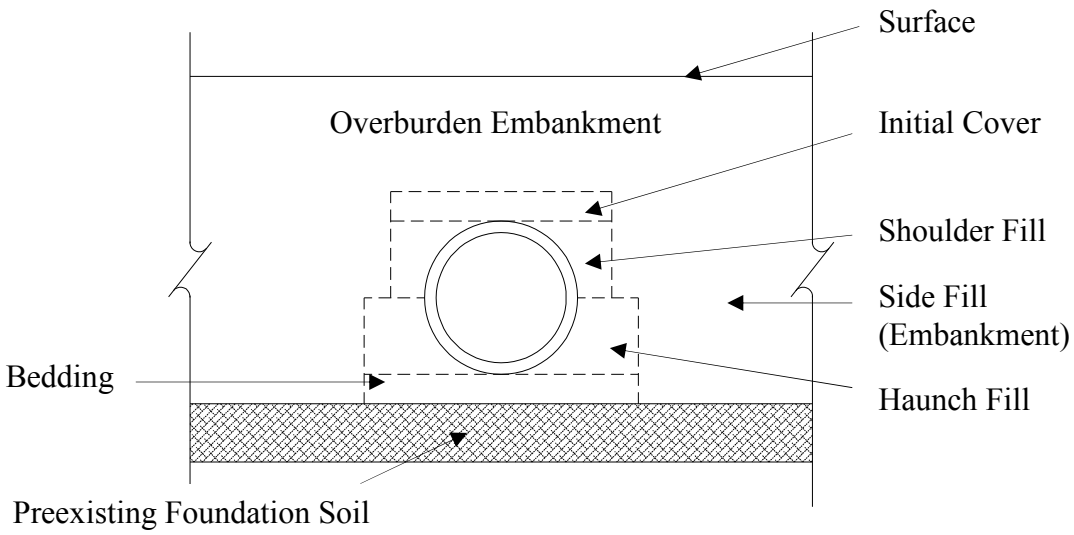

Figure 1.3 Embankment Installation (Positive Projection)

The following terminology is used in this design to describe soils in various parts of the installation.

- Foundation: natural (in-situ) soil or rock below the bottom of the pipe.
- Bedding: placed or natural soil immediately below or adjacent to the bottom of the pipe that is in place before the pipe is positioned in the installation.
- Embedment: soil that is placed around the pipe after the pipe is positioned on the bedding. It usually is located in zones within about one pipe diameter from the pipe exterior surface.
- Haunch fill: soil in the pipe embedment that is placed above the bedding and below the springline.

- Lower side fill: soil between bedding and level of pipe springline located in zones outside the haunch fill (may be placed before or after pipe is positioned in an embankment).
- Shoulder fill: soil in the pipe embedment that is placed adjacent to the top half of the pipe.
- Initial cover: soil in the location immediately over the pipe and shoulder fill extending for at least the width of the outside pipe diameter. A specific thickness for this soil may, or may not, be given in the installation design.
- Backfill: soil placed over the pipe and side fills above the initial cover up to the final ground surface.
- Trench walls: natural (in-situ) soil that extends adjacent to the pipe above the level of the foundation soil. Walls may be vertical or sloped. They may extend to the surface, or they may be partial height with embankment soil over the natural ground surface. Trench walls may also be placed soils when a sub-trench is constructed in a previously placed soil embankment into which the pipe is subsequently installed.
- Pavements and pavement base: asphalt or concrete roadways located at the ground surface and their soil bases.

1.2.2. Bedding and Foundation

Bedding composes of the placed or natural soil immediately below or adjacent to the bottom of the pipe that is in place before the pipe is positioned in the installation. It may consist of a flat configuration of natural in-situ soil, or natural soil that is

loosened, or natural soil that is shaped to the profile of the bottom of the pipe for some portion of the bottom circumference defined as the bedding angle. In installations of higher quality, it often includes a placed soil to provide a cushion and foundation below the pipe, usually with a flat surface configuration, but sometimes shaped to the profile of the bottom of the pipe over the bedding angle. (See Figures 1.1 and 1.2)

Shaped beddings are shown as one of alternative standards used in current design practice. However, the use of flat bedding is much more practical and prevalent in current pipe installation practice. Furthermore, it is doubtful if shaped bedding can produce the desired uniformity of bottom support because of the small tolerance required to achieve uniform bearing with rigid pipe. Unless deliberately cut with a smaller radius than the actual outside radius of the pipe, the support attained with it will be less uniform or less desirable than the support attainable by compacting embedment fill in the haunch below the pipe over a flat bedding.

The ideal bedding consists of a relatively loose soil cushion over the central third of the pipe diameter and a very firm compacted bedding below a well compacted haunch fill over each outer third of the pipe diameter. This concentrates support of the pipe and earth loads away from the central portion of the pipe, reducing critical bending and shear stress resultants in the invert region.

1.2.3. Embedment

The pipe embedment consists of the soil that is placed under and around the pipe immediately above the bedding. It includes the haunch fill, the shoulder fill and the initial cover. The most critical region of embedment is the haunch fill, extending under

the pipe from the springline down to the top of the bedding. If the soil in this region is highly compacted over a similarly compacted bedding under the two outer one-thirds of the pipe outside diameter, the pipe installation will achieve a beneficial distribution of earth support.

The embedment and sidefill soils adjacent to the pipe provide beneficial lateral support. Relatively low lateral pressures are developed in narrow trench installations, with gradually increasing lateral pressures as trench width increases. A stiff or highly compacted soil in the shoulder region above about 10 degrees over the springline of the pipe does not deflect into the soil in this region. Furthermore, a looser soil in this region, relative to the adjacent sidefill, promotes a reduction in load on the pipe and thus, enhances the quality of the pipe-soil installation.

1.2.4. Soil beyond Embedment

The backfill soil over the pipe is the principal source of load on the pipe. The unit weight of this soil is a function of the soil type and compaction. Generally, increasing compaction of backfill over the pipe results in increased load on the pipe for both trench and embankment installations. However, the load on the pipe is also influenced by the soil beyond the embedment adjacent to the pipe.

In trench installations, soil beyond the embedment at the sides of the pipe is the in-situ soil of the trench wall. The location with respect to the outside of the pipe wall and the stiffness of this natural soil affects the load on the pipe. As this soil becomes stiffer and closer to the pipe, the load on the pipe decreases. This is because a portion of

the backfill soil weight is supported by shear forces at the interface between placed backfill and in-situ trench wall.

Increasing compaction of the backfill over the pipe in a trench installation increases the unit weight of the soil above the pipe and thus tends to increase the load on the pipe. However, increased compaction of trench backfill is beneficial for reducing settlement of the trench fill relative to the in-situ soil trench walls and increasing the transfer of a portion of the trench backfill weight to the trench walls due to arching.

In positive projecting embankment installations, the type and compaction of soil beyond the embankment at the sides of the pipe may influence the load on the pipe, since increased settlement in this region causes transfer of more load to the rigid pipe. In these installations, relatively rigid concrete pipe are normally stiffer than the sidefill. However, the magnitude of the additional load is significantly influenced by the level of compaction of the backfill in the region above the top of the pipe relative to the level of compaction of sidefill, in the region adjacent to the pipe. The backfill in the region above the top of the pipe acts as a "shear beam" supported by the elastic spring stiffness of the sidefill soil and the pipe plus its bedding. The load on the pipe is minimized when the sidefill soil is stiffer than the backfill above the top of the pipe and is increased when the sidefill soil is not as stiff as the backfill above the pipe.

1.2.5. Soil Characterization

Soil and rock are the two main categories of natural geologic formations. In relation to pipe installations, rock is generally quite hard, although it may be highly weathered or fractured. Even so, rock may be assumed to be stiffer and stronger than

soil. Soils occur in nature in many forms and compositions. They may be broadly classed as either coarse-grained (more than 50-percent sand and gravel), or fine-grained (more than 50-percent silt and clay). However, coarse-grained soils with more than 35-percent or so of silt and clay will generally behave like fine-grained soils. Natural soils may be saturated or unsaturated and range in consistency from loose or soft to very dense or hard.

Constructed (placed) soils are natural soils that are excavated, placed and recompacted as backfill and embankments, or they are manufactured aggregate that are placed and compacted. They generally have the same range of composition as natural soils and their mechanical properties are influenced by the same factors. However, stress history is much better known since it is a function of a controlled compaction process rather than natural phenomena. Also, in pipeline projects, constructed soils are either unsaturated when compacted or, if placed under water, they are freely draining granular materials. Thus, their mechanical properties can be characterized by more precise models than used for in-situ soils. It is desirable to use non-linear, stress dependent models for constructed soils, particularly in the zones close to the pipe, because they significantly influence pipe loading and deformation.

Soil types are commonly classified by ASTM D 2487 (2005) *Standard Test Method for Classification of Soils for Engineering Purposes*, or by AASHTO M 145 (2005). Descriptions and notation for classification of the principal soil types are given in those standards. These classifications of soil types apply to both natural (pre-existing) soils and to placed soils.

The numbers of soil type classifications described in the above standards are too great and the mechanical properties of the soil types overlap so much that the independent characterization of all standard soil types for use in practical soil-structure interaction analysis is not warranted at this time. Thus, constructed soils have been grouped into four broad classifications and natural soils have been grouped into two broad categories plus rock. These are given in Table 1.1.

Constructed soil characterization for structural purposes also depends on the level of compaction for a given placed soil type. This is related to the density achieved by compaction (densification) following placement of the soil. Various quantitative measures of compaction level or soil density are used in geotechnical engineering practice. Placed or constructed soil properties, as used in the soil-structure interaction procedures are related to compaction levels represented by the commonly specified "Standard Proctor" compaction reference test and "Modified Proctor" compaction reference test. The former is defined in ASTM D 698 (2005) and AASHTO T 99 (2005). The latter is defined in ASTM D 1557 (2005), and AASHTO T 180 (2005). The level of compaction is specified as the ratio of required field dry unit weight to the maximum dry unit weight (at optimum moisture content) in the reference test, expressed as a percent.

Table 1.1. Group Classification of Constructed and Natural Soils

Constructed Soils		
Soil Group	**Soil Classification**	
	Symbol	**Description**
1	SW	Well graded sand
	SP	Poorly graded sand
	GW	Well graded gravel
	GP	Poorly graded gravel
2	ML	Sandy silt
	SM	Silty sand
	GM	Silty gravel
	GC	Clayey gravel, with less than 20% passing #200 sieve
	SC	Clayey sand, with less than 20% passing #200 sieve
3	CL	Silty clay
	MH	Inorganic elastic silt
	GC	Clayey gravel
	SC	Clayey sand
4	CH	Plastic clay
Natural Soils		
Soil Type	**Soil Classification**	
	Symbol	**Description**
1	-	Coarsed-grained soils (greater than 50% sand and gravel sizes)
2	-	Fine-grained soils (greater than 50% silt and clay sizes)
3	-	Weak and competent rock

The Modified Proctor reference test uses a greater compaction effort than the Standard Proctor reference test. Thus, a particular compaction level achieved in the field represents a lower percentage of Modified Proctor than of Standard Proctor densities. For example, if a granular soil is compacted to 90 percent of Standard Proctor density, it

may be at 85 percent of Modified Proctor density. Equivalent soil classifications and modified proctor compaction levels are given in Table 1.2 and 1.3 respectively.

Table 1.2. Equivalent ASTM and AASHTO soil classifications

Basic Soil Type	**ASTM D 2487**	**AASHTO M 145**
Sn (Gravelly sand, SW)	SW, SP GW, GP sands and gravels with 12% or less fines	A1, A3
Si (Sandy silt, ML)	GM, SM, ML also GC and SC with less than 20% passing a No.200 sieve	A-2-4, A-2-5, A4
Cl (Silty clay, CL)	CL, MH, GC, SC also GC and SC with more than 20% passing a No.200 sieve	A-2-6, A-2-7, A5, A6

In Table 1.2, the soil classification listed in parentheses is the type that was tested to develop the constrained soil modulus values. The correlations to other soil types are approximate.

Table 1.3. Compaction Levels Used in Standard Installations

Specified Standard Proctor ASTM D 698 AASHTO T 99 %	**Equivalent Modified Proctor ASTM D 1557 AASHTO T 180 %**
Soil Groups 1 and 2	
100	95
95	90
90	85
85	80
80	75
Soil Groups 3	
100	90
95	85
90	80
85	75
80	70

Soil properties for use in soil-structure interaction analysis are most accurate when obtained by testing the specific soils and compaction levels that are to be specified for a particular pipe-soil installation design. Properties for each soil category have been evaluated by testing a representative soil in each category. These standard placed soil groups and their associated structural properties are given in Table 1.4. Also, six standard natural (pre-existing) soils have been defined for the two soil groups described above with three densities for each type and, in addition, two types of rock are included. These standard pre-existing soils and two types of rock, together with their estimated stiffness properties, are given in Table 1.5.

The soil shear strength and stiffness that is obtained by a given compaction level in terms of percent Standard Proctor dry density (or percent Modified Proctor dry density), varies significantly with soil type. Of the three standard soil types described in the previous section, gravelly sand soils have the largest shear strength and stiffness at a given compaction level while silty clays have the least.

Table 1.4. Soil Properties for Constructed Soil (Placed Backfill)

Soil Type	Std. T 99	Mod. T 180	γ_m (pcf)	K	n	C (psi)	Ø (deg)
SW	100	95	148	1300	0.90	0	54
	95	90	141	950	0.60	0	48
	90	85	134	640	0.43	0	42
	85	80	126	450	0.35	0	38
	80	75	119	320	0.35	0	36
	60	60	91	54	0.85	0	29
ML	100	95	134	800	0.54	5.5	36
	95	90	127	440	0.40	4	34
	90	85	120	200	0.26	3.5	32
	85	80	114	110	0.25	3	30
	80	75	107	75	0.25	2.5	28
	50	45	66	16	0.95	0	23
CL	100	90	125	170	0.37	11	12
	95	85	119	120	0.45	9	15
	90	80	112	75	0.54	7	17
	85	75	106	50	0.60	6	18
	80	70	100	35	0.66	5	19
	50	40	56	16	0.95	0	23

Table 1.5. Soil Properties for Pre-Existing (In-Situ) Soil

Soil Type	State	γ_m (pcf)	K	n	C (psi)	Ø (deg)
1	Dense	145	680	0	100	50
	Medium	130	408	0	100	50
	Loose	115	136	0	100	50
2	Very Stiff	125	408	0	100	50
	Firm to Stiff	117	238	0	100	50
	Soft	110	68	0	100	50

1.3 Load and Pressure Distribution on Buried Pipe

Loads that may cause structural effects on a buried pipe must be taken into account in the structural analysis procedure used to determine the moments, thrusts, and shears that govern the design of the pipe. However, determination of certain loads and the resulting pressures acting on the pipe is complicated by the effects of soil-structure interaction caused by deformations of pipe and soil. Typical loads that must be considered when analyzing or designing a buried pipe installation are:

- Pipe weight
- Earth load
- Fluid weight and internal pressure
- Surface concentrated loads
- Surface surcharge loads

1.3.1. Pipe Weight

Pipe weight may or may not be significant relative to other loads on a buried pipe. However, it should always be included in design procedures for pipe-soil installations. With the pipe inside diameter, D_i, pipe wall thickness, h, and the inside horizontal span, S_i, an approximation of the weight of pipe, W_p, can be calculated from the following:

Circular: $$W_p = 3.3h(D_i + h) \quad (1.1)$$

Arch or horizontal elliptical: $$W_p = 2.8h(S_i + h) \quad (1.2)$$

Vertical elliptical: $$W_p = 4.2h(S_i + h) \quad (1.3)$$

1.3.2. Earth Load

The earth load that acts on a buried pipe is significantly affected by the relative deformation of the pipe and the adjacent soil. A principal objective of a soil-structure interaction analysis is to determent the earth load and its pressure distribution. In finite element (FEM) analysis, earth load is directly taken into account via the unit weight of the earth in each of the elements. The results of the analysis give the pressure distribution at each of the pipe nodes in the pipe model. The summation of upward vertical components of pressure equals the total downward vertical load. This load is also the summation of downward vertical components of pressure. Similarly, the summation of horizontal components of pressure in one direction equals the horizontal load on the pipe.

The prism load, PL, is defined as the unit weight of backfill soil, w, with the height, H, over the top of the pipe times the volume of a one-foot-thick prism over the outside diameter, D_o, of the pipe. For a uniform backfill:

$$PL = \frac{wD_o}{12}(H + 0.00894D_o) \tag{1.4}$$

1.3.3. Fluid Weight and Internal Pressure

The weight of fluid in a concrete pipe, W_f, generally produces bending effects that are about the same magnitude as those caused by pipe weight (except for thrust which is tensile). These effects are of little significance in small diameter pipe but increase in importance as pipe diameter increases. The weight of fluid, γ, in the pipe

should normally be one of the applied loads when designing pipe for the installed condition.

$$W_f = 0.5454 \times 10^{-2} \gamma D_i^{\,2} \tag{1.5}$$

Many culvert and sewer pipelines are designed for gravity flow without any significant internal pressure head above the condition of the pipe flowing full. However, in those cases where significant internal pressure head, above the level of external earth pressure, is anticipated, this pressure should be considered as an additional loading condition.

1.3.4. Surface Concentrated Loads

The most commonly encountered concentrated surface loads are wheel loads from highway trucks. Buried pipe also may pass under railroads or airport runways. Evaluation of the effects of surface concentrated loads on buried pipe requires consideration of the attenuation and distribution of the earth pressure through the pavement and earth over the pipe. The influence of two or more adjacent wheels must also be taken into account for appropriate combinations of wheel spacing, height of earth cover over the crown, and pipe diameter. The tire footprint, and the longitudinal beam stiffness of the pipe also help to distribute the effects of a concentrated surface load. The effect of the pavement is a function of the type of pavement (i.e., plain concrete, reinforced concrete, or asphalt), but the beneficial effect of distribution from rigid pavements is frequently ignored in the design of concrete pipe below roadways.

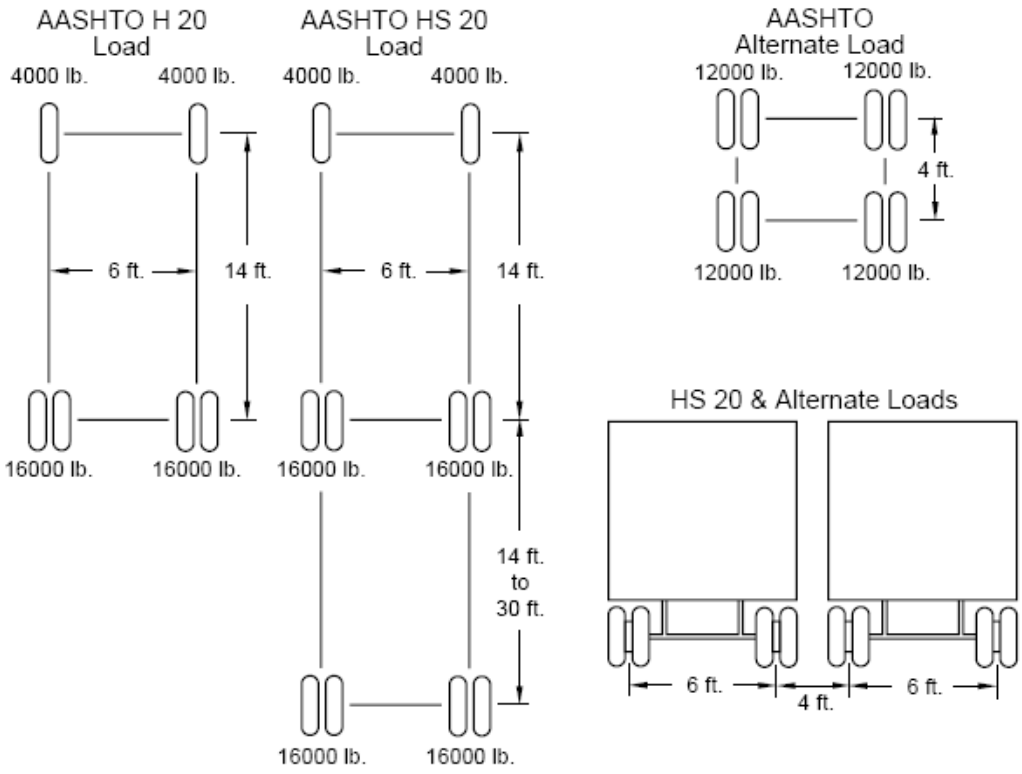

Figure 1.4 AASHTO Live Loads (Ref: AASHTO (2004) Bridge Design Specifications)

The largest effect on a buried pipe from a single surface concentrated load occurs when the least earth pressure attenuation takes place at the shallowest height of cover. However, parametric studies have shown that pipe design requirements for cover heights as low as one foot often are close to what would be provided for practical minimum design of reinforcement in the pipe. In view of this, reasonable approximations for estimating the effects of surface concentrated loads are warranted, rather than an elaborate analytical procedure for determining the theoretical pressure from a concentrated load at various locations below the surface.

One such simplified procedure for determining the below-ground pressures caused by highway truck wheels is given in the AASHTO Bridge Design Specification. Standard trucks have the dimensional arrangement of axles shown in Figure 1.4. The earth pressure caused by a concentrated surface load is assumed to attenuate with increasing depth at an angle of about 41 degrees with the vertical in each direction, as shown in Figure 1.5. This angle increases the sides of the loaded area 1.75 ft (0.5 m). for every foot of depth below the surface.

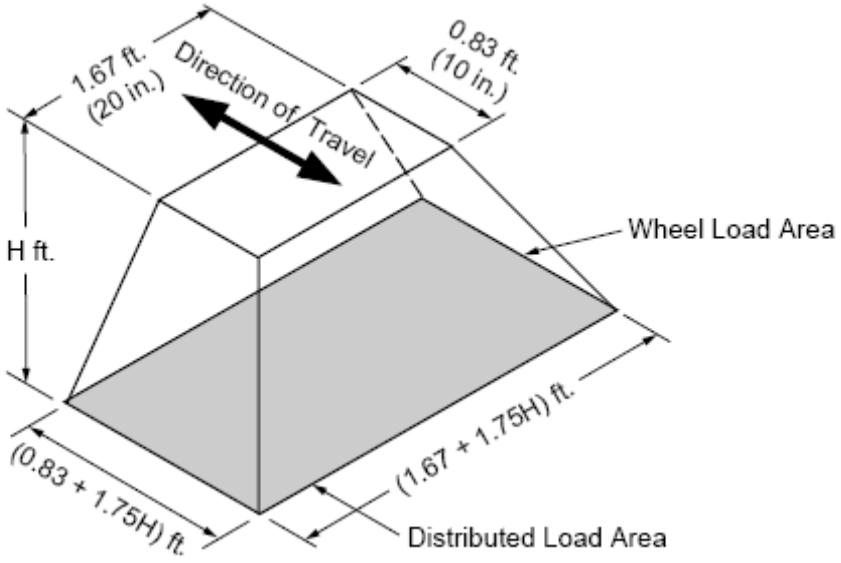

Figure 1.5 Earth Pressure Attenuation at Depth of Earth Cover, H, for Load from Dual Truck Wheel at Surface (Ref: AASHTO (2004) Bridge Design Specifications)

CHAPTER 2

FINITE ELEMENT MODEL

2.1 Introduction

The three-dimensional finite element models of pipe-soil interaction were performed by using computer program, ABAQUS version 6.5-1. Including the different types of soil zones, the models compose of several types of elements, eight-noded linear brick (C3D8R) and six-noded linear triangular prism (C3D6). The pipe-soil interface was a no-slip (bonded) condition. The optimum mesh with regard to element type was selected and the analysis was performed to include geometric and contact nonlinearities.

2.2 Plane-Strain Approximation

Plane-strain implies the pipe-soil installation is a long, prismatic configuration with no variation in the pipe, soil system, or loading along the longitudinal axis. The inference is that there is no deformation in the longitudinal direction and that every cross section deforms in the same manner. Consequently, the boundary value problem reduces to describing a single representative cross section. This description includes the pipe size and shape, wall section properties per unit length, wall material properties, soil geometry and material properties for various zones (e.g. in-situ, backfill, bedding, etc.), and loading conditions.

In reality, pipe-soil installations are three-dimensional systems, and it is well to emphasize the limitations of the plane-strain approximation. In a trench or embankment installation, the soil height above the pipe may vary significantly along the longitudinal axis of the pipe. In such cases it is common practice to select a representative cross-section based on the greatest fill height in order to achieve a conservative design.

2.3 Soil-Structure Interaction

The pipe (structure) and the enveloping soil mass, working in tandem as a composite unit, is one of the most remarkably synergistic systems in engineering. When soil is properly compacted around the pipe, the load-carrying capacity of the pipe-soil system far exceeds the individual capacity of either component by itself. Analysis of soil-structure interaction is the recognition that both the pipe and soil are structural components. Thus, the amount of load carried by the pipe is dependent on the soil stiffness relative to the pipe stiffness for various modes of deformation.

2.4 Finite Element Model

The finite element model used for three-dimensional analysis was constructed with a plane of symmetry representing the longitudinal centerline of the soil prism load, and therefore, only includes half of overburden pressure. Figure 2.1 and Figure 2.2 show the soil zones and the converged finite element mesh used in the analysis respectively. All analysis was completed using an embankment installation, since this generally produces more load and deflection than a trench installation.

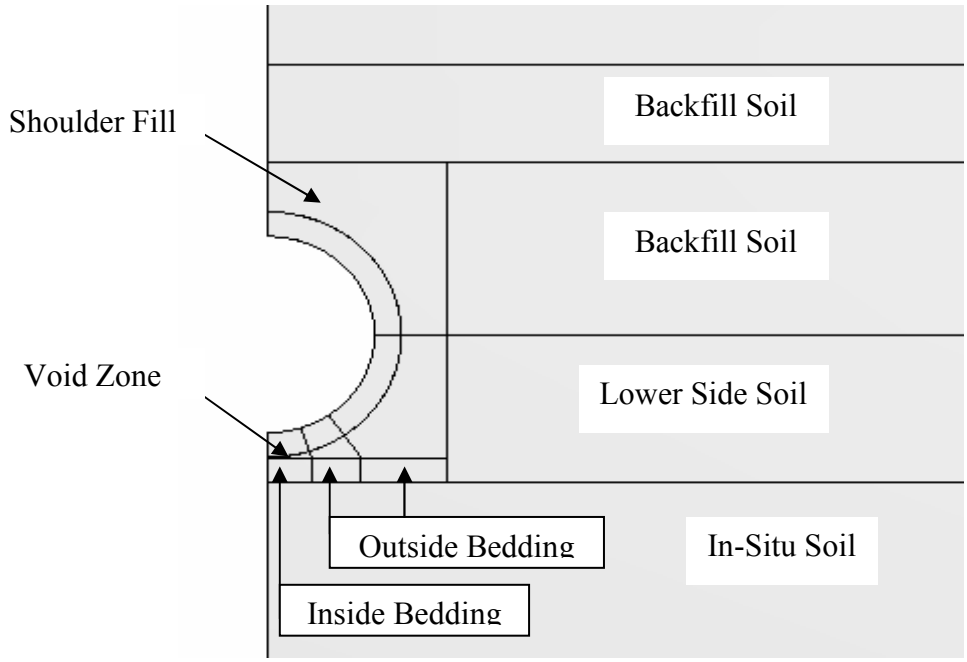

Figure 2.1 Soil Zones used in The FEM Model

2.4.1. Pipe Model

There are three different sizes of concrete pipe used in this FEA which are 24 in (60 cm) inside diameter (D_i) with 3 in (7.5 cm) wall thickness, 60 in (150 cm) inside diameter (D_i) with 6 in (15 cm) wall thickness, and 84 in (210 cm) inside diameter (D_i) with 8 in (20 cm) wall thickness. The pipe properties are presented in Table 2.1.

Table 2.1. Concrete Pipe Properties

Property	**Value**
Mass Density, γ	150 pcf (2,520 kg/m^3)
Compressive Strength, f_c'	4,000 psi (28 MPa)
Poisson's Ratio, υ	0.2
Young's Modulus, E_c	3.605E+06 psi (24,856 MPa)

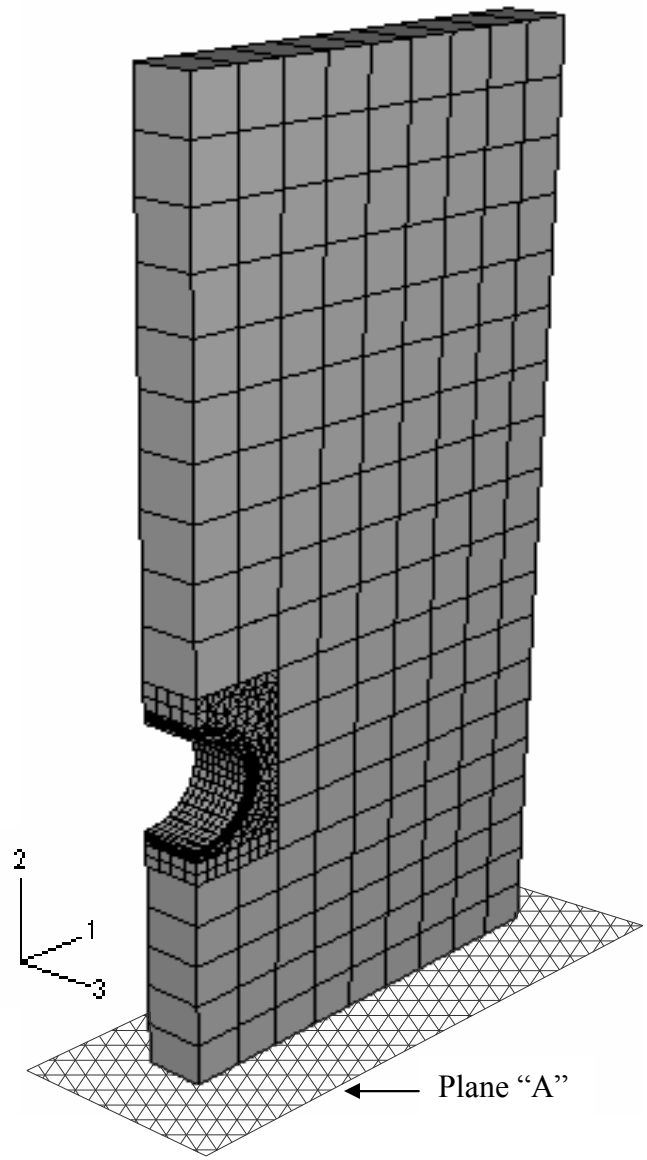

Figure 2.2 Converged Finite Element Mesh

All surfaces above plane “A” (except the surfaces of internal pipe) were restrained to the movement along the 1-direction. Also, all surfaces at plane “A” were restrained to the movement in all directions.

2.4.2. Soil Models

Soil properties were developed by Selig (1988). These properties use the hyperbolic Young's modulus developed by Duncan et al. (1980) and the hyperbolic bulk modulus developed by Selig (1988). There are three general groups of placed backfill soils, which are defined in AASHTO LRFD (1998) as shown in Table 2.3. These groups are coarse-grained soils with little or no fines (Sn), coarse-grained soils with fines or sandy or gravelly fine-grained soils (Si), and fine-grained soils (Cl). General assumptions for soils used in the analyses are as follows:

- In-situ or native soil under the bedding was considered to be a firm fine-grained material.
- A small area, called "void zone", which is difficult to compact in the field was always considered to be filled with a very soft material. Thus, silty material at 50% of Standard Proctor Density, called "Si50", was applied in this zone.
- A larger area above the bedding and below the springline, called "haunch fill", was considered to be filled with a coarse-grained material at 90% of Standard Proctor Density, called "Sn90".
- An area adjacent to the haunch zone and below the springline, called "lower side fill", was considered to be filled with a coarse-grained material at 90% of Standard Proctor Density, called "Sn90".
- Backfill and shoulder fill were also considered to be filled with a coarse-grained material at 90% of Standard Proctor Density, called "Sn90".

- Bedding zone was divided into "inside bedding zone" and "outside bedding zone". Materials used for the inside bedding were varied with Si70, Si90, Sn85, and Sn90. The outside bedding was modeled as Sn90 for all cases.

Table 2.2. Young's Modulus Based on Soil Type and Compaction Condition

P_{sp} Stress level		**Sn100**		**Sn95**		**Sn90**		**Sn85**	
(ksf)	**(kPa)**	**(ksi)**	**(MPa)**	**(ksi)**	**(MPa)**	**(ksi)**	**(MPa)**	**(ksi)**	**(MPa)**
0.150	7.414	2.350	16.725	2.000	14.234	1.275	9.074	0.470	3.345
0.750	37.068	3.450	24.554	2.600	18.505	1.500	10.676	0.520	3.701
1.500	74.137	4.200	29.892	3.000	21.351	1.625	11.565	0.570	4.057
3.000	148.273	5.500	39.144	3.450	24.554	1.800	12.811	0.650	4.626
6.000	296.547	7.500	53.378	4.250	30.248	2.100	14.946	0.825	5.872
9.000	444.820	9.300	66.189	5.000	35.586	2.500	17.793	1.000	7.117
P_{sp} Stress level				**Si95**		**Si90**		**Si85**	
(ksf)	**(kPa)**			**(ksi)**	**(MPa)**	**(ksi)**	**(MPa)**	**(ksi)**	**(MPa)**
0.150	7.414			1.415	10.071	0.670	4.768	0.360	2.562
0.750	37.068			1.670	11.886	0.740	5.267	0.390	2.776
1.500	74.137			1.770	12.597	0.750	5.338	0.400	2.847
3.000	148.273			1.880	13.380	0.790	5.623	0.430	3.060
6.000	296.547			2.090	14.875	0.900	6.405	0.510	3.630
9.000	444.820								
P_{sp} Stress level				**Cl95**		**Cl90**		**Cl85**	
(ksf)	**(kPa)**			**(ksi)**	**(MPa)**	**(ksi)**	**(MPa)**	**(ksi)**	**(MPa)**
0.150	7.414			0.530	3.772	0.255	1.815	0.130	0.925
0.750	37.068			0.625	4.448	0.320	2.277	0.175	1.245
1.500	74.137			0.690	4.911	0.355	2.527	0.200	1.423
3.000	148.273			0.740	5.267	0.395	2.811	0.230	1.637
6.000	296.547			0.815	5.800	0.460	3.274	0.285	2.028
9.000	444.820			0.895	6.370	0.525	3.736	0.345	2.455

Notes: 1. The soil types are defined by a two-letter designation that indicates general soil classification, Sn for sands and gravels, Si for silts, and Cl for clays. Specific soil groups that fall into these categories, based on ASTM D 2487 and AASHTO M 145, are listed in Table 1.2

2. The numerical suffix to the soil type indicates the compaction level of the soil as a percentage of maximum dry density determined in accordance with AASHTO T 99.

Analyses were completed for varied backfill depths of 20 ft (6 m), 40 ft (12 m), 60 ft (18 m), 80 ft (24 m), and 100 ft (30 m) and also, varied bedding thicknesses of 3 in (7.5 cm), 5 in (12.5 cm), 7 in (17.5 cm), and 9 in (22.5 cm).

2.4.3. Incremental Construction and Soil Compaction

This model is defined by Young's modulus and Poisson's ratio whose values are dependent upon the current level of overburden pressure. In this model, the soil Young's modulus increases with increasing overburden stress.

When the pipe is installed, the fill soil is usually compacted in about 6 in lifts, beginning near the pipe invert and symmetrically incremented on both sides, and then over the pipe crown up to the final fill height. During the side compaction process, the pipe side walls are pushed inward due to the "Poisson effect" of soil from compaction pressure and the soil gravity weight. In this model, the use of thick construction increments in conjunction with a "squeeze pressure" technique was simulated. Consequently, horizontal element rows (backfill soils in this case) adjacent to the side of the pipe were assigned. At the same time, each construction increment was assigned equal and opposite pressures at its top and bottom surface. Thus, as each construction increment entered the system in sequence, it was compressed in the vertical direction, thereby, causing a lateral pressure to develop on the pipe.

2.4.4. Boundary Conditions

The boundaries of the soil mesh must be located far enough away from the pipe so as not to appreciably influence the solution. The convergence distance for lateral boundaries was three diameters from the center of the pipe. The soil nodes along lateral

boundaries of the model were fixed against horizontal translation. All nodes along the bottom of the model were fixed against translation. Nodes along the end faces of the model (Plane 1-2) are fixed from translating longitudinally.

2.5 Pipe Wall Stiffness

The thicknesses of pipe wall were 3 in (7.5 cm), 6 in (15 cm), and 8 in (20 cm) for the diameter of 24 in (60 cm), 60 in (150 cm), and 84 in (210 cm) respectively. Modeled by using 8-node linear brick elements, each pipe wall thickness was meshed into 5 layers of brick elements for delineating the difference values between compressive and tensile stresses. The pipe wall stiffness was comprised of bending stiffness, $E_c I_{eff}$, and axial stiffness, $E_c A_{eff}$, where E_c is the modulus of elasticity of concrete, I_{eff} is the effective moment of inertia of the pipe cross section, and A_{eff} is the effective area of the pipe wall. The normal-weight concrete pipes were modeled as linear-elastic with a Young's modulus (E_c) of 3.605×10^6 psi (24,856 MPa), calculated by:

$$E_c = 57{,}000\sqrt{f'_c} \tag{2.1}$$

where f'_c is compressive strength of concrete ($f'_c = 4{,}000$ psi. (28 MPa))

The effective area, A_{eff}, and effective moment of inertia, I_{eff}, were computed by:

$$A_{eff} = \frac{\pi}{4}\left(D_o^{\,2} - D_i^{\,2}\right) \tag{2.2}$$

$$I_{eff} = \frac{\pi}{64}\left(D_o^{\,4} - D_i^{\,4}\right) \tag{2.3}$$

where D_o is the pipe outside diameter, and D_i is the pipe inside diameter

2.6 Soil Stiffness

Soil was modeled using 6-node linear triangular prism elements. The stress-strain relationships were assumed as linear elastic for in-situ soil and nonlinear for all backfill soil. The in-situ soil was assigned a Young's modulus of 15,000 psi (103 MPa) and a Poisson's ratio of 0.3, based on the assumption that the in-situ was considered to be a firm fine-grained material.

Nonlinear stress-strain relationships were defined using the Duncan hyperbolic Young's modulus (Duncan et al, 1980) and the Selig hydrostatic hyperbolic bulk modulus (Selig 1988). The model nonlinearity allows for a shear failure criterion and gives increased soil stiffness and shear strength for increased lateral confinement.

2.6.1. Mohr-Coulomb Model (Perfect Plasticity)

The elastic-plastic Mohr-Coulomb model involves five input parameters, i.e. E and υ for soil elasticity, ϕ and c for soil plasticity, and ψ as an angle of dilatancy. Plasticity is associated with the development of irreversible strains.

2.6.2. Elastic Perfectly-Plastic Behavior

The basic principle of elastoplasticity is that strains and strain rates are decomposed into an elastic part and a plastic part:

$$\varepsilon = \varepsilon^e + \varepsilon^p \qquad\qquad \dot{\varepsilon} = \dot{\varepsilon}^e + \dot{\varepsilon}^p \qquad (2.4)$$

Hooke's law is used to relate the stress rates to the elastic strain rates. Substitution of Eq.(2.2) into Hooke's law (2.3) leads to:

$$\dot{\sigma}' = D^e \dot{\varepsilon}^e = D^e \left(\dot{\varepsilon} - \dot{\varepsilon}^p \right) \qquad (2.5)$$

According to the classical theory of plasticity (Hill, 1950), plastic strain rates are proportional to the derivative of the yield function with respect to the stresses. This means that the plastic strain rates can be represented as vectors perpendicular to the yield surface. This classical form of the theory is referred to as associated plasticity. However, for Mohr-Coulomb type yield functions, the theory of associated plasticity leads to an overprediction of dilatancy. Therefore, in addition to the yield function, a plastic potential function g is introduced. The case $g \neq f$ is denoted as non-associated plasticity. In general, the plastic strain rates are written as:

$$\dot{\varepsilon}^p = \lambda \frac{\partial g}{\partial \sigma'} \tag{2.6}$$

in which λ is the plastic multiplier. For purely elastic behavior λ is zero, whereas in the case of plastic behavior λ is positive:

$$\lambda = 0 \quad for: \quad f < 0 \quad or: \quad \frac{\partial f^T}{\partial \sigma'} D^e \dot{\varepsilon} \leq 0 \quad (Elasticity) \tag{2.7a}$$

$$\lambda > 0 \quad for: \quad f = 0 \quad or: \quad \frac{\partial f^T}{\partial \sigma'} D^e \dot{\varepsilon} > 0 \quad (Plasticity) \tag{2.7b}$$

These equations may be used to obtain the following relationship between the effective stress rates and strain rates for elastoplasticity (smith & Griffith, 1982; Vermeer & de Borst, 1984):

$$\dot{\sigma}' = \left(D^e - \frac{\alpha}{d} D^e \frac{\partial g}{\partial \sigma'} \frac{\partial f^T}{\partial \sigma'} D^e \right) \dot{\varepsilon} \tag{2.8a}$$

where:

$$d = \frac{\partial f^T}{\partial \sigma'} D^e \frac{\partial g}{\partial \sigma'} \tag{2.8b}$$

The above theory of plasticity is restricted to smooth yield surfaces and does not cover a multi surface yield contour as present in the Mohr-Coulomb model. For such a yield surface the theory of plasticity has been extended by Koiter (1960) and others to account for flow vertices involving two or more plastic potential functions:

$$\dot{\varepsilon}^{p} = \lambda_1 \frac{\partial g_1}{\partial \sigma'} + \lambda 2 \frac{\partial g 2}{\partial \sigma'} + \ldots \tag{2.9}$$

Similarly, several quasi independent yield functions $(f_1, f_2, \ldots)$ are used to determine the magnitude of the multipliers $(\lambda_1, \lambda_2, \ldots)$.

2.6.3. Yield Criterion

The Mohr-Coulomb criterion assumes that failure occurs when the shear stress on any point in a material reaches a value that depends linearly on the normal stress in the same plane. The Mohr-Coulomb model is based on plotting Mohr's circle for states of stress at failure in the plane of the maximum and minimum principal stresses. The failure line is the best straight line that touches these Mohr's circles.

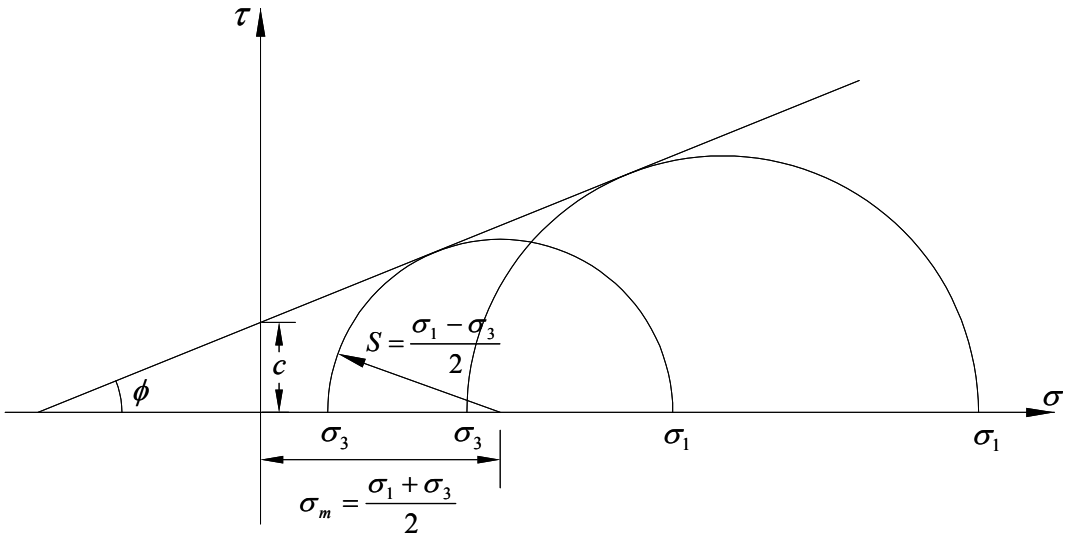

Figure 2.3 Mohr-Coulomb failure model

Therefore, the Mohr-Coulomb model is defined by

$$\tau = c + \sigma \tan\phi \tag{2.10}$$

where σ is negative in compression. From Mohr's circle,

$$\tau = s\cos\phi \tag{2.11}$$

$$\sigma = \sigma_m + s\sin\phi \tag{2.12}$$

Substituting for τ and σ, multiplying both sides by $\cos\phi$, and reducing, the Mohr-Coulomb model can be written as:

$$s + \sigma_m \sin\phi - c\cos\phi = 0 \tag{2.13}$$

where

$$s = \frac{1}{2}(\sigma_1 - \sigma_3) \tag{2.14}$$

is half of the difference between the maximum principal stress, σ_1, and the minimum principal stress, σ_3 (and is, therefore, the maximum shear stress),

$$\sigma_m = \frac{1}{2}(\sigma_1 + \sigma_3) \tag{2.15}$$

is the average of the maximum and minimum principal stresses, and ϕ is the friction angle.

For general states of stress the model is more conveniently written in terms of three stress invariants as

$$F = R_{mc} q - p \tan\phi - c = 0 \tag{2.16}$$

where

$$R_{mc}(\theta,\phi) = \frac{1}{\sqrt{3}\cos\phi}\sin\left(\theta + \frac{\pi}{3}\right) + \frac{1}{3}\cos\left(\theta + \frac{\pi}{3}\right)\tan\phi \tag{2.17}$$

ϕ is the slope of the Mohr-Coulomb yield surface in the $p - R_{mc} q$ stress plane (see Figure 2.4), which is commonly referred to as the friction angle of the material and can depend on temperature and predefined field variables;

c is the cohesion of the material; and

θ is the deviatoric polar angle defined as

$$\cos(3\theta) = \left(\frac{r}{q}\right)^3 \tag{2.18}$$

and

$$p = -\frac{1}{3} trace(\sigma) \tag{2.19}$$

p is the equivalent pressure stress,

$$q = \sqrt{\frac{3}{2}(S : S)} \tag{2.20}$$

q is the Mises equivalent stress,

$$r = \left(\frac{9}{2} S \cdot S : S\right)^{\frac{1}{3}} \tag{2.21}$$

r is the third invariant of deviatoric stress,

$$S = \sigma + pI \tag{2.22}$$

S is the deviatoric stress.

The friction angle ϕ controls the shape of the yield surface in the deviatoric plane as shown in Figure 2.4. The friction angle can range from $0^\circ \le \phi < 90^\circ$. In the case of $\phi = 0^\circ$ the Mohr-Coulomb model reduces to the pressure-independent Tresca model with a perfectly hexagonal deviatoric section. In the case of $\phi = 90^\circ$ the Mohr-Coulomb model reduces to the "tension cut-off" Rankine model with a triangular deviatoric section and $R_{mc} = \infty$ (this limiting case is not permitted within the Mohr-Coulomb model described here).

While using one-element tests to verify the calibration of the model, it should be noted that the ABAQUS/Standard output variables SP1, SP2, and SP3 correspond to the principal stresses σ_3, σ_2 and σ_1, respectively.

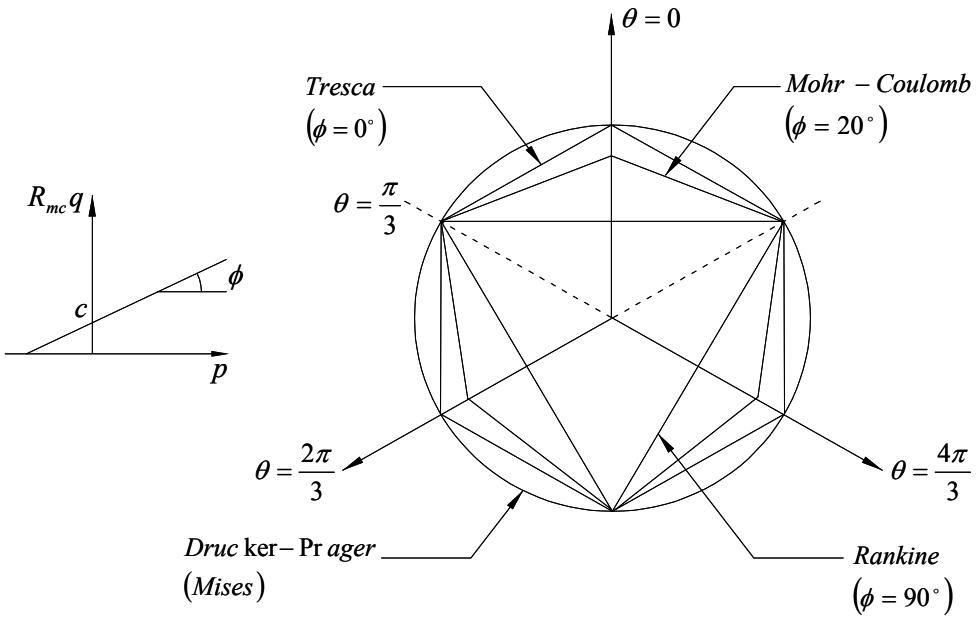

Figure 2.4 Mohr-Coulomb yield surface in meridional and deviatoric planes

The bulk modulus is defined as the change in mean stress (average change in stress in three orthogonal directions) divided by the change in volumetric strain. The bulk modulus is assumed to vary only with the confining stress.

2.7 Preliminaries on Material Modeling

A material model is a set of mathematical equations that describes the relationship between stress and strain. Material models are often expressed in a form in which infinitesimal increments of stress (or "stress rates") are related to infinitesimal increments of strain (or "strain rates"). All material models implemented in this study are based on a relationship between the effective stress rates, σ' and the strain rates, ε'.

2.7.1. General Definitions of Stress

Stress is a tensor which can be represented by a matrix in Cartesian coordinates:

$$\sigma = \begin{bmatrix} \sigma_{xx} & \sigma_{xy} & \sigma_{xz} \\ \sigma_{yx} & \sigma_{yy} & \sigma_{yz} \\ \sigma_{zx} & \sigma_{zy} & \sigma_{zz} \end{bmatrix} \tag{2.23}$$

In the standard deformation theory, the stress tensor is symmetric such that $\sigma_{xy} = \sigma_{yx}$, $\sigma_{yz} = \sigma_{zy}$, $\sigma_{zx} = \sigma_{xz}$. In this situation, stresses can be written in vector notation, which involve only six different components:

$$\sigma = \begin{pmatrix} \sigma_{xx} & \sigma_{yy} & \sigma_{zz} & \sigma_{xy} & \sigma_{yz} & \sigma_{zx} \end{pmatrix}^T \tag{2.24}$$

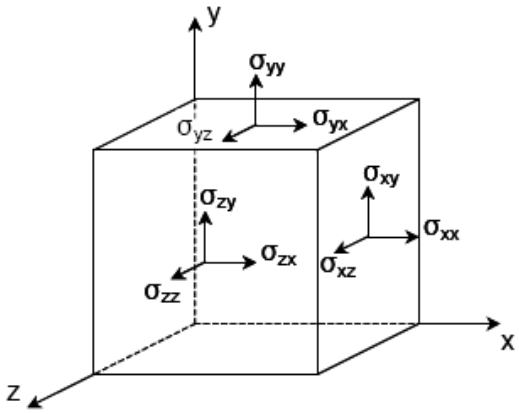

Figure 2.5 General three-dimensional coordinate system for stresses

In plane strain condition,

$$\sigma_{yz} = \sigma_{zx} = 0 \tag{2.25}$$

According to Terzaghi's principle, stresses in the soil are divided into effective stresses, σ', and pore pressures, σ_w:

$$\sigma = \sigma' + \sigma_w \tag{2.26}$$

Water is considered not to sustain any shear stresses. As a result, effective shear stresses are equal to total shear stresses. Positive normal stress components are considered to represent tension, whereas negative normal stress components indicate pressure (or compression). However, the effect of pore pressures, σ_w, was not included in this study for the embankment installation.

Material models for soil are generally expressed as a relationship between infinitesimal increments of effective stress and infinitesimal increments of strain. In such a relationship, infinitesimal increments of effective stress are represented by stress rates (with a dot above the stress symbol):

$$\dot{\sigma}' = \begin{pmatrix} \dot{\sigma}'_{xx} & \dot{\sigma}'_{yy} & \dot{\sigma}'_{zz} & \dot{\sigma}'_{xy} & \dot{\sigma}'_{yz} & \dot{\sigma}'_{zx} \end{pmatrix}^T \tag{2.27}$$

It is often useful to use principal stresses rather than Cartesian stress components when formulating material models. Principal stresses are the stresses in such a coordinate system direction that all shear stress components are zero. Principal stresses are the eigenvalues of the stress tensor. Principal effective stresses can be determined in the following:

$$\det\left(\sigma' - \sigma' I\right) = 0 \tag{2.28}$$

where I is the identity matrix. This equation gives three solutions for σ', i.e. the principal effective stresses $\left(\sigma'_1, \sigma'_2, \sigma'_3\right)$. The principal effective stresses are arranged in algebraic order:

$$\sigma'_1 \le \sigma'_2 \le \sigma'_3 \tag{2.29}$$

Hence, σ'_1 is the largest compressive principal stress and σ'_3 is the smallest compressive principal stress.

In addition to principal stresses, it is also useful to define invariants of stress, which are stress measures that are independent of the orientation of the coordinate system. Two useful stress invariants are:

$$p' = -\frac{1}{3}\left(\sigma'_{xx} + \sigma'_{yy} + \sigma'_{zz}\right) = -\frac{1}{3}\left(\sigma'_1 + \sigma'_2 + \sigma'_3\right) \tag{2.30}$$

$$q = \sqrt{\frac{1}{2}\left(\left(\sigma'_{xx} - \sigma'_{yy}\right)^2 + \left(\sigma'_{yy} - \sigma'_{zz}\right)^2 + \left(\sigma'_{zz} - \sigma'_{xx}\right)^2 + 6\left(\sigma^2{}_{xy} + \sigma^2{}_{yz} + \sigma^2{}_{zx}\right)^2\right)} \tag{2.31}$$

where p' is the isotropic effective stress, or mean effective stress, and q is the equivalent shear stress. The convention adopted for p' is positive for compressive in

contrast to other stress measures. The equivalent shear stress, q, has the important property that it reduces to $q = \left|\sigma_1' - \sigma_3'\right|$ for triaxial stress states with $\sigma_2' = \sigma_3'$.

Principal effective stresses can be written in terms of the invariants:

$$-\sigma_1' = p' + \frac{2}{3} q \sin\left(\theta - \frac{2}{3}\pi\right) \tag{2.32}$$

$$-\sigma_2' = p' + \frac{2}{3} q \sin(\theta) \tag{2.33}$$

$$-\sigma_3' = p' + \frac{2}{3} q \sin\left(\theta + \frac{2}{3}\pi\right) \tag{2.34}$$

In which θ is referred to as Lode's angle (a third invariant), which is defined as:

$$\theta = \frac{1}{3} \arcsin\left(\frac{27}{2} \frac{J_3}{q^3}\right) \tag{2.35}$$

with

$$J_3 = (\sigma_{xx}' - p')(\sigma_{yy}' - p')(\sigma_{zz}' - p') - (\sigma_{xx}' - p')\sigma^2{}_{yz} - (\sigma_{yy}' - p')\sigma^2{}_{zx}$$
$$-(\sigma_{zz}' - p')\sigma^2{}_{xy} + 2\sigma_{xy}\sigma_{yz}\sigma_{zx} \tag{2.36}$$

2.7.2. General Definitions of Strain

Strain is a tensor which can be represented by a matrix in Cartesian coordinates:

$$\varepsilon = \begin{bmatrix} \varepsilon_{xx} & \varepsilon_{xy} & \varepsilon_{xz} \\ \varepsilon_{yx} & \varepsilon_{yy} & \varepsilon_{yz} \\ \varepsilon_{zx} & \varepsilon_{zy} & \varepsilon_{zz} \end{bmatrix} \tag{2.37}$$

According to the small deformation theory, only the sum of complementing Cartesian shear strain components ε_{ij} and ε_{ji} result in shear stress. This sum is denoted

as the shear strain γ. Hence, instead of $\varepsilon_{xy,}\varepsilon_{yx,}\varepsilon_{yz,}\varepsilon_{zy,}\varepsilon_{zx,}\varepsilon_{xz}$ the shear strain components $\gamma_{xy},\gamma_{yz},\gamma_{zx}$ are used respectively. Under the above conditions, strains are often written in vector notation, which involve only six different components:

$$\varepsilon = \begin{pmatrix} \varepsilon_{xx} & \varepsilon_{yy} & \varepsilon_{zz} & \varepsilon_{xy} & \varepsilon_{yz} & \varepsilon_{zx} \end{pmatrix}^T \tag{2.38}$$

$$\varepsilon_{xx} = \frac{\partial u_x}{\partial x} \tag{2.39a}$$

$$\varepsilon_{yy} = \frac{\partial u_y}{\partial y} \tag{2.39b}$$

$$\varepsilon_{zz} = \frac{\partial u_z}{\partial z} \tag{2.39c}$$

$$\gamma_{xy} = \varepsilon_{xy} + \varepsilon_{yx} = \frac{\partial u_x}{\partial y} + \frac{\partial u_y}{\partial x} \tag{2.39d}$$

$$\gamma_{yz} = \varepsilon_{yz} + \varepsilon_{zy} = \frac{\partial u_y}{\partial z} + \frac{\partial u_z}{\partial y} \tag{2.39e}$$

$$\gamma_{zx} = \varepsilon_{zx} + \varepsilon_{xz} = \frac{\partial u_z}{\partial x} + \frac{\partial u_x}{\partial z} \tag{2.39f}$$

Positive normal strain components refer to extension, whereas negative normal strain components indicate compression. In the formulation of material models, where infinitesimal increments of strain are considered, these increments are represented by strain rates (with a dot above the strain symbol).

$$\dot{\varepsilon} = \begin{pmatrix} \dot{\varepsilon}_{xx} & \dot{\varepsilon}_{yy} & \dot{\varepsilon}_{zz} & \dot{\varepsilon}_{xy} & \dot{\varepsilon}_{yz} & \dot{\varepsilon}_{zx} \end{pmatrix}^T \tag{2.40}$$

For plane strain condition,

$$\varepsilon_{zz} = \gamma_{xz} = \gamma_{yz} = 0 \tag{2.41}$$

In analogy to the invariants of stress, it is also useful to define invariants of strain. A strain invariant that is often used is the volumetric strain, ε_v, which is defined as the sum of all normal strain components:

$$\varepsilon_v = \varepsilon_{xx} + \varepsilon_{yy} + \varepsilon_{zz} = \varepsilon_1 + \varepsilon_2 + \varepsilon_3 \tag{2.42}$$

The volumetric strain is defined as negative for compaction and as positive for dilatancy.

2.7.3. Elastic Strains

Material models for soil are generally expressed as a relationship between infinitesimal increments of effective stress (effective stress rates) and infinitesimal increments of strain (strain rates). This relationship can be expressed in the form:

$$\dot{\sigma}' = M\dot{\varepsilon} \tag{2.43}$$

M is a material stiffness matrix. Note that in this type of approach, pore-pressures are explicitly excluded from the stress-strain relationship.

The simplest material model is based on Hooke's law for isotropic linear elastic behavior. This model is available under the name Linear Elastic model, but it is also the basis of other models. Hook's law can be given by the equation:

$$\begin{bmatrix} \dot{\sigma}'_{xx} \\ \dot{\sigma}'_{yy} \\ \dot{\sigma}'_{zz} \\ \dot{\sigma}'_{xy} \\ \dot{\sigma}'_{yz} \\ \dot{\sigma}'_{zx} \end{bmatrix} = \frac{E}{(1-2\nu')(1+\nu')} \begin{bmatrix} 1-\nu' & \nu' & \nu' & 0 & 0 & 0 \\ \nu' & 1-\nu' & \nu' & 0 & 0 & 0 \\ \nu' & \nu' & 1-\nu' & 0 & 0 & 0 \\ 0 & 0 & 0 & \frac{1}{2}-\nu' & 0 & 0 \\ 0 & 0 & 0 & 0 & \frac{1}{2}-\nu' & 0 \\ 0 & 0 & 0 & 0 & 0 & \frac{1}{2}-\nu' \end{bmatrix} \begin{bmatrix} \dot{\varepsilon}_{xx} \\ \dot{\varepsilon}_{yy} \\ \dot{\varepsilon}_{zz} \\ \dot{\gamma}_{xy} \\ \dot{\gamma}_{yz} \\ \dot{\gamma}_{zx} \end{bmatrix} \tag{2.44}$$

The relationship between Young's modulus E and other stiffness moduli, such as the shear modulus G, the bulk modulus K, and the oedometer modulus E_{oed}, is given by:

$$G = \frac{E}{2(1+\nu)} \tag{2.45a}$$

$$K = \frac{E}{3(1-2\nu)} \tag{2.45b}$$

$$E_{oed} = \frac{(1-\nu)E}{(1-2\nu)(1+\nu)} \tag{2.45c}$$

2.8 Element Types

Continuum or solid elements were used to model the various components in pipe-soil interaction. Conceptually, continuum elements simply modeled small blocks of material in a component. All elements were connected together on any of their faces, continuum element, like bricks, were used to create models of nearly shape, subjected to nearly any loading. Continuum stress/displacement elements in ABAQUS have names that begin with the letter "C". The next two letters indicate the dimensionality and usually the active degree of freedom in the element. The letters "3D" indicate a three-dimensional element. The letter "R" at the end of the element name specifies the reduced-integration elements.

The expression "full integration" refers to the number of Gauss points required to integrate the polynomial terms in element's stiffness matrix exactly when the element has a regular shape. For hexahedral and quadrilateral elements, a "regular shape" means

that the edges are straight and meet at the right angles and that any edge nodes are at the midpoint of the edge. Fully integrated, linear elements use two integration points in each direction. Thus, the three-dimensional element C3D8 uses a 2 × 2 × 2 array of integration points in the element. Fully integrated, quadratic elements use three integration points in each direction as shown in Figure 2.6.

Table 2.3. Element Types used in Pipe-Soil Model (Ref. ABAQUS (2005) version 6.5)

Element	Description and Shape	D.O.F.
C3D6	6-node linear triangular prism. 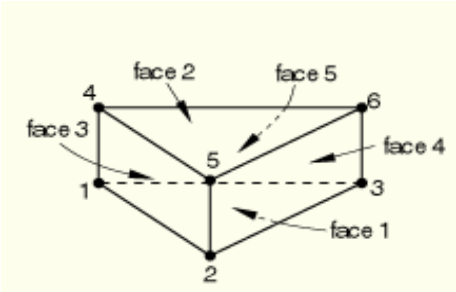	6
C3D8R	8-node linear brick, reduced integration. 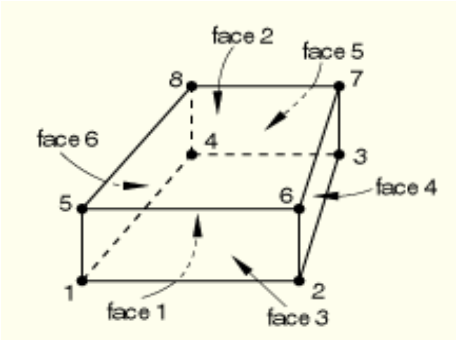	8

(a) (b)

Figure 2.6 Integration points in two-dimensional elements with fully integration; (a) Linear element and (b) Quadratic element (Ref: ABAQUS (2005) version 6.5)

Only quadrilateral and hexahedral elements can use a reduced-integration scheme; all wedge, tetrahedral, and triangular solid elements use full integration, although they can be used in the same mesh with reduced-integration hexahedral or quadrilateral elements. Reduced-integration elements use one fewer integration point in each direction than the fully integrated elements. Reduced-integration, linear elements have just a single integration point located at the element's centroid. Reduce-integration, quadratic elements use two integration points in each direction as shown in Figure 2.7.

(a) (b)

Figure 2.7 Integration points in two-dimensional elements with reduced integration; (a) Linear element and (b) Quadratic element (Ref: ABAQUS (2005) version 6.5)

2.9 Solid Element Formulation

All the solid elements in ABAQUS allow for finite strain and rotation in large-displacement analysis. For kinematically linear analysis the strain is defined as

$$\varepsilon = sym\left(\frac{\partial u}{\partial X}\right) \tag{2.46}$$

where u is the total displacement;

X is the spatial position of the point under consideration.

This measure of strain is useful only if the strains and rotations are small (all components of the strain and rotation matrices are negligible compared to unity). For cases where the strains and/or rotations are no longer small, two ways of measuring strain are used in the solid elements. When the hyperelastic or hyperfoam material definition is used with an element, ABAQUS internally uses the stretch values calculated directly from the deformation gradient matrix, $\mathbf{F}$, to compute the material behavior. With any other material behavior it is assumed that any elastic strains are small compared to unity, so the appropriate reference configuration for the elasticity is only infinitesimally different from the current configuration and the appropriate stress measure is, therefore, the Cauchy ("true") stress. (More precisely, the appropriate stress measure should be the Kirchhoff stress defined with respect to the elastic reference configuration, but the assumption that this reference configuration and the current configuration are only infinitesimally different makes the Kirchhoff and Cauchy stress measures almost the same: the differences are on the order of the elastic strains

compared to unity). The conjugate strain rate to Cauchy stress is the rate of deformation,

$$D = sym\left(\frac{\partial v}{\partial X}\right) \tag{2.47}$$

where v is the velocity at a point;

X is the spatial position of the point under consideration.

The strain is, therefore, defined as the integral of the rate of deformation. This integration is nontrivial, particularly in the general case where the principal axes of strain rotate during the deformation. The total strain is constructed by integrating the strain rate approximately over the increment by the central difference algorithm; and, when the strain components are referred to a fixed coordinate basis, the strain at the start of the increment must also be rotated to account for the rigid body rotation that occurs in the increment. This is also done approximately, using the Hughes-Winget (1980) method. This integration algorithm defines the integration of a tensor associated with the material behavior as

$$a_{t+\Delta t} = \Delta R \cdot a_t \cdot \Delta R^T + \Delta a(\Delta D) \tag{2.48}$$

where a is the tensor; Δa is the increment in the tensor associated with the material's constitutive behavior, and, therefore, dependent on the strain increment, ΔD, defined by the central difference formula as

$$\Delta D = sym\left(\frac{\partial \Delta u}{\partial x_{t+\Delta t/2}}\right) \tag{2.49}$$

where $x_{t+\Delta t/2} = (1/2)(x_t + x_{t+\Delta t})$; and ΔR is the increment in rotation, defined by Hughes and Winget as

$$\Delta R = \left(I - \frac{1}{2}\Delta W \right)^{-1} \cdot \left(I + \frac{1}{2}\Delta W \right) \tag{2.50}$$

where ΔW is the central difference integration of the rate of spin:

$$\Delta W = asym\left(\frac{\partial \Delta u}{\partial x_{t+\Delta t/2}} \right) \tag{2.51}$$

The contribution of the internal work terms to the Jacobian of the Newton method that is often used in ABAQUS/Standard, in tensor notation, is

$$\int_V (d\sigma : \delta D + \sigma : d\delta D) dV \tag{2.52}$$

where σ and $d\sigma$ are evaluated at the end of the increment.

By using the integration definition above, it can be shown that

$$d\sigma_{t+\Delta t} = d\Delta R \cdot \Delta R^T \cdot (\sigma_{t+\Delta t} - C : \Delta D) + (\sigma_{t+\Delta t} - C : \Delta D) \cdot \Delta R \cdot d\Delta R^T + C : d\Delta D \tag{2.53}$$

where C is the Jacobian matrix of the constitutive model:

$$C = \frac{\partial d\sigma}{\partial d\Delta D} \tag{2.54}$$

However, rather than computing the tangent matrix for the Newton method on this basis, we approximate this by using

$$d\sigma_{t+\Delta t} = dW \cdot \sigma_{t+\Delta t} + \sigma_{t+\Delta t} \cdot dW^T + C : dD \tag{2.55}$$

which yields the Jacobian

$$\int_V \left(\delta D : C : dD - \frac{1}{2}\sigma : \delta \left(2D \cdot D - \frac{\partial v^T}{\partial x} \cdot \frac{\partial v}{\partial x} \right) \right) dV \qquad (2.56)$$

This Jacobian is the tangent stiffness of the rate form of the problem. Experience with practical cases suggests that this approximation provides an acceptable rate of convergence in the Newton iterations in most applications with real materials.

2.10 Triangular, Tetrahedral, and Wedge Elements

Solid elements in ABAQUS include first- and second-order triangles, tetrahedra, and wedge elements for three-dimensional analysis. Second-order tetrahedra are not suitable for the analysis of contact problems: a constant pressure on an element face produces zero equivalent loads at the corner nodes. In contact problems this makes the contact condition at the corners indeterminate, with failure of the solution likely because of excessive gap chatter. The same argument holds true for contact on triangular faces of a wedge element.

2.10.1. Interpolation

The interpolation is defined in terms of the element coordinates g, h and r shown in Figure 2.8. Since ABAQUS is a Lagrangian code for most applications, these are also material coordinates. They each span a range from 0 to 1 in an element but satisfy the constraint that $g + h \le 1.0$ for triangles and wedges and $g + h + r \le 1.0$ for tetrahedra. The node numbering convention used in ABAQUS for these elements is also shown in Figure 2.8. Corner nodes are numbered first, and then the midside nodes for second-order elements. The interpolation functions are as follows.

First-order triangle (3 nodes):

$$u = (1-g-h)u_1 + gu_2 + hu_3 \tag{2.57}$$

Second-order triangle (6 nodes):

$$u = 2\left(\frac{1}{2}-g-h\right)(1-g-h)u_1 + 2g\left(g-\frac{1}{2}\right)u_2 + 2h\left(h-\frac{1}{2}\right)u_3$$
$$+ 4g(1-g-h)u_4 + 4ghu_5 + 4h(1-g-h)u_6 \tag{2.58}$$

First-order tetrahedron (4 nodes):

$$u = (1-g-h-r)u_1 + gu_2 + hu_3 + ru_4 \tag{2.59}$$

Second-order tetrahedron (10 nodes):

$$u = (2(1-g-h-r)-1)(1-g-h-r)u_1 + (2g-1)gu_2 + (2h-1)hu_3$$
$$+ (2r-1)ru_4 + 4(1-g-h-r)gu_5 + 4ghu_6 + 4(1-g-h-r)hu_7 \tag{2.60}$$
$$+ 4(1-g-h-r)ru_8 + 4gru_9 + 4hru_{10}$$

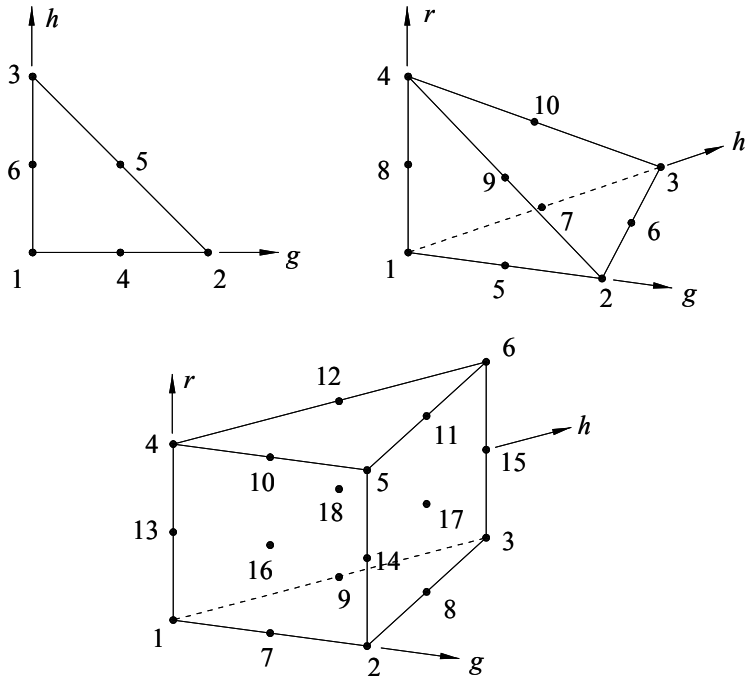

Figure 2.8 Isoparametric Master Elements

First-order wedge (6 nodes):

$$u = \frac{1}{2}(1-g-h)(1-r)u_1 + \frac{1}{2}g(1-r)u_2 + \frac{1}{2}h(1-r)u_3$$
$$+ \frac{1}{2}(1-g-h)(1+r)u_4 + \frac{1}{2}g(1+r)u_5 + \frac{1}{2}h(1+r)u_6 \qquad (2.61)$$

Second-order wedge (15 nodes):

$$u = \frac{1}{2}\left((1-g-h)(2(1-g-h)-1)(1-r) - (1-g-h)\left(1-r^2\right)\right)u_1$$
$$+ \frac{1}{2}\left(g(2g-1)(1-r) - g\left(1-r^2\right)\right)u_2 + \frac{1}{2}\left(h(2h-1)(1-r) - h\left(1-r^2\right)\right)u_3$$
$$+ \frac{1}{2}\left((1-g-h)(2(1-g-h)-1)(1+r) - (1-g-h)\left(1-r^2\right)\right)u_4$$
$$+ \frac{1}{2}\left(g(2g-1)(1+r) - g\left(1-r^2\right)\right)u_5 + \frac{1}{2}\left(h(2h-1)(1+r) - h\left(1-r^2\right)\right)u_6 \qquad (2.62)$$
$$+ 2(1-g-h)g(1-r)u_7 + 2gh(1-r)u_8 + 2h(1-g-h)(1-r)u_9$$
$$+ 2(1-g-h)g(1+r)u_{10} + 2gh(1+r)u_{11} + 2h(1-g-h)(1+r)u_{12}$$
$$+ (1-g-h)\left(1-r^2\right)u_{13} + g\left(1-r^2\right)u_{14} + h\left(1-r^2\right)u_{15}$$

Second-order variable 15–18 node wedge (assuming all 18 nodes are defined):

$$u = \left(\frac{1}{2}\left((1-g-h)(2(1-g-h)-1)(1-r) - (1-g-h)\left(1-r^2\right)\right) + \frac{1}{4}\left(N_{16}+N_{18}\right)\right)u_1$$
$$+ \left(\frac{1}{2}\left(g(2g-1)(1-r) - g\left(1-r^2\right)\right) + \frac{1}{4}\left(N_{16}+N_{17}\right)\right)u_2$$
$$+ \left(\frac{1}{2}\left(h(2h-1)(1-r) - h\left(1-r^2\right)\right) + \frac{1}{4}\left(N_{17}+N_{18}\right)\right)u_3$$
$$+ \left(\frac{1}{2}\left((1-g-h)(2(1-g-h)-1)(1+r) - (1-g-h)\left(1-r^2\right)\right) + \frac{1}{4}\left(N_{16}+N_{18}\right)\right)u_4$$

$$+\left(\frac{1}{2}\left(g\left(2g-1\right)\left(1+r\right)-g\left(1-r^2\right)\right)+\frac{1}{4}\left(N_{16}+N_{17}\right)\right)u_5$$

$$+\left(\frac{1}{2}\left(h\left(2h-1\right)\left(1+r\right)-h\left(1-r^2\right)\right)+\frac{1}{4}\left(N_{17}+N_{18}\right)\right)u_6 \tag{2.63}$$

$$+\left(2\left(1-g-h\right)g\left(1-r\right)-\frac{1}{2}N_{16}\right)u_7+\left(2gh\left(1-r\right)-\frac{1}{2}N_{17}\right)u_8$$

$$+\left(2h\left(1-g-h\right)\left(1-r\right)-\frac{1}{2}N_{16}\right)u_9+\left(2\left(1-g-h\right)g\left(1+r\right)+\frac{1}{2}N_{16}\right)u_{10}$$

$$+\left(2gh\left(1+r\right)+\frac{1}{2}N_{17}\right)u_{11}+\left(2h\left(1-g-h\right)\left(1+r\right)+\frac{1}{2}N_{18}\right)u_{12}$$

$$+\left(\left(1-g-h\right)\left(1-r^2\right)-\frac{1}{2}\left(N_{16}+N_{18}\right)\right)u_{13}+\left(g\left(1-r^2\right)-\frac{1}{2}\left(N_{16}+N_{17}\right)\right)u_{14}$$

$$+\left(h\left(1-r^2\right)-\frac{1}{2}\left(N_{17}+N_{18}\right)\right)u_{15}+N_{16}u_{16}+N_{17}u_{17}+N_{18}u_{18}$$

where

$$N_{16}=4g\left(1-g-h\right)\left(1-r^2\right)$$

$$N_{17}=4gh\left(1-r^2\right)$$

$$N_{18}=4h\left(1-g-h\right)\left(1-r^2\right)$$

2.10.2. Integration

The first-order triangle and tetrahedron are constant stress elements and use a single integration point for the stiffness calculation when used in stress/displacement applications. A lumped mass matrix is used for both elements, with the total mass divided equally over the nodes. For heat transfer applications a three-point integration scheme is used for the conductivity and heat capacity matrices of the first-order triangle,

with the integration points midway between the vertices and the centroid of the element; and a four-point integration scheme is used for the first-order tetrahedron. Distributed loads are integrated with two and three points for first-order triangles and tetrahedrons, respectively.

The three-point scheme is also used for the stiffness of the second-order triangle when it is used in stress/displacement applications. The mass matrix is integrated with a six-point scheme that integrates fourth-order polynomials exactly. Distributed loads are integrated using three points. The heat transfer versions of the element use the six-point scheme for the conductivity and heat capacity matrices.

For stress/displacement applications the second-order tetrahedron uses 4 integration points for its stiffness matrix and 15 integration points for its consistent mass matrix. For heat transfer applications the conductivity and heat capacity matrices are integrated using 15 integration points. The first-order wedge uses 2 integration points for its stiffness matrix but 6 integration points for its lumped mass matrix. The second-order wedge uses 9 integration points for its stiffness matrix but 18 integration points for its consistent mass matrix.

2.11 Contact Modeling

Contact simulations in pipe-soil model were surface based. Surfaces, involved in contact were created on the various components in the model. Then, the pairs of surfaces that contacted each other, known as contact pairs, must be identified. Also, the

constitutive models governing the interactions between the various surfaces must be defined. Friction behaviors were included in these surface interactions.

Since it is possible that there is a relative slide between the regions between each soil layer or between pipe and soil, nonlinear contact elements were used to model the contact between the mentioned regions. When surfaces were in contact, they usually transmitted shear as well as normal forces across their interface. Thus, frictional forces, which resist the relative sliding of the surfaces, were taken into account. Coulomb friction was a common friction model used to describe the interaction of contacting surfaces. The model characterized the frictional behavior between the surfaces using a friction coefficient, μ of 0.5, according to the following equation:

$$\tau = \mu N \tag{2.64}$$

where μ is the coefficient of friction;

N is the contact pressure between the two surfaces.

This equation gives the limiting frictional shear stress for the contacting surfaces. The contacting surfaces will not slip (slide relative to each other) until the shear stress across their interface equals the limiting frictional shear stress, μN .

2.12 Typical Finite Element Results

The output database files in ABAQUS were read by the visualization module to create contour plots, animations, X-Y plots, and tabular output of the results. In this section, the results of pipe-soil model are shown graphically via the deflection shape and stress contour.

2.12.1. Deflection Shape

After loaded by buried backfill soils, the pipe wall vertically deformed in downward direction and horizontally deformed in lateral direction as shown in Figure 2.9. The vertical deflection, maximum at crown, was resulted by the gravity weight of backfill soils which was directly concentrated to the vertical center line of the pipe. Simultaneously, the Poisson effect induced the lateral deflection in the pipe wall, maximum at springline.

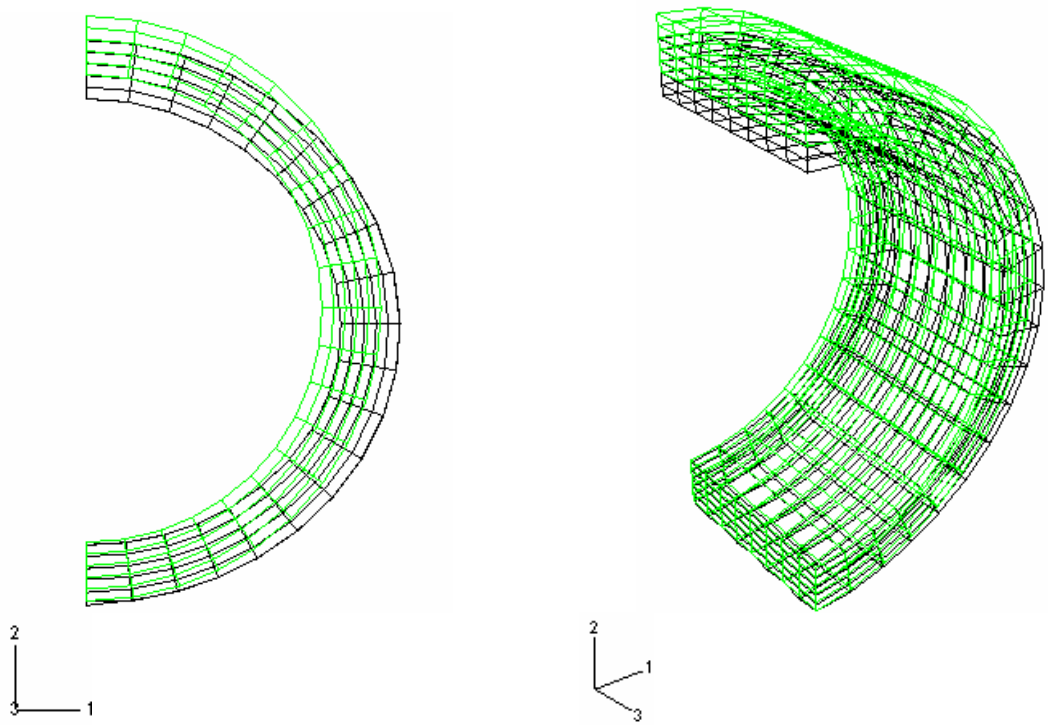

(a) (b)

Figure 2.9 Typical deflection shape of the pipe wall; (a) In plane 1-2 and (b) In 3-dimension view (The green lines show the original shape, and the black lines show the deformed shape)

2.12.2. Stress Contour

The stress contours shown in Figure 2.10 are the combined effects of moment and thrust in the pipe wall. Three locations of critical stress in the pipe wall were studied: at invert, crown, and springline. The sections of maximum stress with tension at the inside and compression at the outside of the pipe occurred at the invert and crown of the pipe as shown in Figure 2.10(a). Also, the sections of maximum stress with tension at the outside and compression at the inside of the pipe occurred at springline as shown in Figure 2.10(b). However, because of the pipe-soil interaction system, the surrounding soil has a great effect on the distribution of these stresses in the pipe wall.

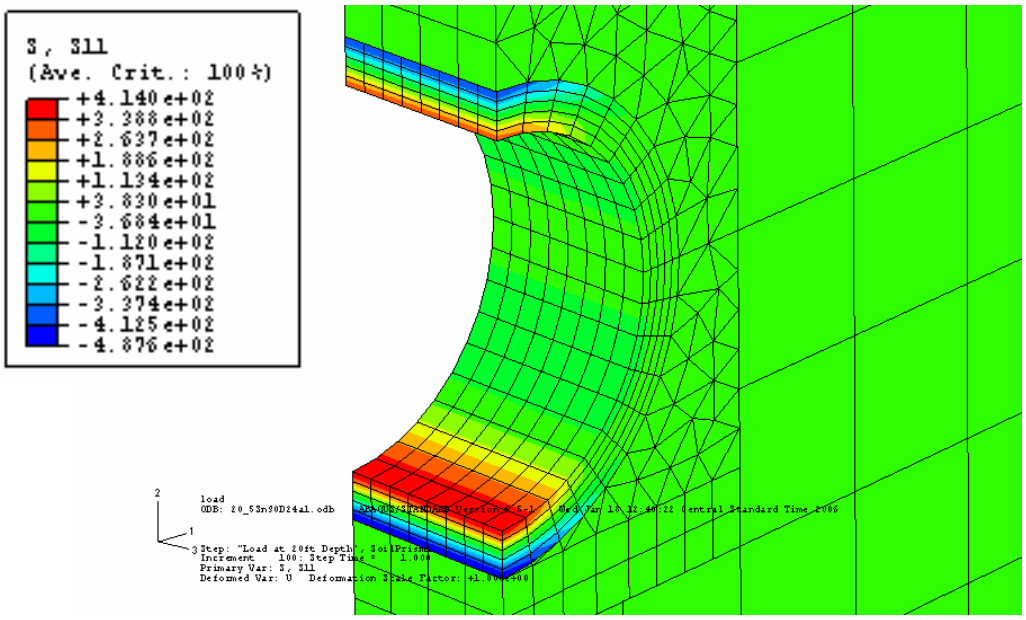

(a)

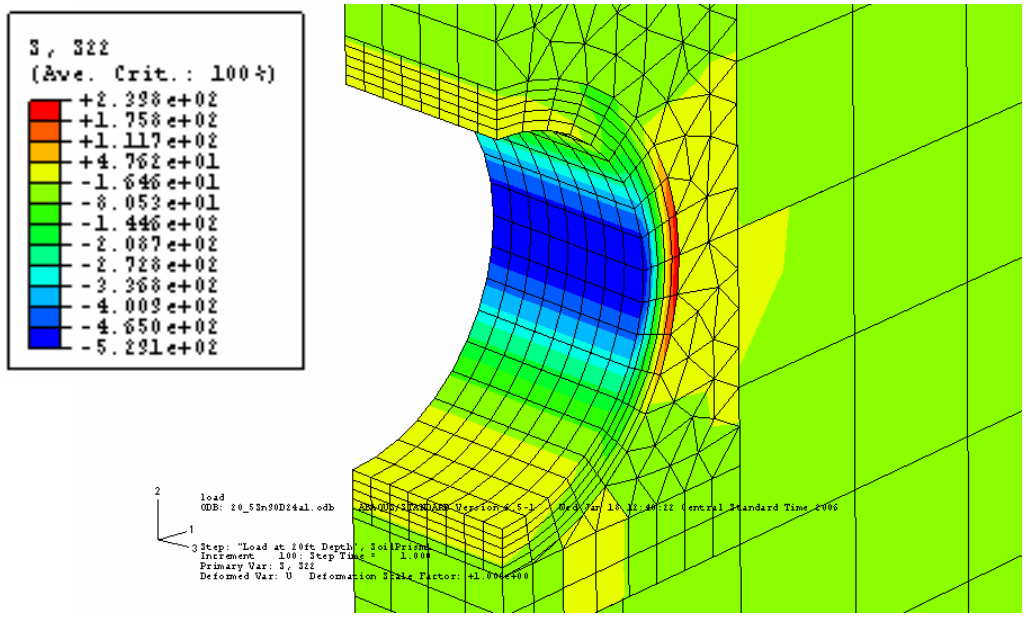

(b)

Figure 2.10 Typical stress contour in the pipe wall; (a) Hoop stresses at invert and crown and (b) Hoop stresses at springline

CHAPTER 3

PARAMETRIC STUDY

3.1 Introduction

A parametric study is conducted to study the effects of parameters relating to the behavior of pipe-soil interaction. These parameters include with the dimension of model, interaction between surfaces, backfill depth, bedding thickness, and material. The resulting stresses are considered at the invert, crown, and springline of the pipe.

3.2 The effect of model length

The different values of model length in longitudinal axis of the pipe were created for studying the effect of model length on the stress and deflection results. The model length was varied at 1 in (2.5 cm), 12 in (30 cm), and 72 in (180 cm) as shown in Figure 3.1.

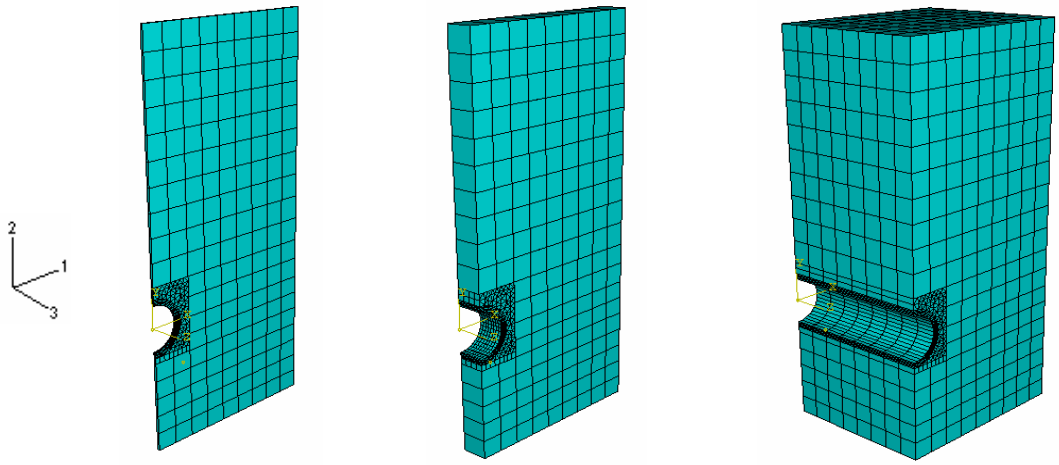

(a) (b) (c)

Figure 3.1 The variation of the pipe lengths in the FEM model; (a) 1in-length model, (b) 12in-length model, and (c) 72in-length model

Furthermore, the consistency of soil in this longitudinal direction was continuous as in reality. Thus, the boundary condition of FEM model in longitudinal (3-direction) was modeled with and without restraint. The results in Figure 3.2 show the nearly constant values of deflection in percentage when the model length was increased from 12 in (30 cm) to 72 in (180 cm). However, the deflection results remarkably varied at the region of model length from 1 in (2.5 cm) to 12 in (30 cm) when the longitudinal restraint was neglected. The model with the longitudinal restraint yielded the higher deflection. The results in Figure 3.3 show the nearly constant values of tensile stresses when the model length was increased with the values of 1 in (2.5 cm), 12 in (30 cm), and 72 in (180 cm) respectively and the restraint in longitudinal direction was applied.

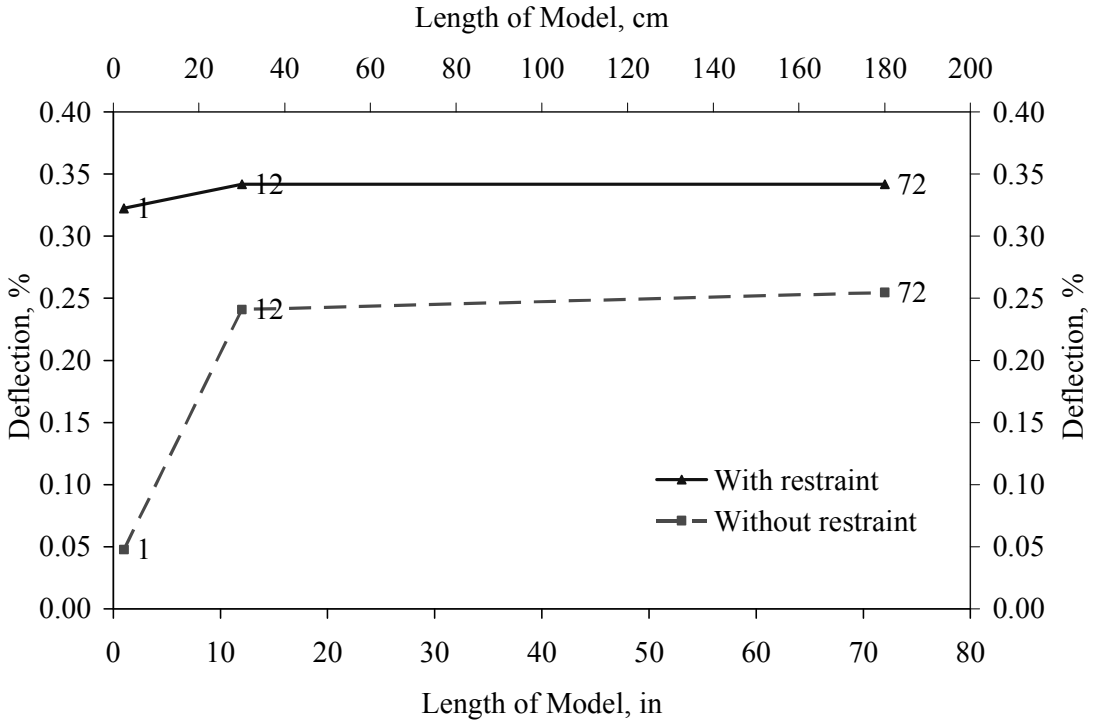

Figure 3.2 % Deflection in the pipe wall with the variation of model lengths

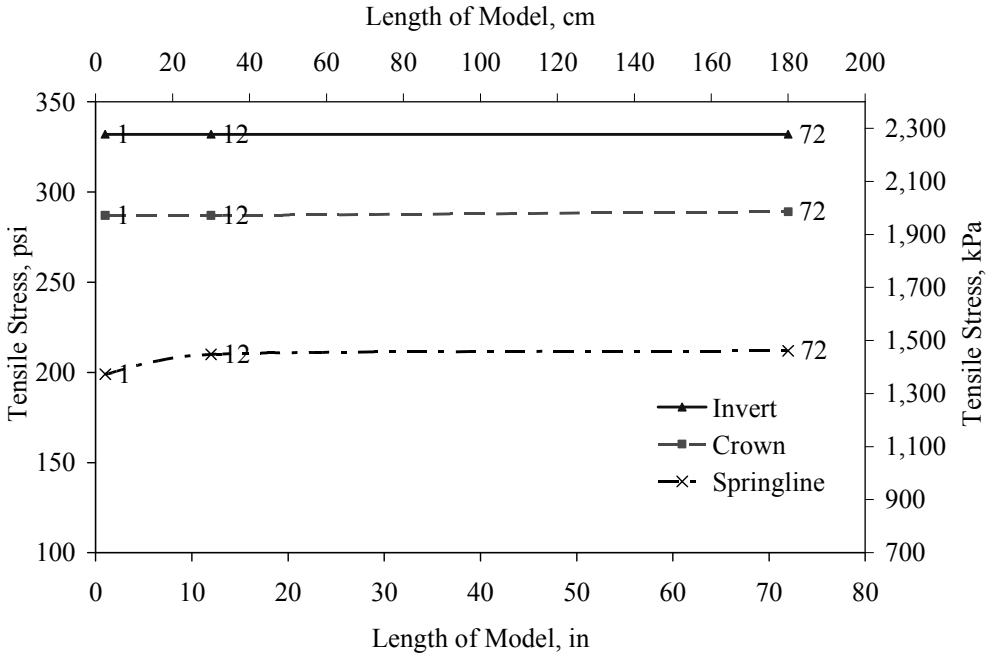

Figure 3.3 Tensile stresses in the pipe wall with the variation of model lengths

3.3 The effect of model width

The width of model relates to soil weight above the pipe and lateral soil supporting the pipe. The boundaries of the soil must be located far enough away from the pipe so as not to remarkably influence the solutions. In this case, lateral boundaries should be restrained with vertical rollers to allow the deformation in vertical direction (2-direction). The study on model width was preceded using the distance of $1D_0$, and $2.5D_0$ from the outside diameter of pipe wall to lateral boundaries, where D_0 is the pipe outside-diameter as shown in Figure 3.4.

The results from $1D_0$ and $2.5D_0$ for lateral boundaries are close together and higher in the model with $2.5D_0$ width as shown in Figure 3.5.

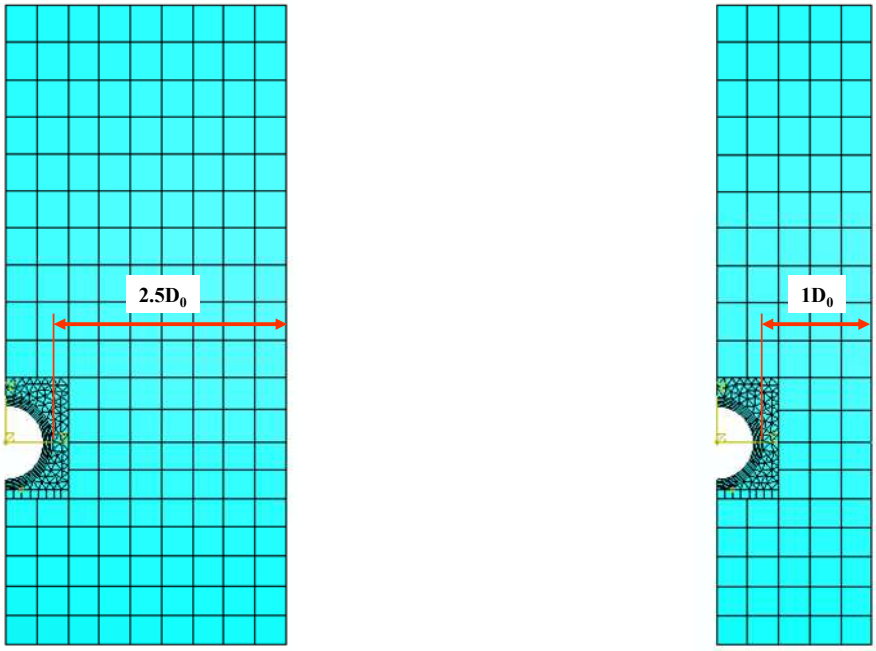

Figure 3.4 The difference in lateral boundaries used for study; (a) Model with $1D_0$ width and (b) Model with $2.5D_0$ width

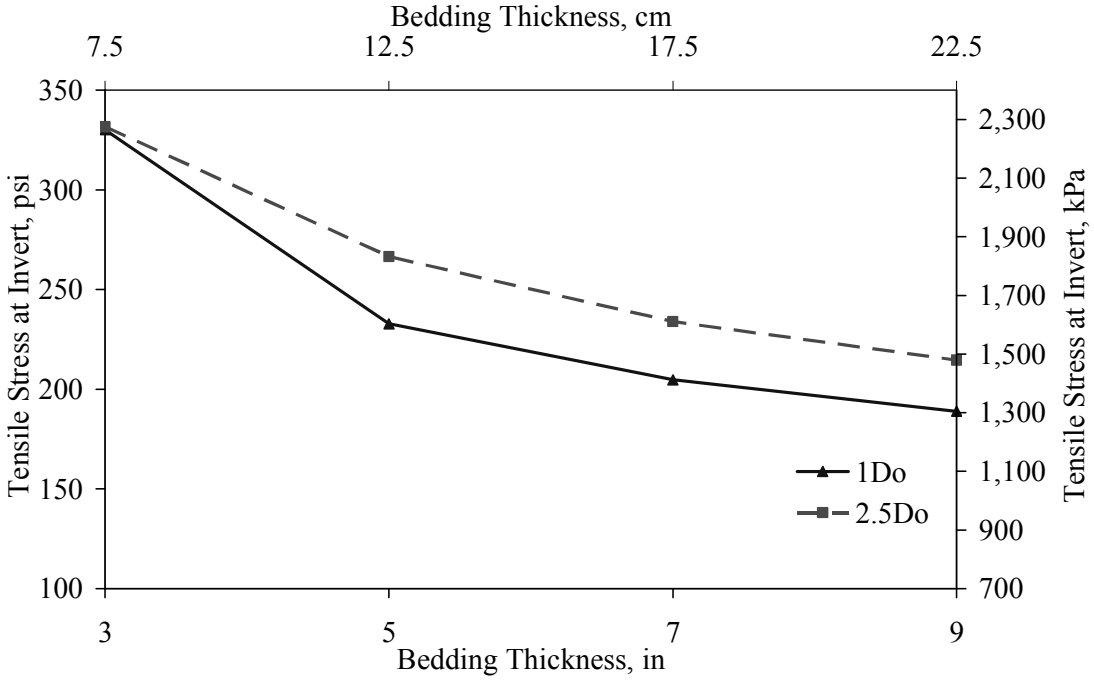

Figure 3.5 Tensile stresses at invert in the pipe wall with the different model width

3.4 The effect of friction

The friction force between each soil zone and between pipe and soils is one of interesting factors effecting on analysis results. By using ABAQUS, the interaction properties of this model were created using both tangential and normal behavior. For the study of interaction process, the values of friction coefficient were varied from 0.1 to 0.9 for the surfaces between pipe and surrounding soils. The results in Figure 3.6 show that the variation in friction coefficient has a small effect on the pipe deflection. Also, The use of 0.5 as friction coefficient is converged.

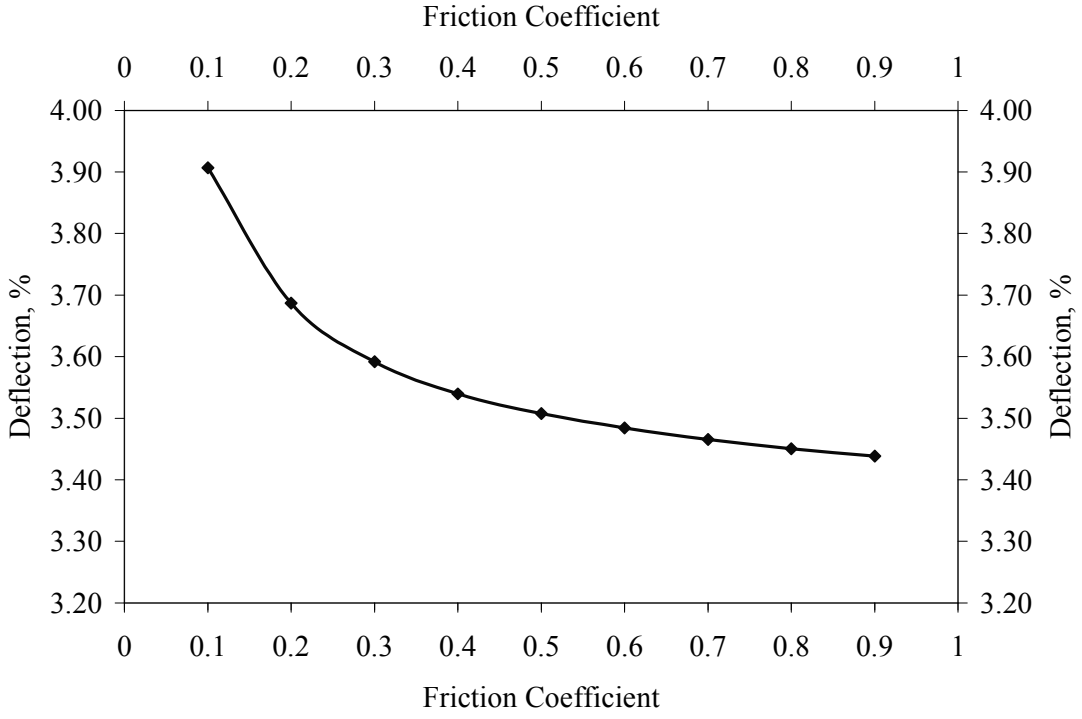

Figure 3.6 The effect of friction coefficient on the deflection of pipe wall

3.5 The parametric study on bedding thicknesses and materials

The parametric study is conducted to study the effects of backfill depths and bedding thicknesses on the tensile stresses at the invert, crown, and springline of pipe wall. Also, the effects of different types of inside bedding materials were studied by varying the soil types and compaction levels. The total cases used in FEM are shown in Table 3.1.

Table 3.1 Total cases in parametric study

Pipe Diameter	24 in. (60 cm.)	60 in. (150 cm.)	84 in. (210 cm.)		
Depth of Backfill	20 ft. (6 m.)	40 ft. (12 m.)	60 ft. (18 m.)	80 ft. (24 m.)	100 ft. (30 m.)
Bedding Thickness	3 in. (7.5 cm.)	5 in. (12.5 cm.)	7 in. (17.5 cm.)	9 in. (22.5 cm.)	
Backfill Material	Sn90				
Inside Bedding Material	Si70	Si90	Sn85	Sn90	
Outside Bedding Material	Sn90				
Lower Side Material	Sn90				
Haunch Material	Sn90				
Void Material	Si50				

The geometric related variables were the pipe and soil zones which compose of in-situ soil, bedding zone, haunch zone, lower side zone, shoulder zone, and backfill soil. The geometric dimensions of soils around the pipe were depended on the pipe outside diameter, D_o as described in section 3.3. These boundaries of soil mesh must be located far enough away from the pipe so as not to appreciably influence the solution. The distance of 2.5 diameters from the center of the pipe was used for lateral boundaries and two diameters below the center of pipe for a bottom boundary.

For the parametric study, the finer elements were used for modeling the pipe and surrounding soils and the coarser elements were used for modeling the soil zones beyond the interesting areas. The converged mesh contained total elements depending on each model case as shown in Table 3.2, 3.3, and 3.4. This converged mesh was used through out the parametric study. The tensile stresses at the invert, crown, and springline of pipe wall in response to backfill depth, bedding material and thickness was the outcome variable for the parametric study.

Table 3.2 Total DOFs, elements, and nodes for 24in pipe-soil model

24in-diameter Pipe				
Bedding Thickness	Backfill Height	Total Number of		
		DOFs	Elements	Nodes
3 in. (7.5 cm.)	20 ft. (6 m.)	17088	1545	2848
	40 ft. (12 m.)	21888	1725	3648
	60 ft. (18 m.)	26688	1905	4448
	80 ft. (24 m.)	31488	2085	5248
	100 ft. (30 m.)	36288	2265	6048
Bedding Thickness	Backfill Height	Total Number of		
		DOFs	Elements	Nodes
5 in. (12.5 cm.)	20 ft. (6 m.)	17418	1577	2903
	40 ft. (12 m.)	22218	1757	3703
	60 ft. (18 m.)	27018	1937	4503
	80 ft. (24 m.)	31818	2117	5303
	100 ft. (30 m.)	36618	2297	6103
Bedding Thickness	Backfill Height	Total Number of		
		DOFs	Elements	Nodes
7 in. (17.5 cm.)	20 ft. (6 m.)	17748	1609	2958
	40 ft. (12 m.)	22548	1789	3758
	60 ft. (18 m.)	27348	1969	4558
	80 ft. (24 m.)	32148	2149	5358
	100 ft. (30 m.)	36948	2329	6158
Bedding Thickness	Backfill Height	Total Number of		
		DOFs	Elements	Nodes
9 in. (22.5 cm.)	20 ft. (6 m.)	18078	1641	3013
	40 ft. (12 m.)	22878	1821	3813
	60 ft. (18 m.)	27678	2001	4613
	80 ft. (24 m.)	32478	2181	5413
	100 ft. (30 m.)	37278	2361	6213

Table 3.3 Total DOFs, elements, and nodes for 60in pipe-soil model

60in-diameter Pipe				
Bedding Thickness	Backfill Height	Total Number of		
		DOFs	Elements	Nodes
3 in. (7.5 cm.)	20 ft. (6 m.)	21276	2100	3546
	40 ft. (12 m.)	26076	2280	4346
	60 ft. (18 m.)	30876	2460	5146
	80 ft. (24 m.)	35676	2640	5946
	100 ft. (30 m.)	40476	2820	6746
Bedding Thickness	Backfill Height	Total Number of		
		DOFs	Elements	Nodes
5 in. (12.5 cm.)	20 ft. (6 m.)	21276	2100	3546
	40 ft. (12 m.)	26076	2280	4346
	60 ft. (18 m.)	30876	2460	5146
	80 ft. (24 m.)	35676	2640	5946
	100 ft. (30 m.)	40476	2820	6746
Bedding Thickness	Backfill Height	Total Number of		
		DOFs	Elements	Nodes
7 in. (17.5 cm.)	20 ft. (6 m.)	21276	2100	3546
	40 ft. (12 m.)	26076	2280	4346
	60 ft. (18 m.)	30876	2460	5146
	80 ft. (24 m.)	35676	2640	5946
	100 ft. (30 m.)	40476	2820	6746
Bedding Thickness	Backfill Height	Total Number of		
		DOFs	Elements	Nodes
9 in. (22.5 cm.)	20 ft. (6 m.)	21276	2100	3546
	40 ft. (12 m.)	26076	2280	4346
	60 ft. (18 m.)	30876	2460	5146
	80 ft. (24 m.)	35676	2640	5946
	100 ft. (30 m.)	40476	2820	6746

Table 3.4 Total DOFs, elements, and nodes for 84in pipe-soil model

84in-diameter Pipe				
Bedding Thickness	Backfill Height	Total Number of		
		DOFs	Elements	Nodes
3 in. (7.5 cm.)	20 ft. (6 m.)	23388	1966	3898
	40 ft. (12 m.)	31068	2266	5178
	60 ft. (18 m.)	38748	2566	6458
	80 ft. (24 m.)	46428	2866	7738
	100 ft. (30 m.)	54108	3166	9018
Bedding Thickness	Backfill Height	Total Number of		
		DOFs	Elements	Nodes
5 in. (12.5 cm.)	20 ft. (6 m.)	23388	1966	3898
	40 ft. (12 m.)	31068	2266	5178
	60 ft. (18 m.)	38748	2566	6458
	80 ft. (24 m.)	46428	2866	7738
	100 ft. (30 m.)	54108	3166	9018
Bedding Thickness	Backfill Height	Total Number of		
		DOFs	Elements	Nodes
7 in. (17.5 cm.)	20 ft. (6 m.)	23388	1966	3898
	40 ft. (12 m.)	31068	2266	5178
	60 ft. (18 m.)	38748	2566	6458
	80 ft. (24 m.)	46428	2866	7738
	100 ft. (30 m.)	54108	3166	9018
Bedding Thickness	Backfill Height	Total Number of		
		DOFs	Elements	Nodes
9 in. (22.5 cm.)	20 ft. (6 m.)	23388	1966	3898
	40 ft. (12 m.)	31068	2266	5178
	60 ft. (18 m.)	38748	2566	6458
	80 ft. (24 m.)	46428	2866	7738
	100 ft. (30 m.)	54108	3166	9018

3.6 Discussion of parametric study

The results of parametric study are divided into three parts related to Figures A.1 through A.28 in Appendix A, and Figure 3.7 in Chapter 3 as follows:

3.6.1. Decrease in tensile stresses versus bedding materials and bedding thicknesses

As shown in Figures A.1 through A.15, the increase in bedding thicknesses and the decrease in the stiffness of bedding materials decrease the resulting tensile stresses at invert, crown, and springline. Especially at the invert, the tensile stresses greatly decrease because the concrete pipe stands on the bedding via the invert zone. Also, the effect of the bedding material is more significant than the effect of the bedding thickness. For an example of 24 in (60 cm) diameter pipe under 20 ft (6 m) backfill soil: the increase in bedding thicknesses from 3 in (7.5 cm) to 9 in (22.5 cm) decreases the tensile stress at invert for 22%, when Sn90 is used for the bedding material. In contrary, when Si70 is used for the bedding material, the tensile stress at invert can be decreased up to 58%. Moreover, as the pipe diameter increases, the effects from the bedding material and the bedding thickness become diminished.

3.6.2. Tensile stresses versus backfill heights

From Figures A.16 through A.27 showing the values of tensile stresses induced in the pipe wall, the maximum tensile stresses occur at the locations of invert and crown. As the backfill heights increase, the tensile stresses at invert, crown, and springline become increased, especially at invert. These tensile stresses reduce with the increase in bedding thicknesses. Additionally, the use of loosed material, Si70, greatly distributes tensile stresses in pipe wall, thus decreasing the peak stress. For an example

of 84 in (210 cm) diameter pipe under 100 ft (30 m) backfill soil: the maximum tensile stress of 2,385 psi (16,445 kPa) when using Sn90 for bedding material can be reduced to 1,790 psi (12,342 kPa) when using Si70 for bedding material. In contrary, the use of compacted material, Sn90, reduce the effect of the bedding thickness. As shown in the case of 84 in (210 cm) diameter pipe under 100 ft (30 m) backfill soil: the increase in bedding thicknesses from 3 in (7.5 cm) to 9 in (22.5 cm) decreases the tensile stresses at invert from 1,790 psi (12,342 kPa) to 1,130 psi (7,791 kPa), when Si70 is used for the bedding material. In contrary, when Sn90 is used for the bedding material, the tensile stress at invert decreased only from 2,385 psi (16,445 kPa) to 2,370 psi (16,341 kPa).

3.6.3. Stress differentials between upper and lower bounds of the bedding thicknesses

Figure 3.7 shows the stress differential between upper and lower bounds of the bedding thicknesses. The bedding thickness of 3 in (7.5 cm) yields the upper bound of the tensile stress results, and the bedding thickness of 9 in (22.5 cm) yields the lower bound of the tensile stress results. As the stiffness and compaction levels of the bedding material increase, the stress differential between upper and lower bounds of bedding thickness decreases. Thus, the stress differential results show that the effect of bedding thickness becomes less significant, when the stiffness and compaction levels of the bedding material increase. The drop in stress differential at invert is maximum for 84-in (210-cm) diameter pipe when the bedding material changes property from Si70 to Si90. This is followed by the next noticeable stress differential reduction at invert for the 60-in (150-cm) diameter pipe. The change in stress reduction at crown and invert is almost similar for different pipe diameters as the bedding changes properties.

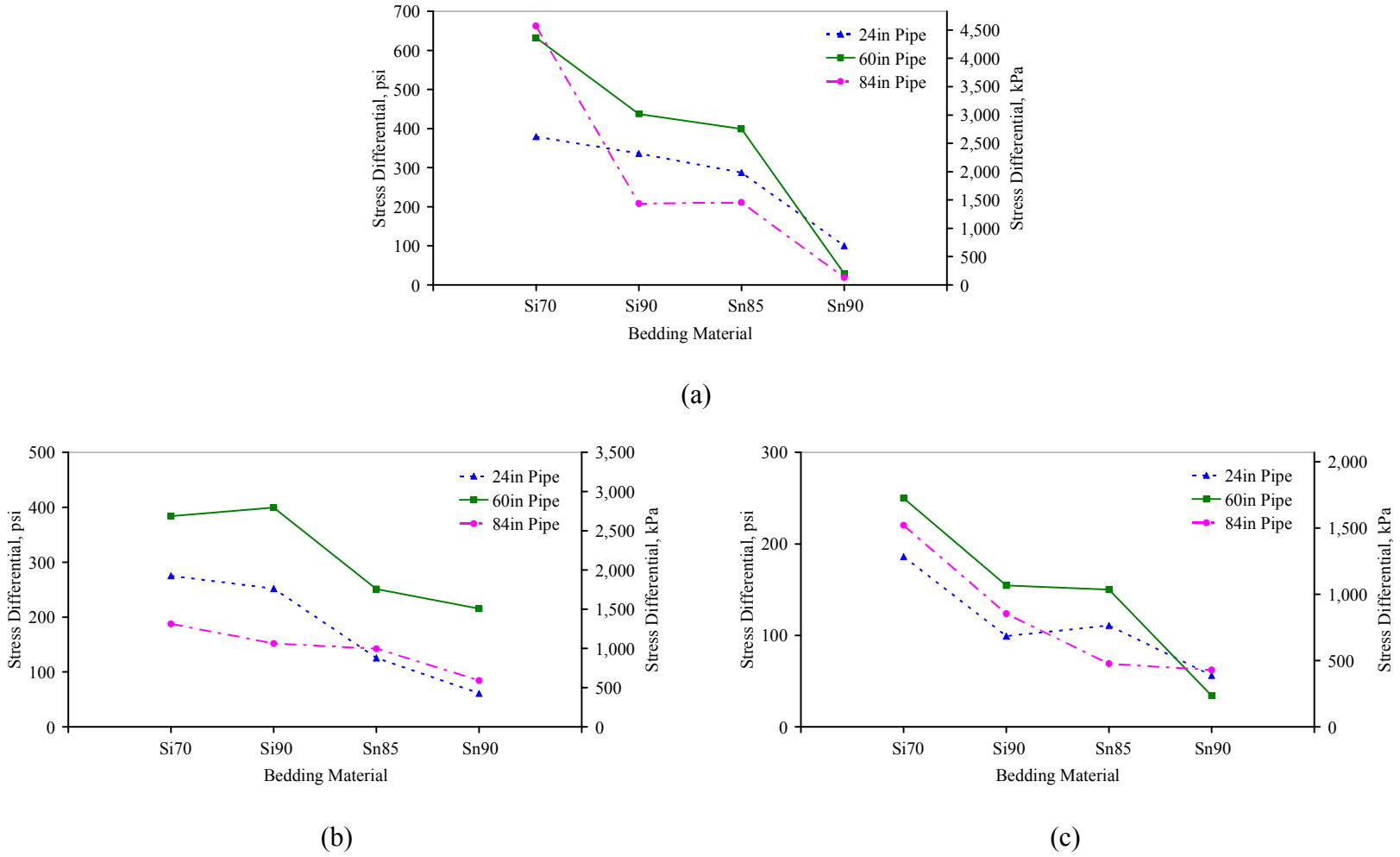

Figure 3.7 Stress differentials between upper and lower bounds of bedding thicknesses;
(a) At invert, (b) At crown, and (c) At springline

CHAPTER 4

SUMMARY, CONCLUSIONS, AND RECOMMENDATIONS

4.1 Summary

In this study, the nonlinear finite element models (FEM) of the pipe-soil interaction were developed using the concept of symmetry. The dimensions of the concrete pipe and corresponding soils around the pipe were created by employing the standard embankment installation, which was the most critical case for underground pipe installations. This standard was introduced by the Concrete Pipe Technology Handbook (2001). Because the pipe-soil structure was symmetric, only one half of the model was used. After several trials, an appropriate converged mesh was carefully selected for the model to represent as the best mesh for the parametric study. The elements used were eight node linear brick for the concrete pipe, bedding, and backfill soil materials. Also, the six noded triangular prism was used for the haunch and shoulder fill located around the pipe. An incremental construction of backfill height was applied to the pipe-soil system to obtain the stresses induced in pipe wall. These stresses were analyzed with different types of bedding material and thickness. Three standard sizes of concrete pipe were considered in this study; 24 in (60 cm) inside diameter (D_i) with 3 in (7.5 cm) wall thickness, 60 in (150 cm) inside diameter (D_i) with 6 in (15 cm) wall thickness, and 84 in (210 cm) inside diameter (D_i) with 8 in (20 cm) wall thickness.

The developed model was analyzed using the incremental geometric nonlinear finite element solution algorithm. The converged solution was obtained using energy-based convergence criteria. Also, to study the interactions between the soil zones and the pipe and soils, contact elements were introduced at the interfaces between the regions. When surfaces were in contact, they transmitted shear as well as normal forces across their interfaces.

A parametric study was conducted to study the effects of force, material, and geometry related variables on the pipe-soil structure. This was done by considering the conditions, usually used in the construction.

The force related variables were increased corresponding to the backfill soil height, buried from 20 ft (6 m) to 100 ft (30 m). These backfill soils acted as prism loads transferring their weight to the pipe.

The material related variables were varied by the types and compaction levels of soil: sandy silt (Si70); sandy silt (Si90); gravelly sand (Sn85); and gravelly sand (Sn90) applied for the inside bedding material. These variables showed the stiffness of soil, effecting on the stress distribution in pipe wall.

The geometric related variables were assessed by using three standard sizes of concrete pipe: 24 in (60 cm); 60 in (150 cm); and 84 in (210 cm) for the pipe inside diameters with the pipe wall thicknesses of 3 in (7.5 cm), 6 in (15 cm), and 8 in (20 cm), respectively. Because the boundaries of soil around the pipe depended on the pipe diameter, the dimensions of overall model were different for each pipe size.

4.2 Conclusions

The conclusion of this study advances in the following forefront:

- As the height of the backfill soil increases, the tensile stresses induced in the pipe wall increase. This demonstrates the effect of incremental construction of the embankment installation. Each layer of backfill soils transfers pressure loads to the pipe via its weight.
- The effects of tensile stresses induced are more predominant at the location of invert than crown and springline of the pipe wall. This is because the pipe is directly supported by the bedding zone at the location of invert. Thus, the tensile stresses are remarkably transferred at this location.
- As the bedding thickness increases, the tensile stresses induced in the pipe wall decrease depending on the properties of the bedding material. The bedding thickness acts as a cushion to support a pipe structure and to dissipate stress especially at pipe invert.
- As the bedding material stiffness and compaction levels decrease, the tensile stresses induced in the pipe wall decrease. The results confirm the fact that the soil with fine materials, called “sandy silt or Si”, and low compaction level can profoundly distribute tensile stresses at the pipe invert, when applying for the inside bedding material. In contrast, the soil with less or no fine materials, called “gravelly sand or Sn” and high compaction level yields the concentrated reaction force at the pipe invert.
- The effects of the bedding thickness and material on induced tensile stresses diminish as the pipe diameter increases. As shown in the results, maximum decreases in

tensile stress are 58%, 54%, and 49% for 24in-diameter pipe, 60in-diameter pipe, and 84in-diameter pipe, respectively. This is because when the same bedding thickness in a smaller diameter pipe is applied to a larger diameter pipe, the difference in the proportions between the bedding thickness and the pipe diameter becomes larger. This means that for a large diameter pipe, the contact area between the pipe surface and the bedding material increases which alleviates the stress concentration and diminishes the pipe stress.

- This study concluded that the effects of the bedding material stiffness and the compaction levels on the induced stresses are more significant than the effect of bedding thickness.
- For normal bedding material generally used by the contractors (Sn85, Sn90, etc.), this study concludes that the effect of bedding thickness (between 3 in (7.5 cm) to 9 in (22.5 cm)) on the pipe stress is minimal and should be ignored.

4.3 Recommendations

The critical parameters for the strength of the concrete pipe are the type and compaction levels of the surrounding soil. The variation of materials used in this study mainly focuses on the bedding zone. However, the existing standard installations do not define the quantitative requirements for other embedment soils around the pipe. Those soil zones beyond the bedding, such as haunch zone and lower side zone, also have major effects on the stress distribution in the pipe. The further study should be extended to incorporate the most effective condition for the pipe-soil installation.

Moreover, some of the traditional standard installations require construction practices to shape the bedding configurations that can not be performed with sufficiently reliable tolerances to assure the uniformity of the support assumed for the installation. These beddings may be shaped to the profile of the bottom of the pipe for some portion of the bottom circumference defined as the bedding angle.

A fully developed FEM model of the pipe-soil installation would have significant data for evaluating the required property of soil, the depth of bedding, and understanding the behavior of pipe-soil interaction. To eliminate the shortcomings of existing analyses and to take advantage of modern knowledge in structural and geotechnical engineering, a variety of special installations that might be more economical and effective should be studied.

Finally, the author strongly recommends that this study to be extended to develop a user friendly software for the use by design engineer. This is due to the fact that the FEM study presented here is more realistic for understanding the pipe-soil behavior than these currently in markets.

APPENDIX A

PARAMETRIC STUDY RESULT PLOTS

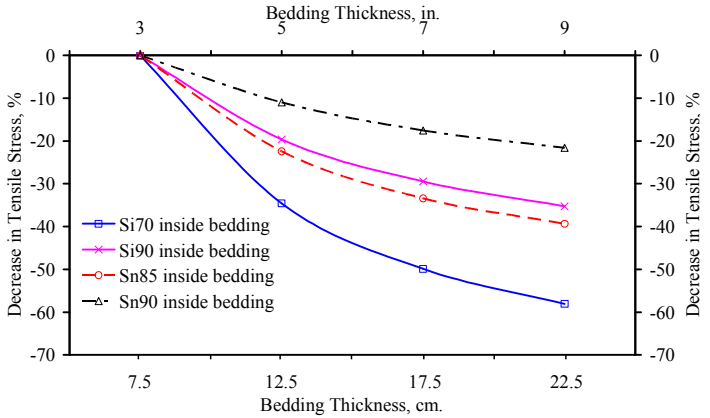

(a)

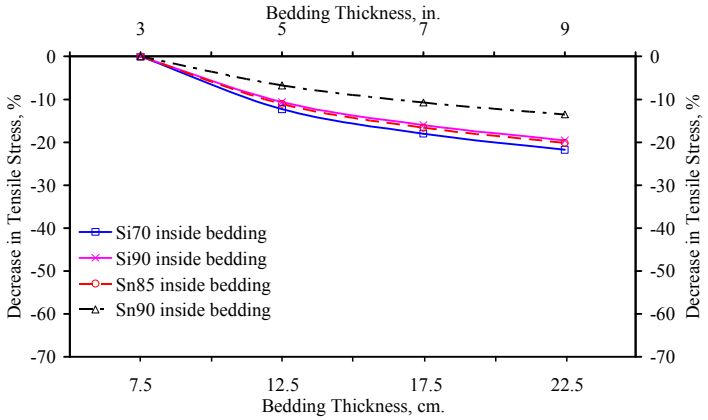

(b)

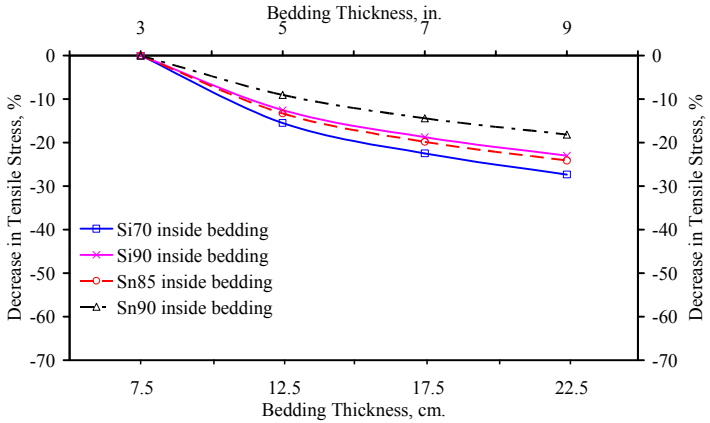

(c)

Figure A.1 Decrease in tensile stresses versus bedding thicknesses for 24in-dia pipe in 20ft-height backfill; (a) At invert, (b) At crown, and (c) At springline

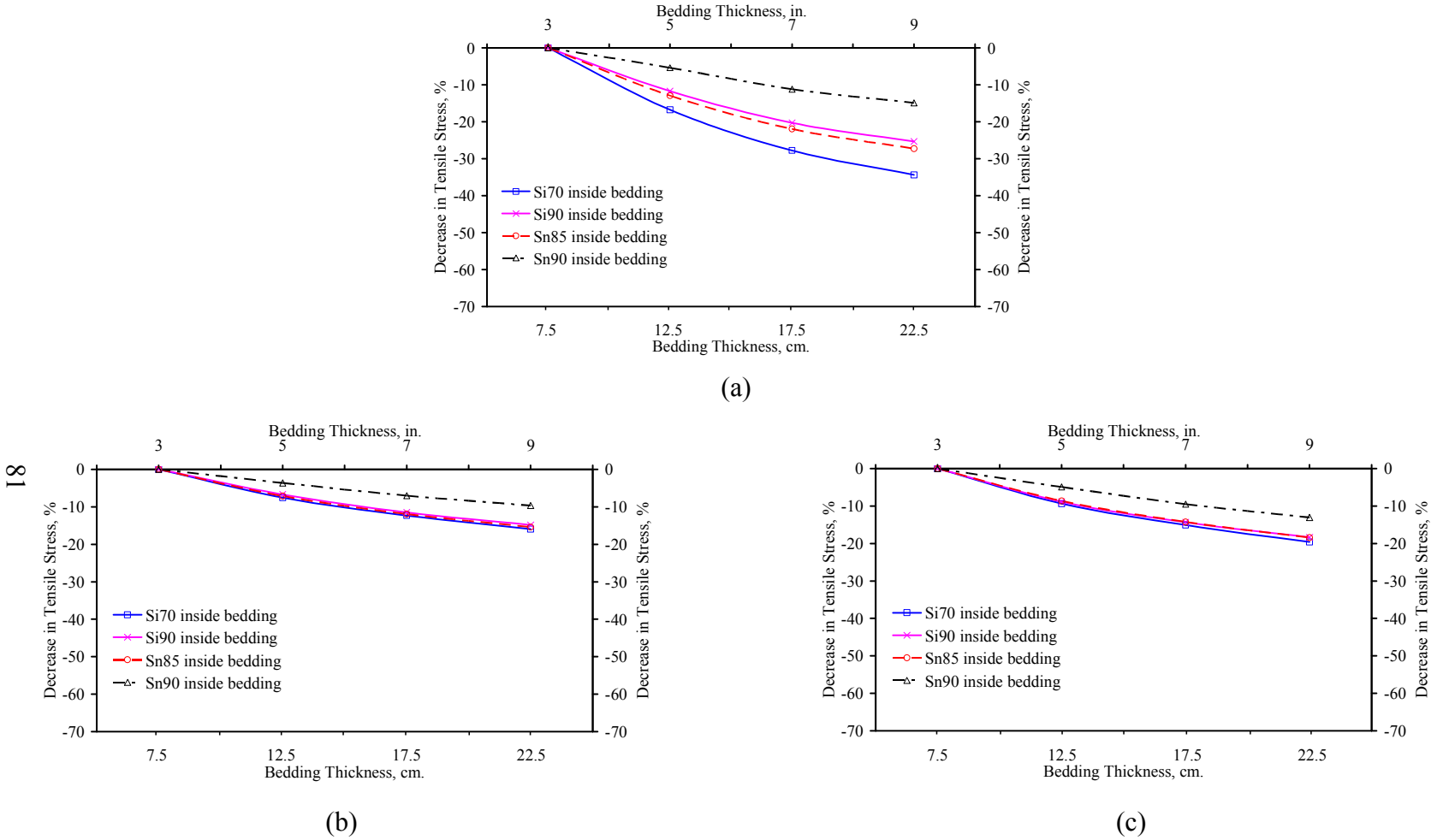

Figure A.2 Decrease in tensile stresses versus bedding thicknesses for 24in-dia pipe in 40ft-height backfill; (a) At invert, (b) At crown, and (c) At springline

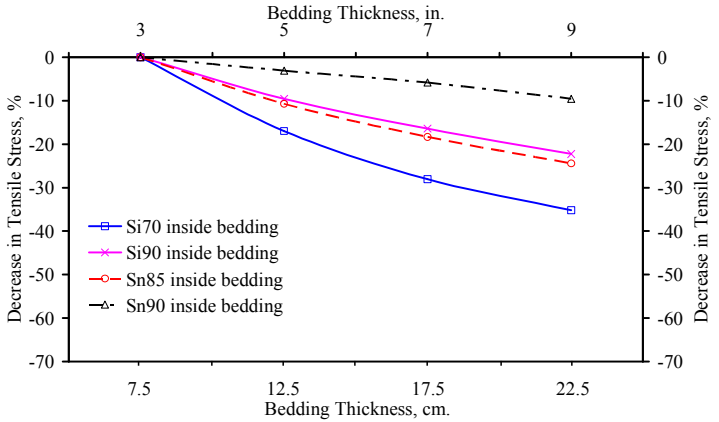

(a)

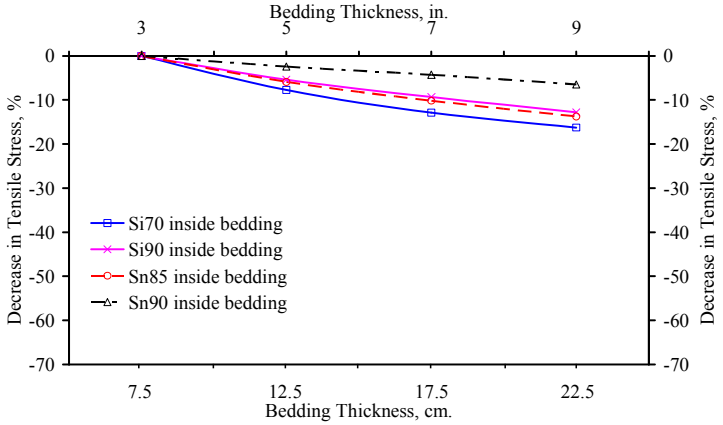

(b)

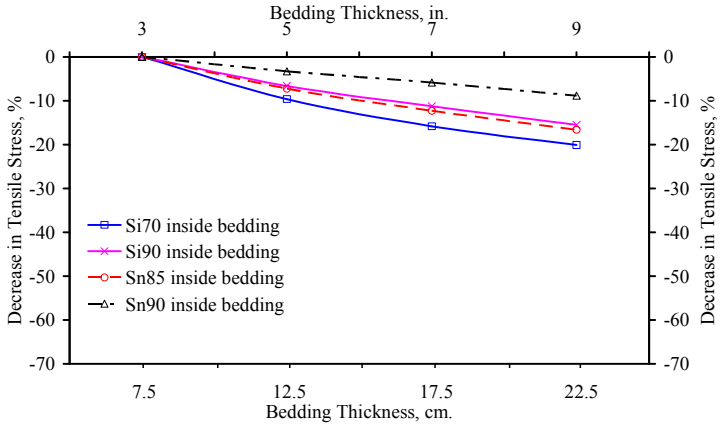

(c)

Figure A.3 Decrease in tensile stresses versus bedding thicknesses for 24in-dia pipe in 60ft-height backfill; (a) At invert, (b) At crown, and (c) At springline

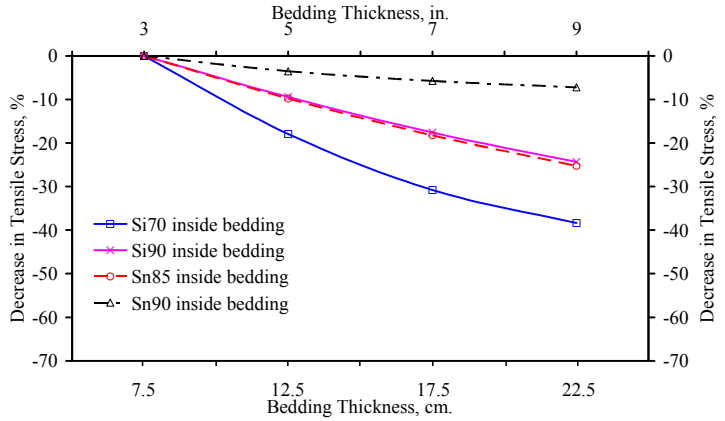

(a)

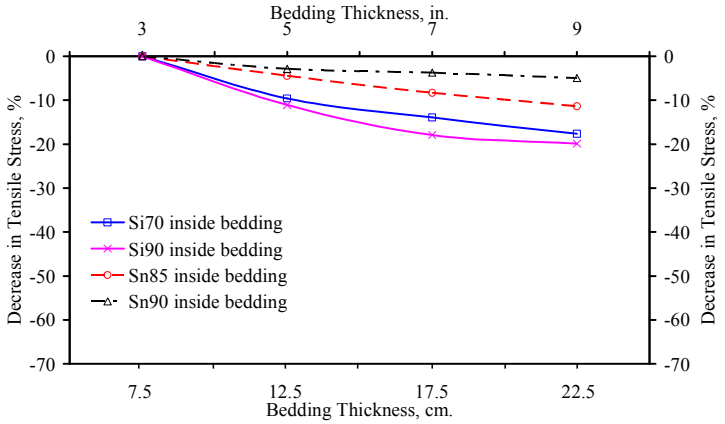

(b)

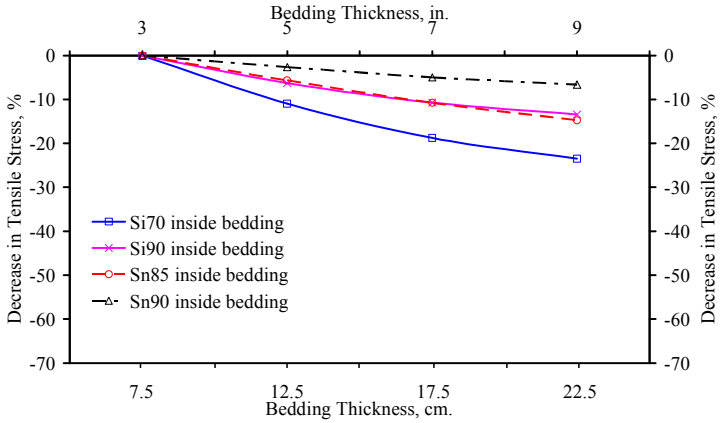

(c)

Figure A.4 Decrease in tensile stresses versus bedding thicknesses for 24in-dia pipe in 80ft-height backfill; (a) At invert, (b) At crown, and (c) At springline

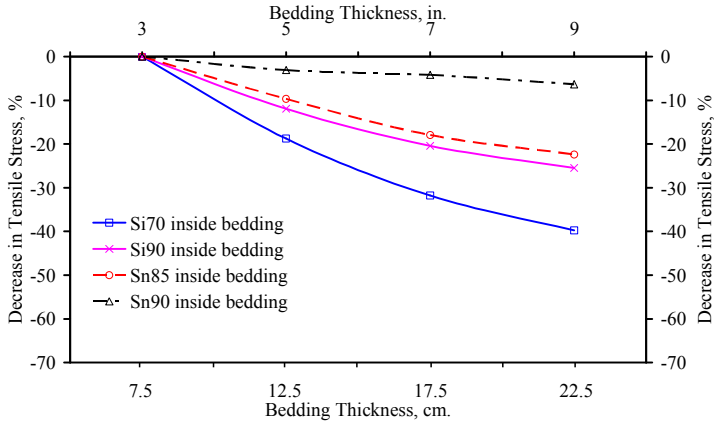

(a)

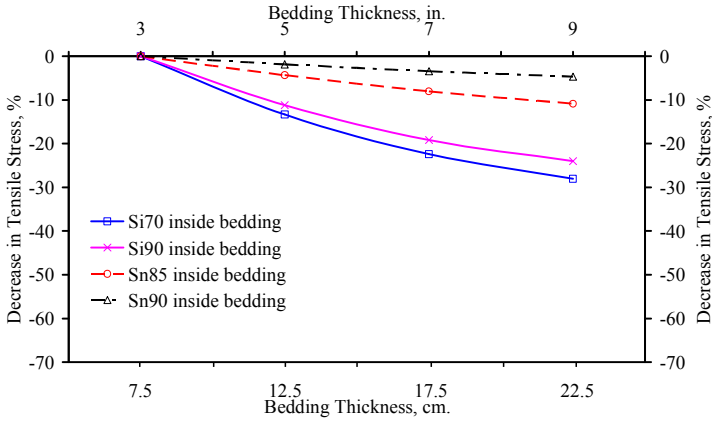

(b)

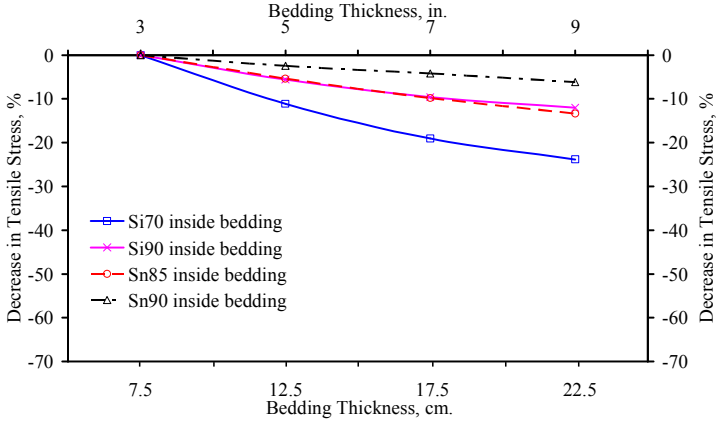

(c)

Figure A.5 Decrease in tensile stresses versus bedding thicknesses for 24in-dia pipe in 100ft-height backfill; (a) At invert, (b) At crown, and (c) At springline

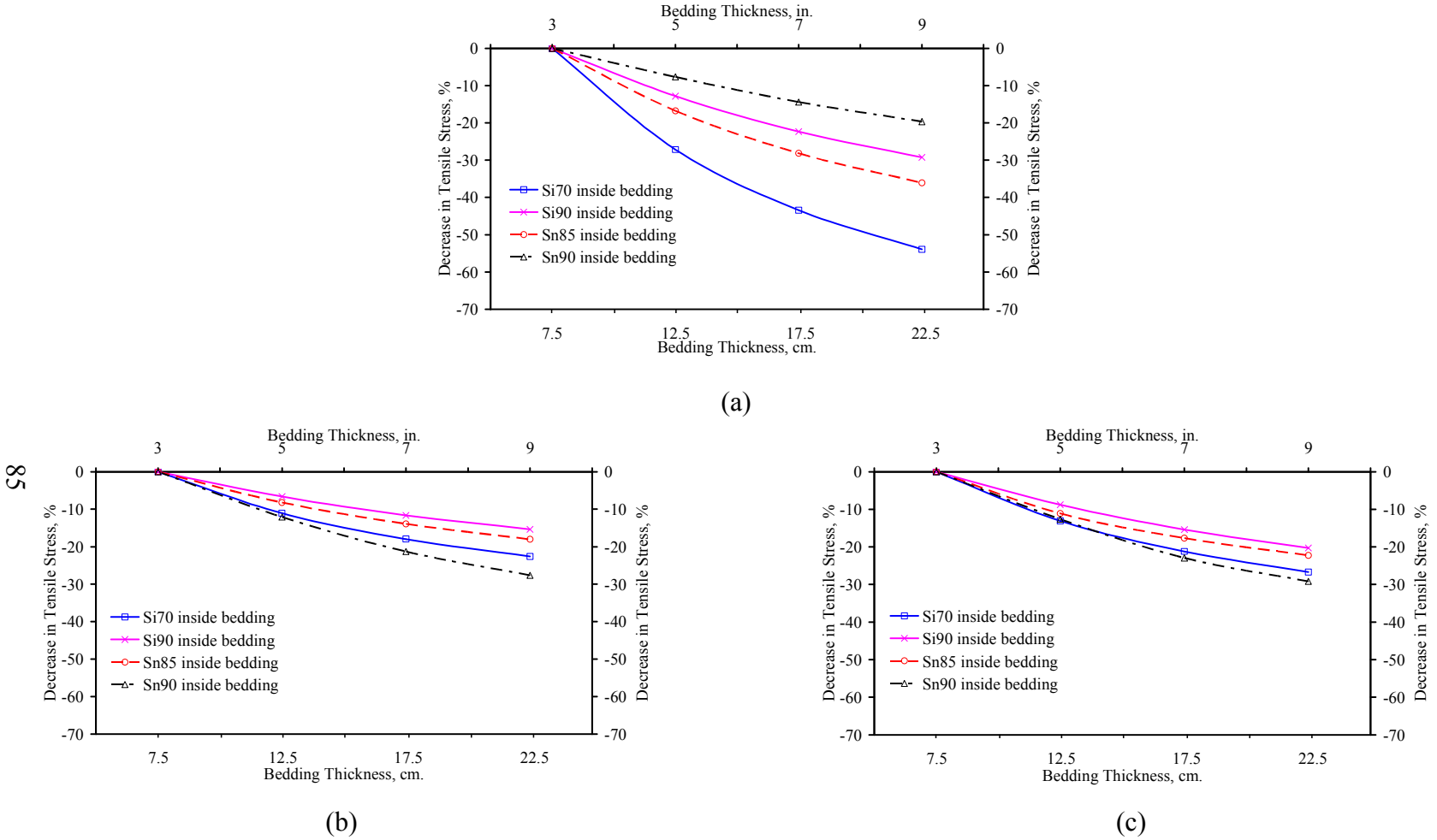

Figure A.6 Decrease in tensile stresses versus bedding thicknesses for 60in-dia pipe in 20ft-height backfill; (a) At invert, (b) At crown, and (c) At springline

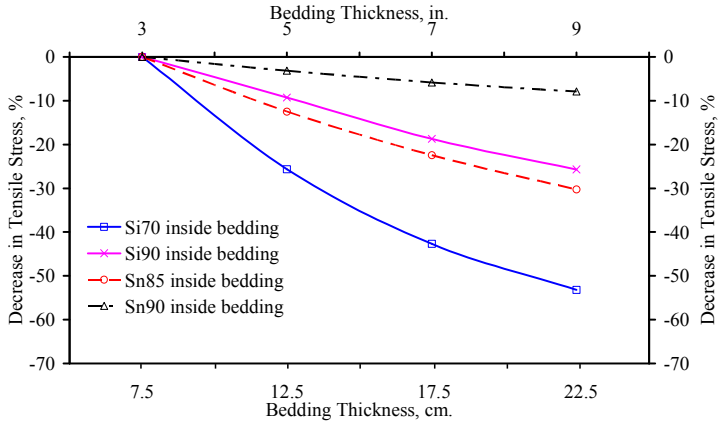

(a)

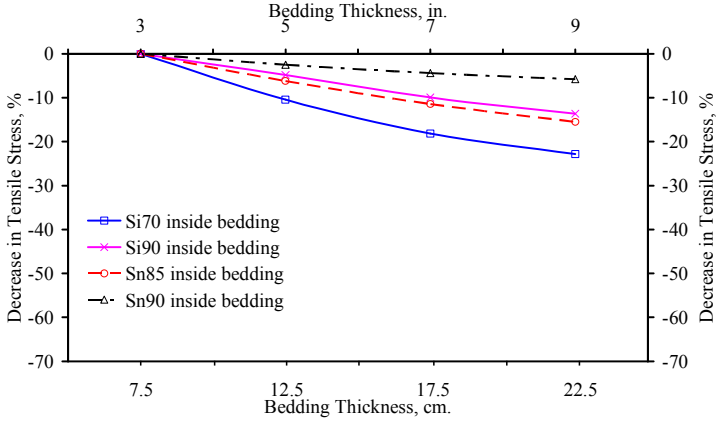

(b)

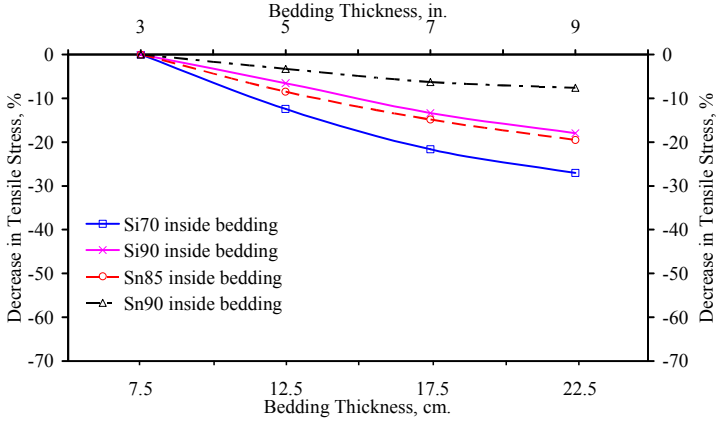

(c)

Figure A.7 Decrease in tensile stresses versus bedding thicknesses for 60in-dia pipe in 40ft-height backfill; (a) At invert, (b) At crown, and (c) At springline

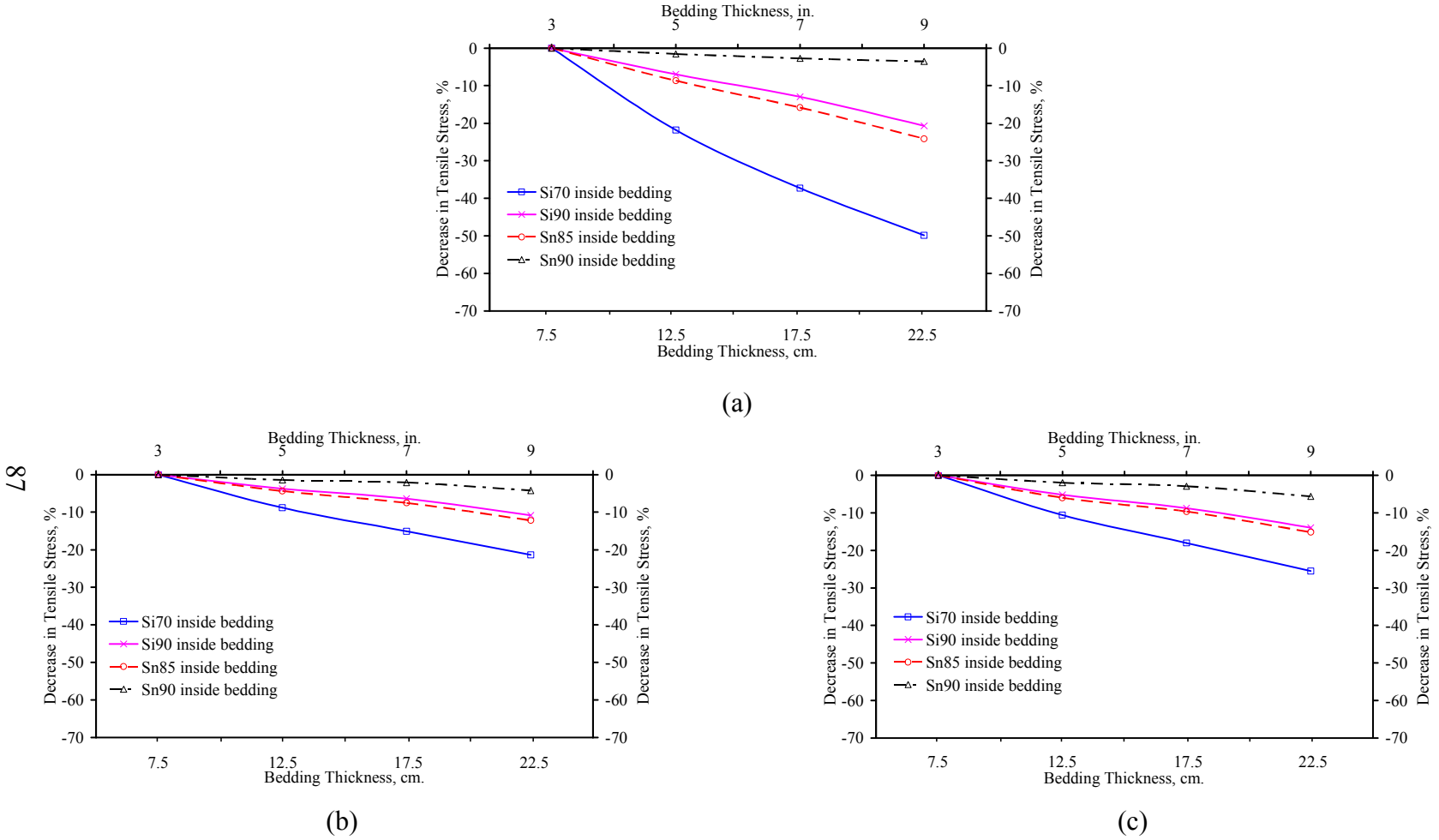

Figure A.8 Decrease in tensile stresses versus bedding thicknesses for 60in-dia pipe in 60ft-height backfill; (a) At invert, (b) At crown, and (c) At springline

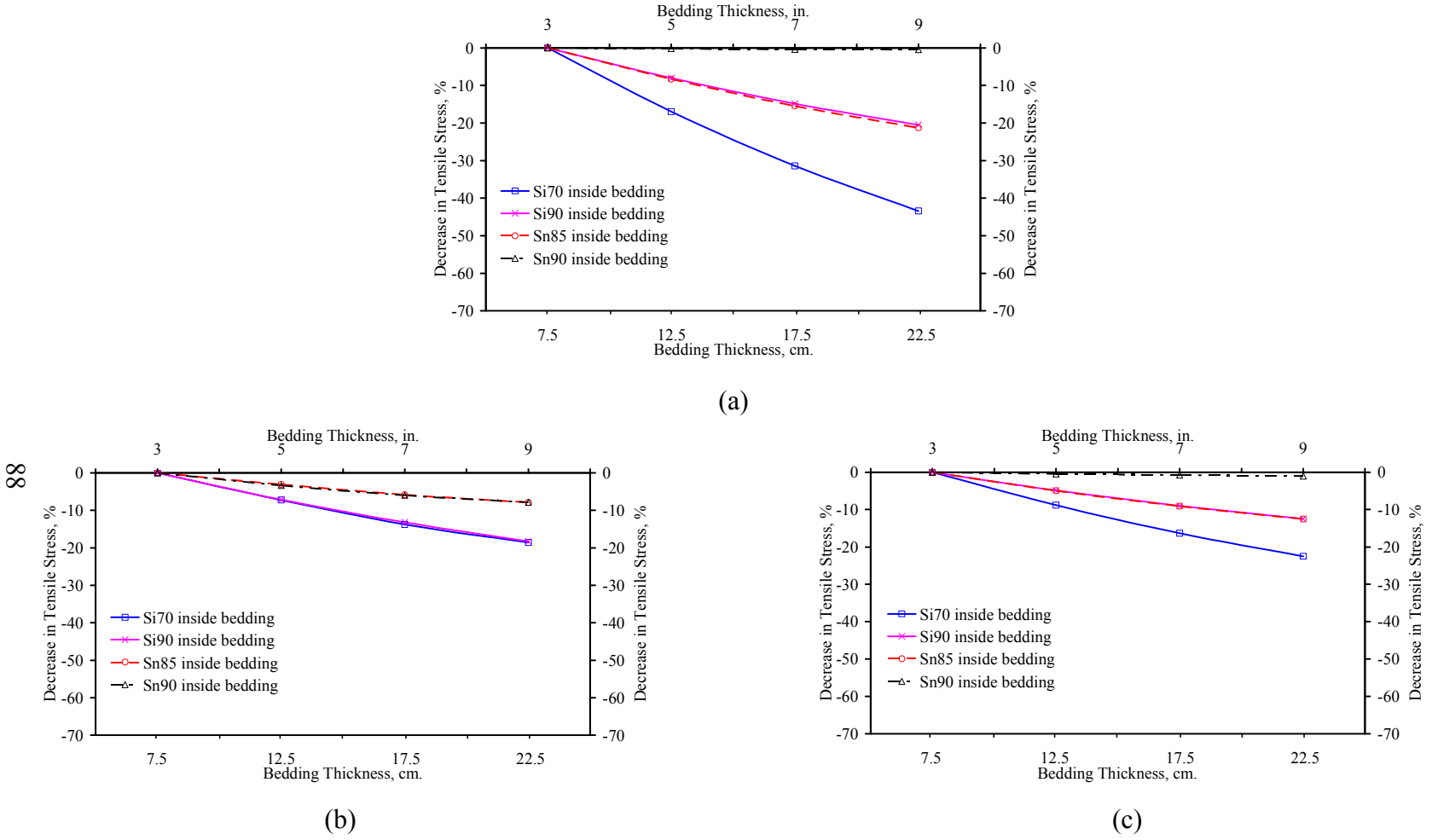

Figure A.9 Decrease in tensile stresses versus bedding thicknesses for 60in-dia pipe in 80ft-height backfill; (a) At invert, (b) At crown, and (c) At springline

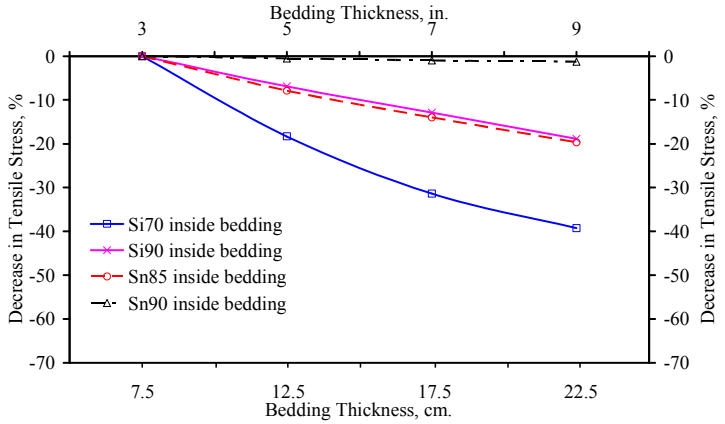

(a)

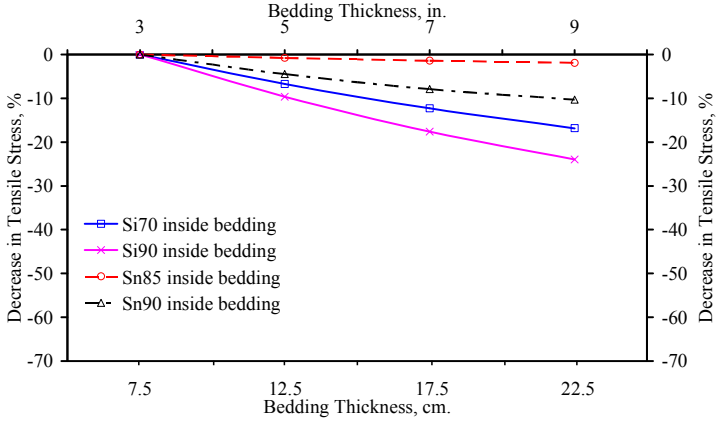

(b)

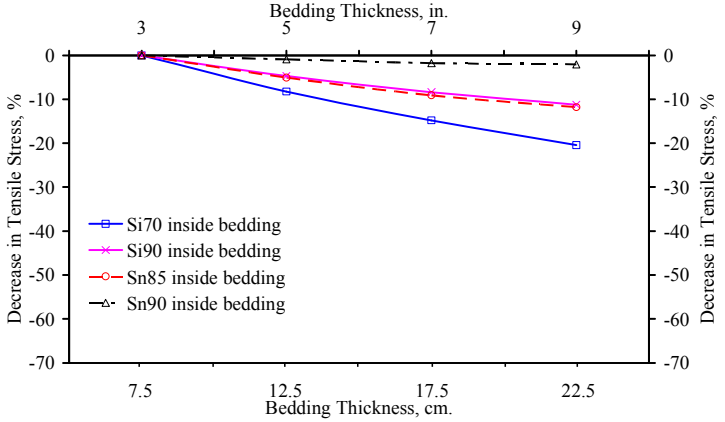

(c)

Figure A.10 Decrease in tensile stresses versus bedding thicknesses for 60in-dia pipe in 100ft-height backfill; (a) At invert, (b) At crown, and (c) At springline

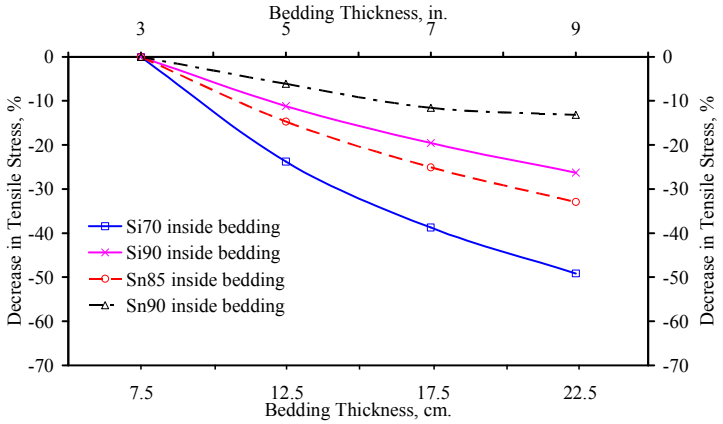

(a)

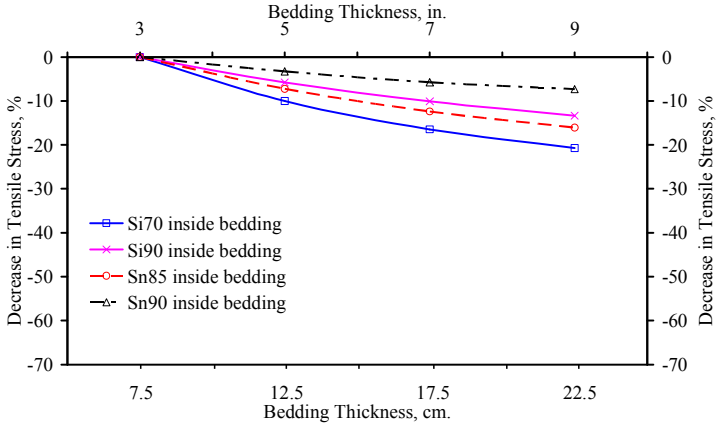

(b)

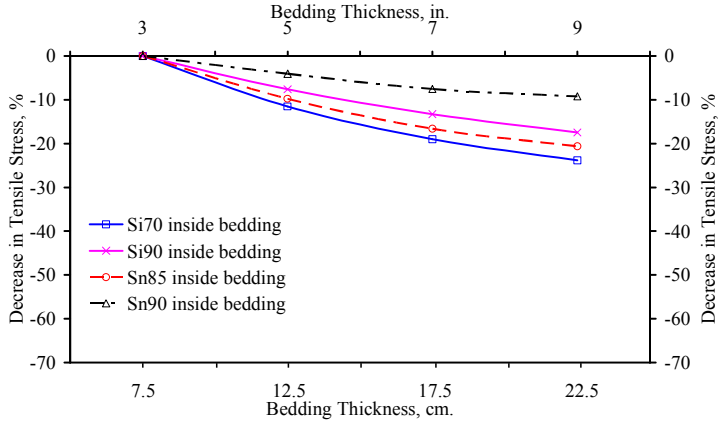

(c)

Figure A.11 Decrease in tensile stresses versus bedding thicknesses for 84in-dia pipe in 20ft-height backfill; (a) At invert, (b) At crown, and (c) At springline

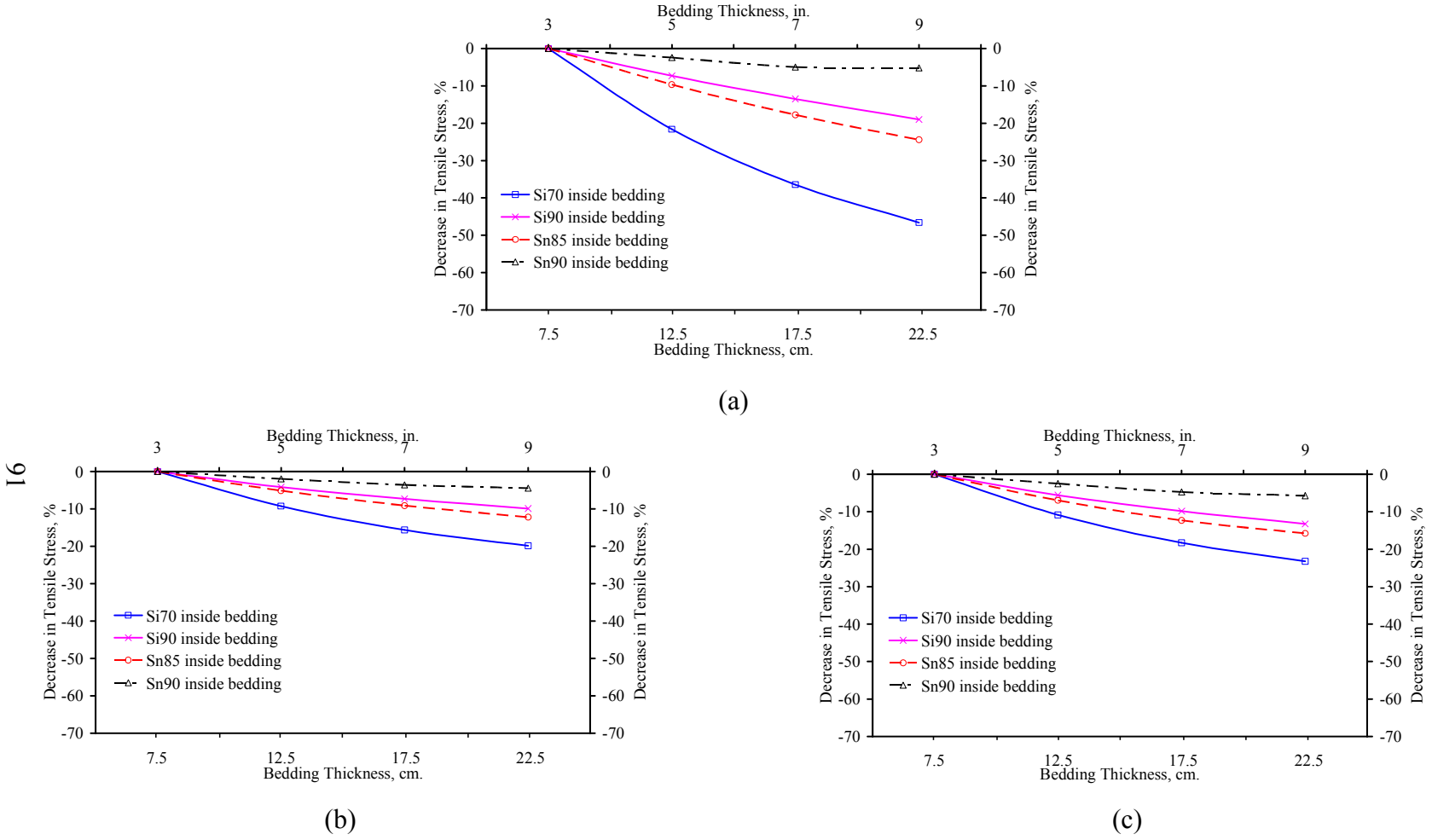

Figure A.12 Decrease in tensile stresses versus bedding thicknesses for 84in-dia pipe in 40ft-height backfill; (a) At invert, (b) At crown, and (c) At springline

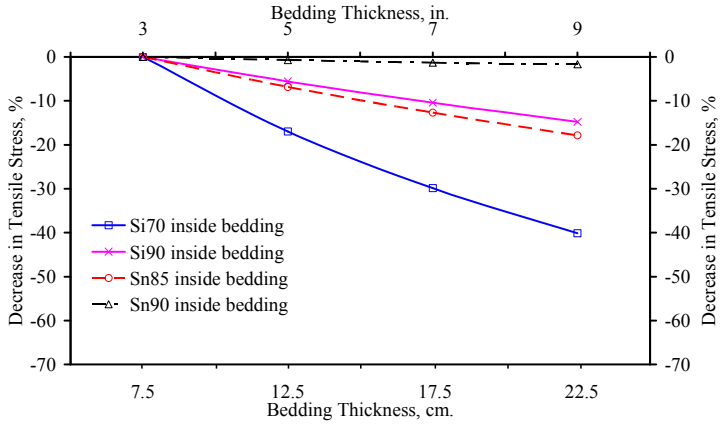

(a)

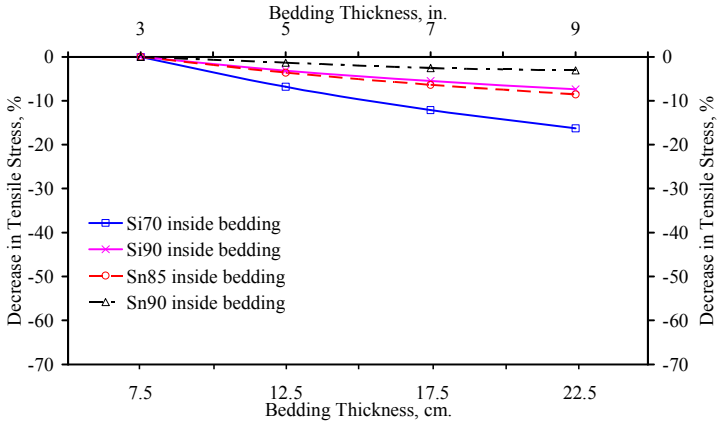

(b)

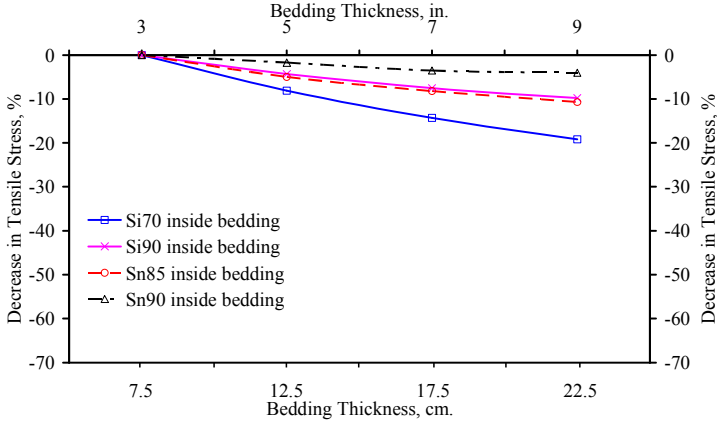

(c)

Figure A.13 Decrease in tensile stresses versus bedding thicknesses for 84in-dia pipe in 60ft-height backfill; (a) At invert, (b) At crown, and (c) At springline

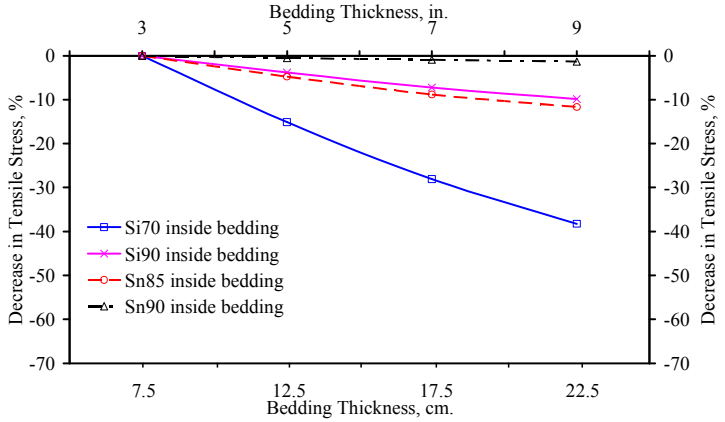

(a)

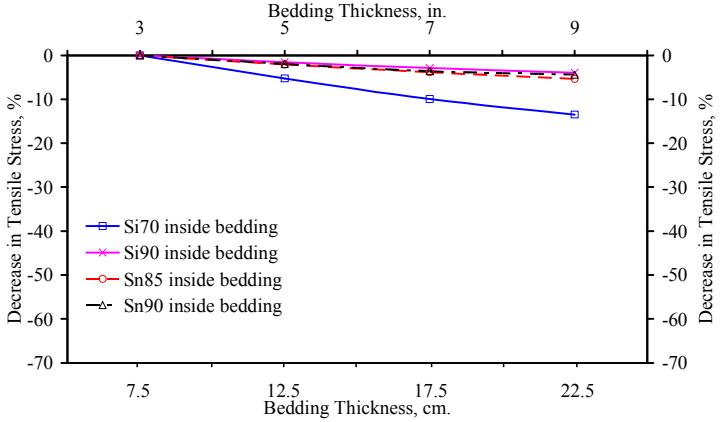

(b)

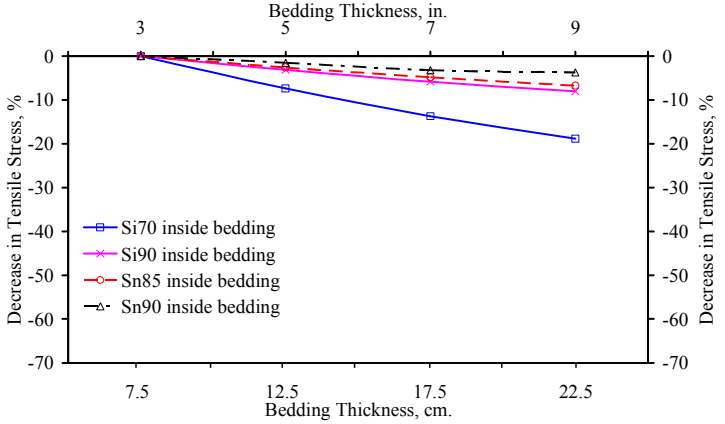

(c)

Figure A.14 Decrease in tensile stresses versus bedding thicknesses for 84in-dia pipe in 80ft-height backfill; (a) At invert, (b) At crown, and (c) At springline

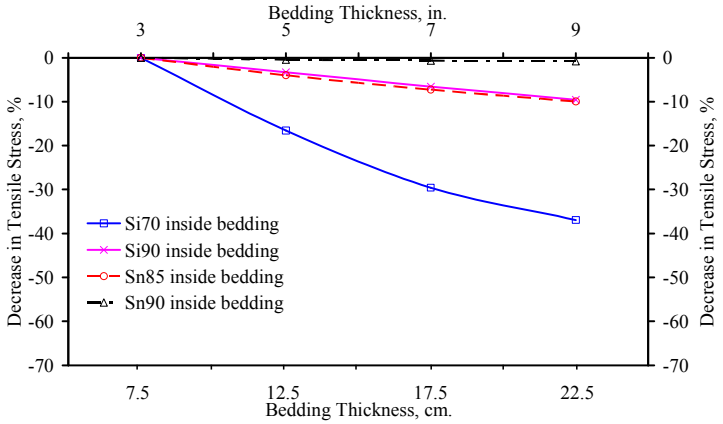

(a)

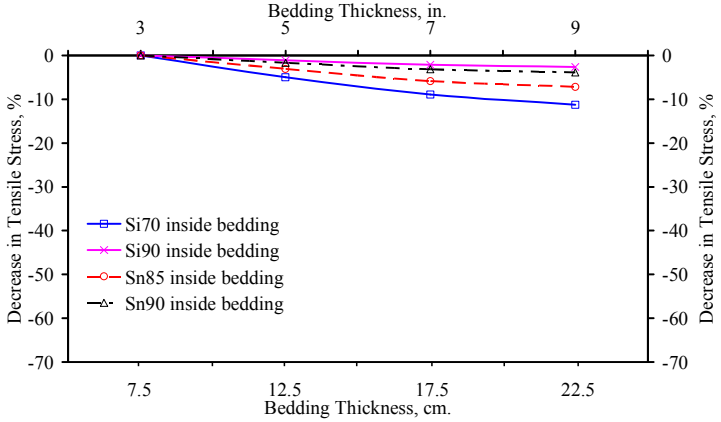

(b)

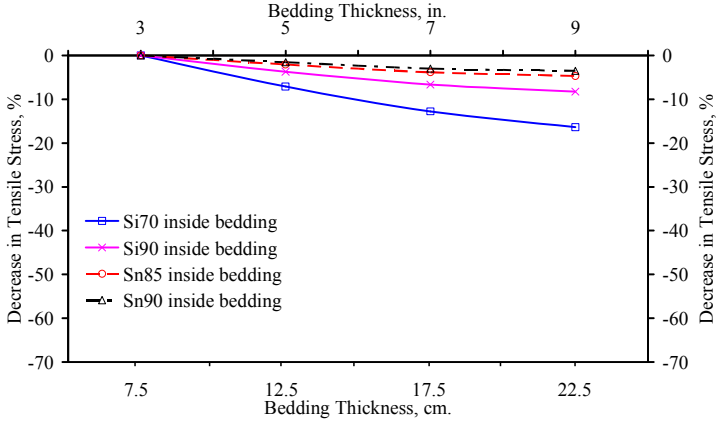

(c)

Figure A.15 Decrease in tensile stresses versus bedding thicknesses for 84in-dia pipe in 100ft-height backfill; (a) At invert, (b) At crown, and (c) At springline

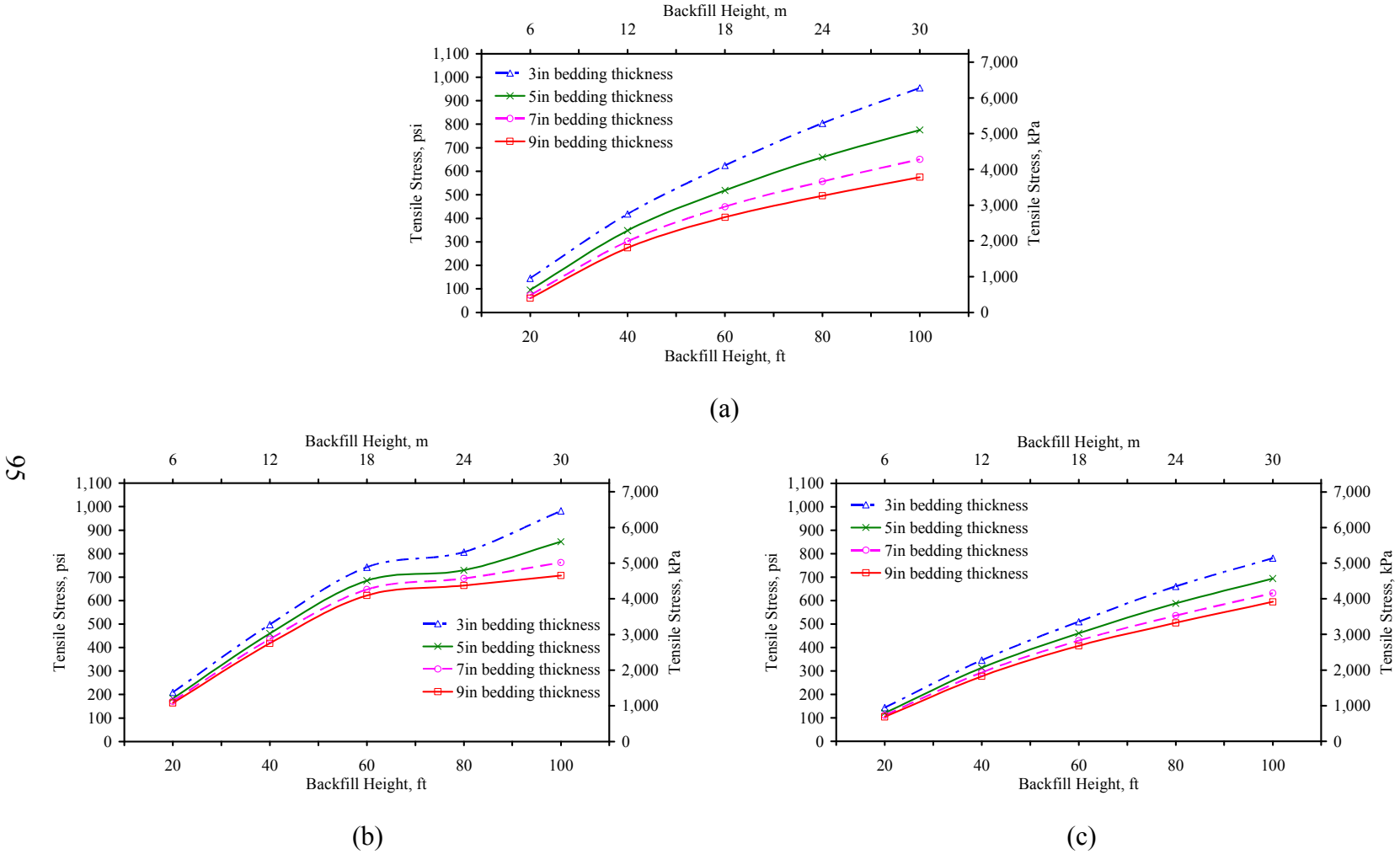

Figure A.16 Comparison of tensile stresses of 24in-dia pipe versus backfill heights (Si70 for inside bedding); (a) At invert, (b) At crown, and (c) At springline

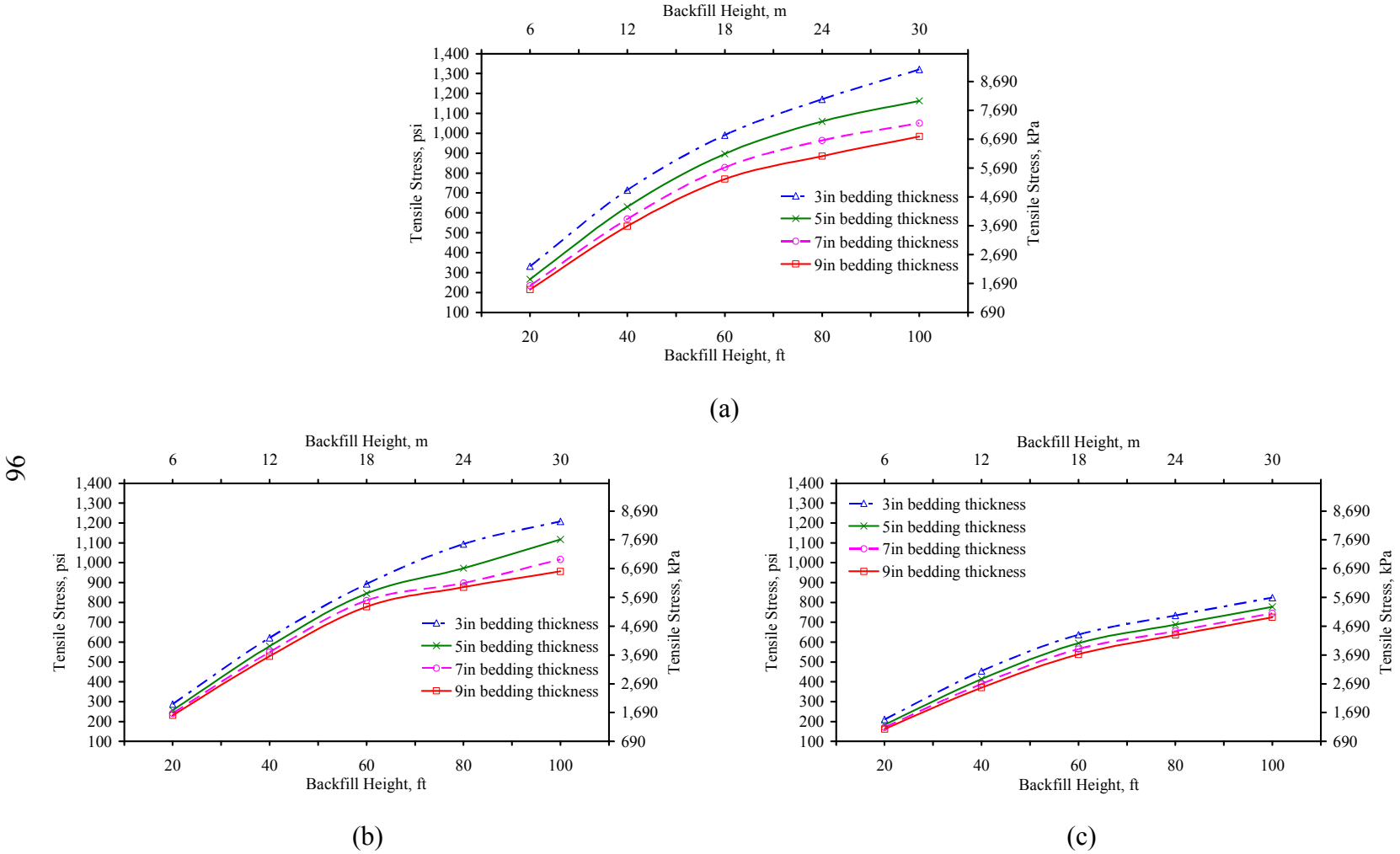

Figure A.17 Comparison of tensile stresses of 24in-dia pipe versus backfill heights (Si90 for inside bedding); (a) At invert, (b) At crown, and (c) At springline

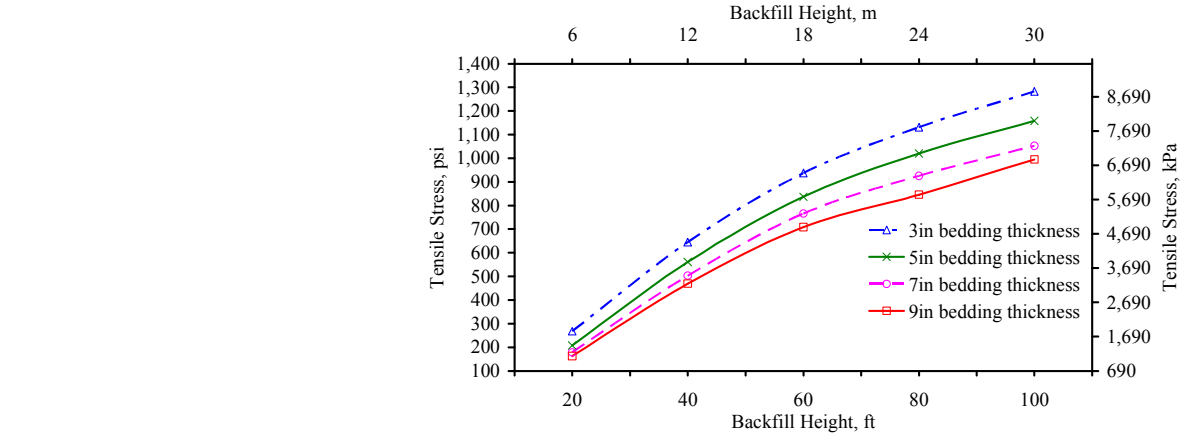

(a)

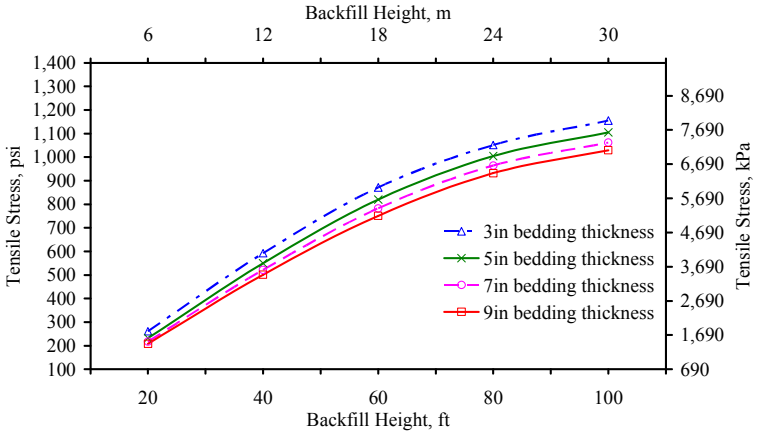

(b)

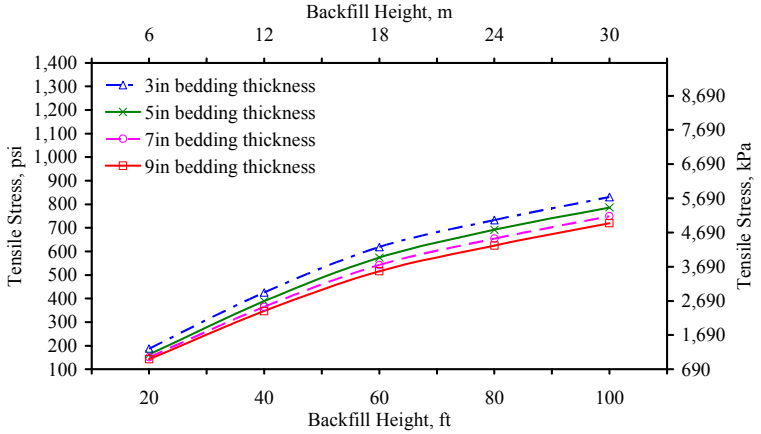

(c)

Figure A.18 Comparison of tensile stresses of 24in-dia pipe versus backfill heights (Sn85 for inside bedding); (a) At invert, (b) At crown, and (c) At springline

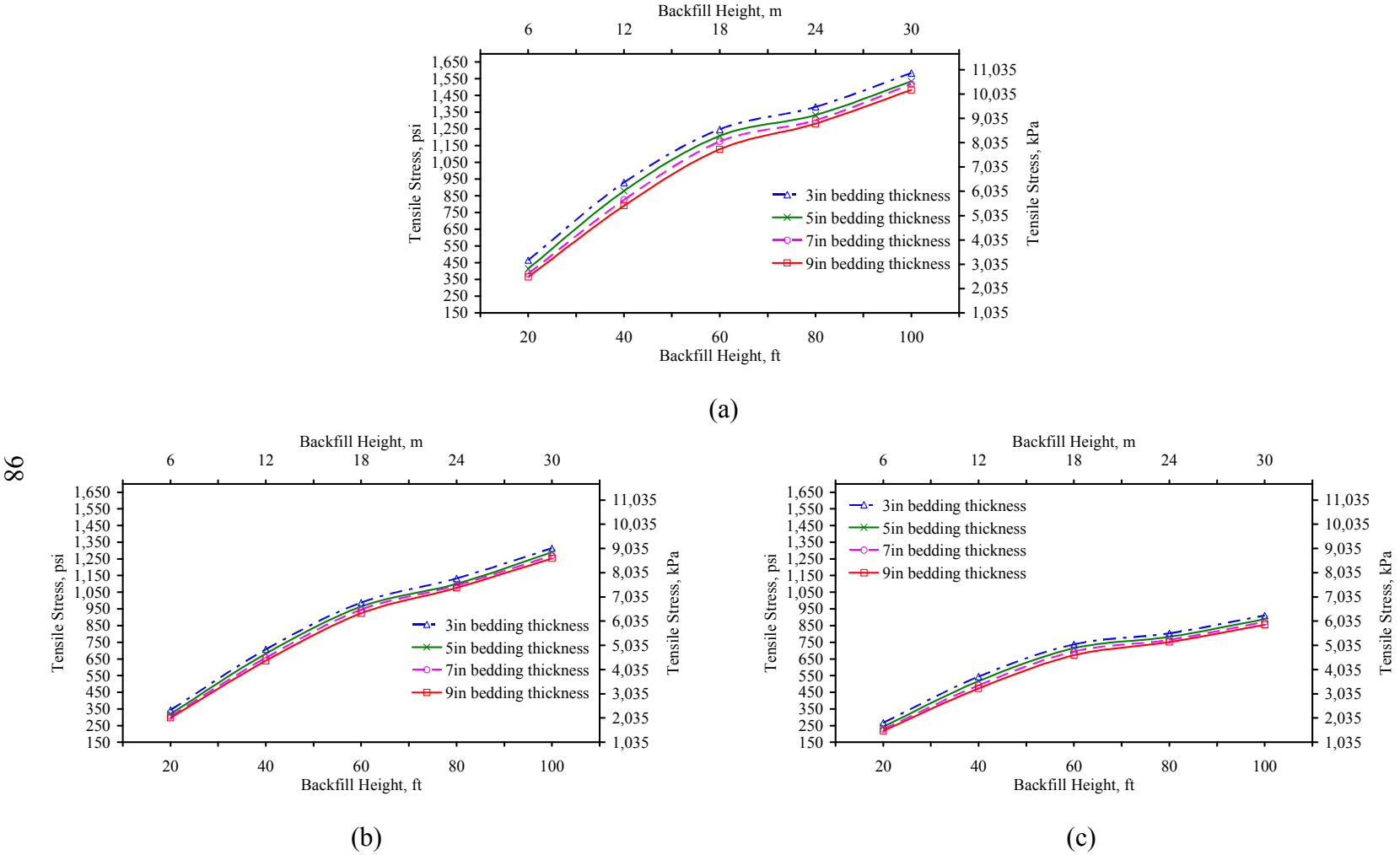

Figure A.19 Comparison of tensile stresses of 24in-dia pipe versus backfill heights (Sn90 for inside bedding); (a) At invert, (b) At crown, and (c) At springline

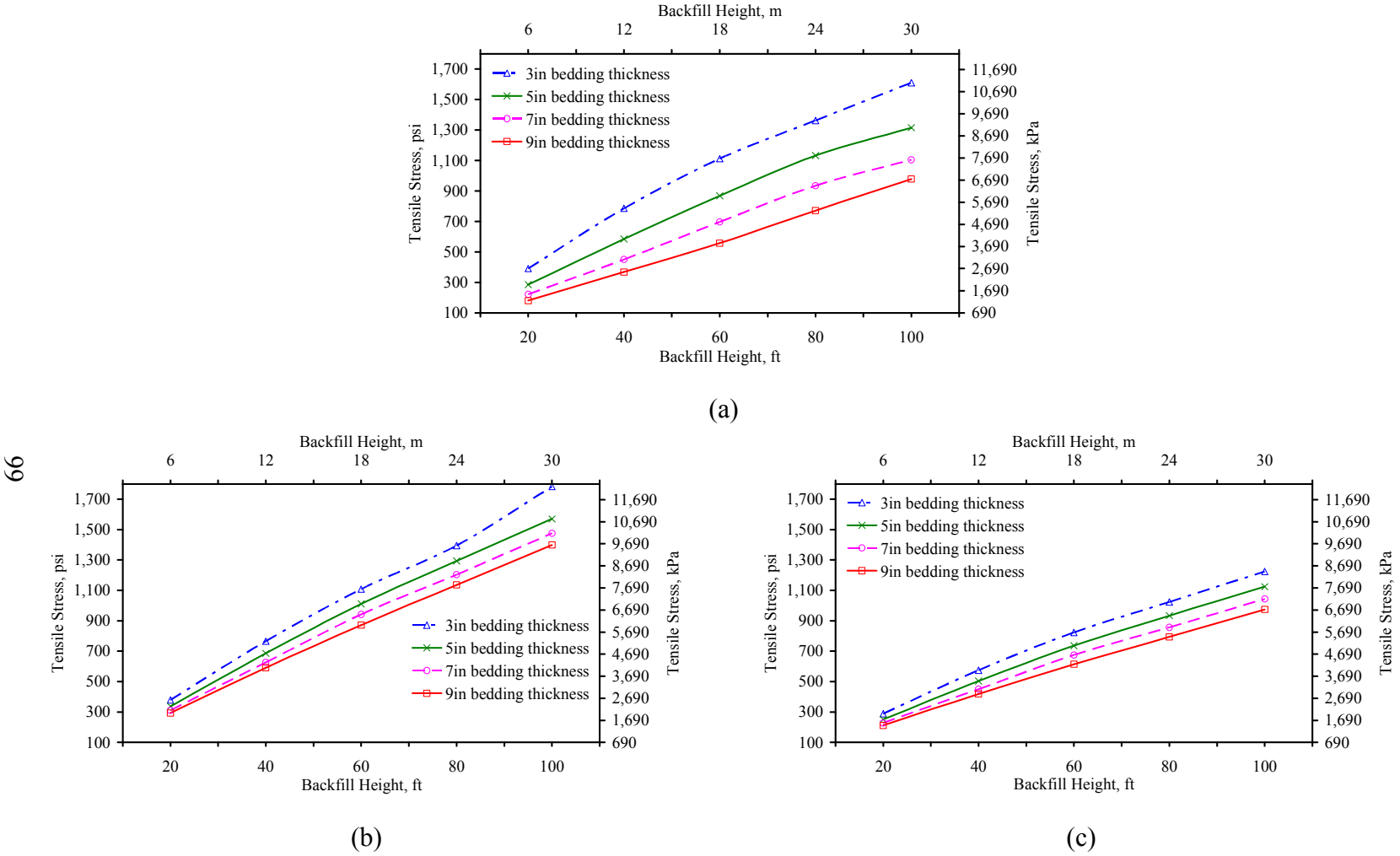

Figure A.20 Comparison of tensile stresses of 60in-dia pipe versus backfill heights (Si70 for inside bedding); (a) At invert, (b) At crown, and (c) At springline

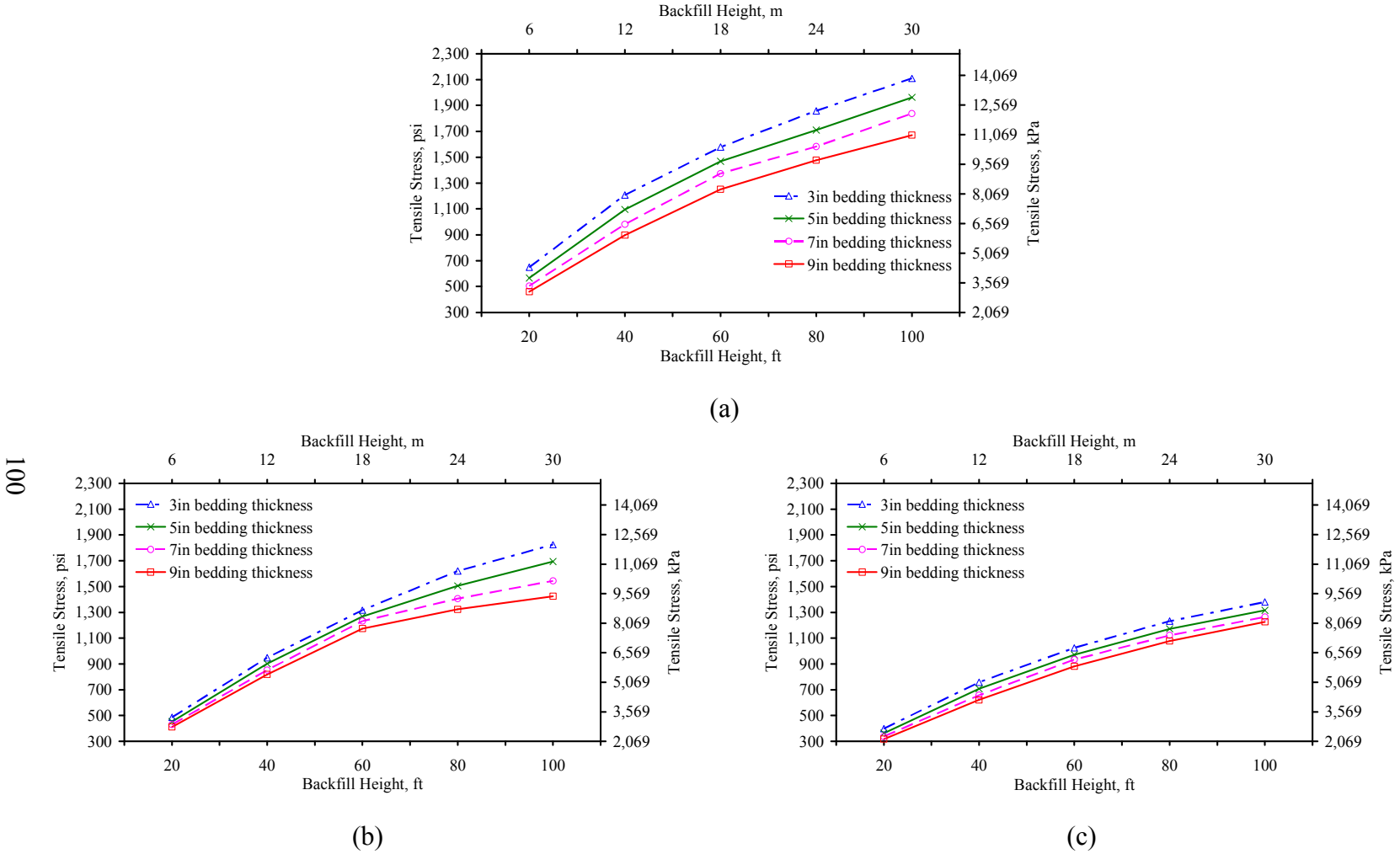

Figure A.21 Comparison of tensile stresses of 60in-dia pipe versus backfill heights (Si90 for inside bedding); (a) At invert, (b) At crown, and (c) At springline

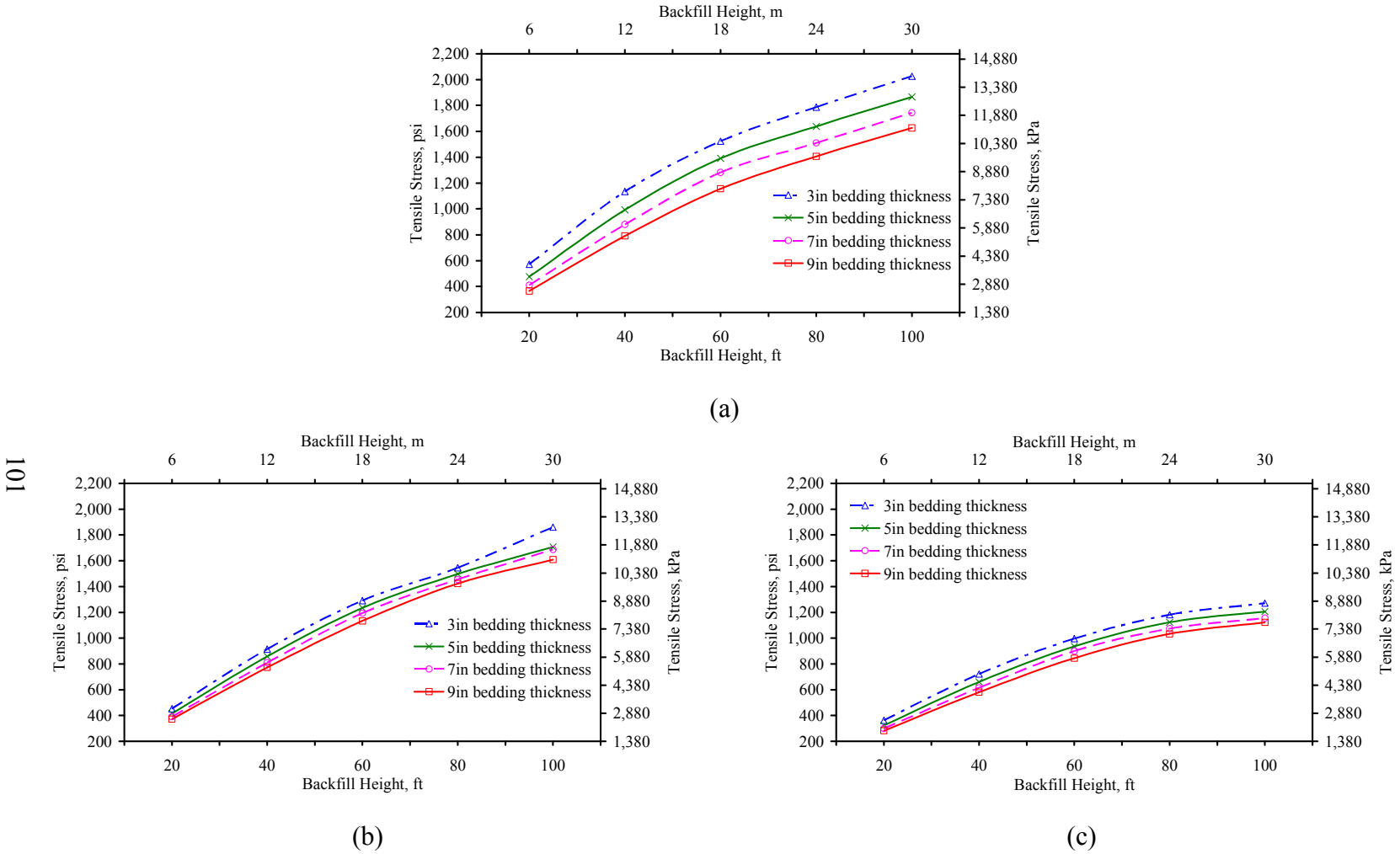

Figure A.22 Comparison of tensile stresses of 60in-dia pipe versus backfill heights (Sn85 for inside bedding); (a) At invert, (b) At crown, and (c) At springline

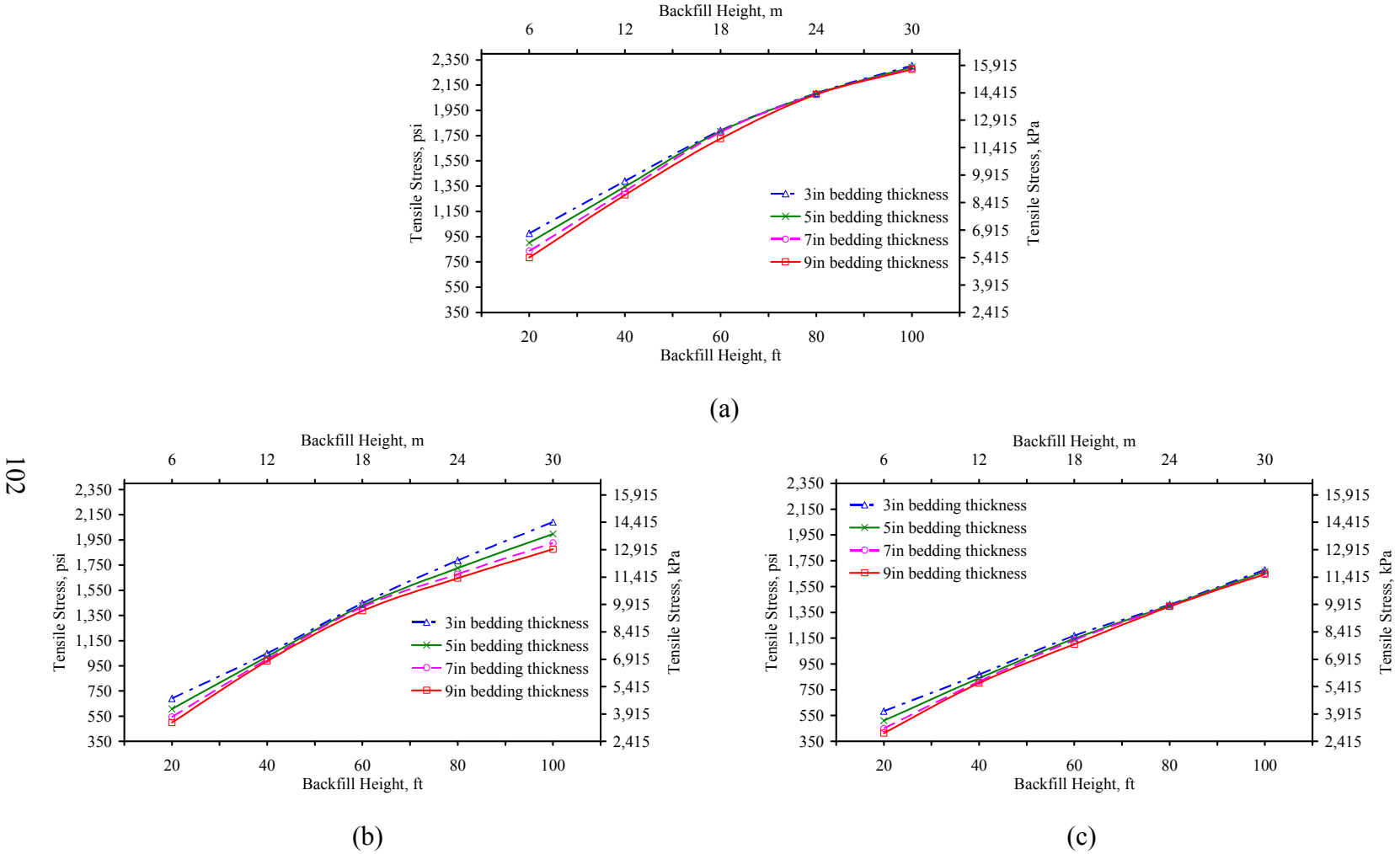

Figure A.23 Comparison of tensile stresses of 60in-dia pipe versus backfill heights (Sn90 for inside bedding); (a) At invert, (b) At crown, and (c) At springline

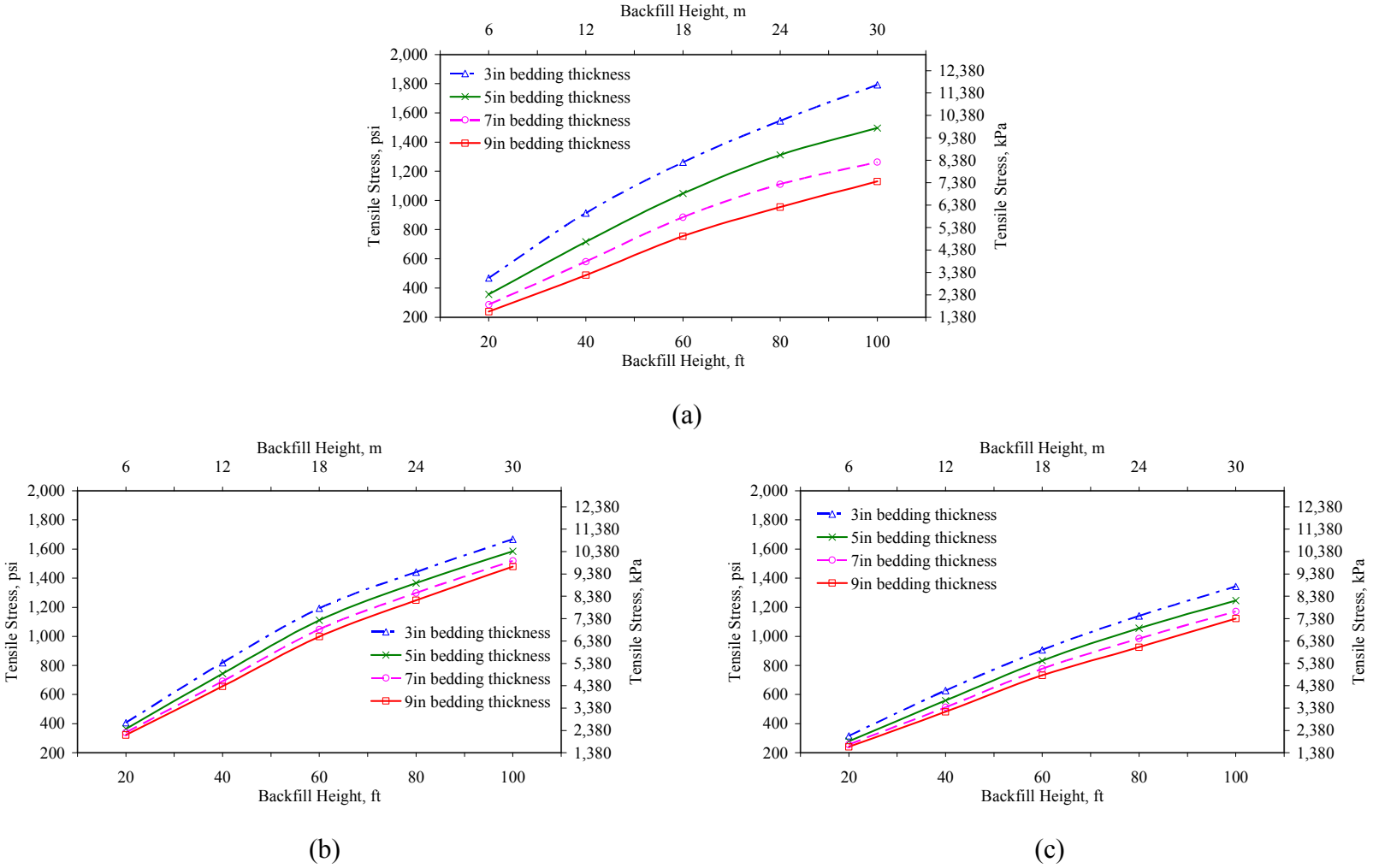

Figure A.24 Comparison of tensile stresses of 84in-dia pipe versus backfill heights (Si70 for inside bedding); (a) At invert, (b) At crown, and (c) At springline

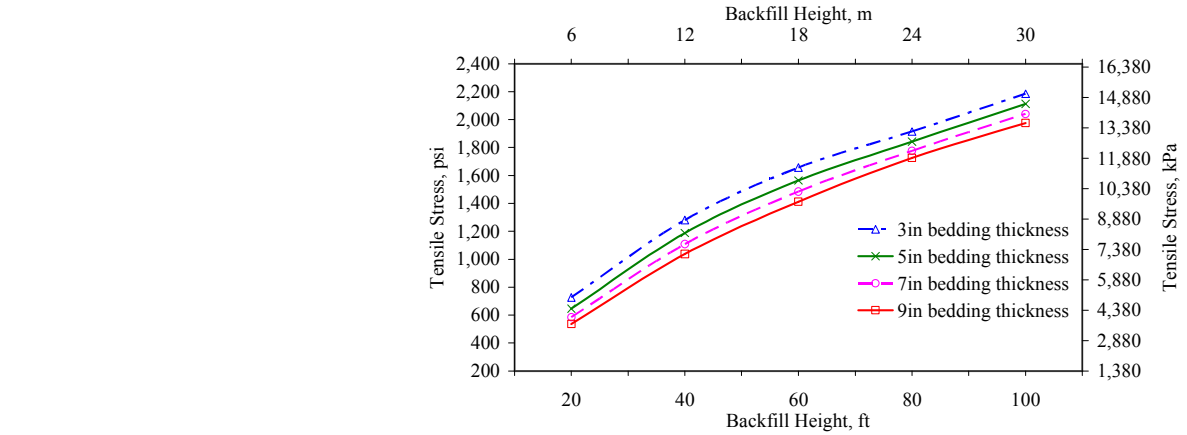

(a)

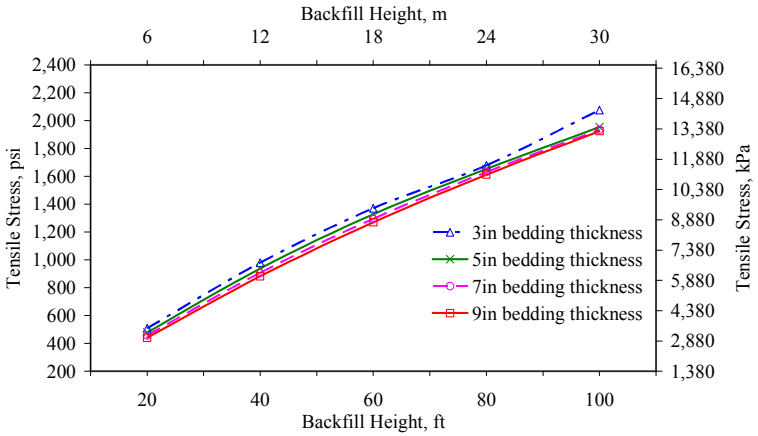

(b)

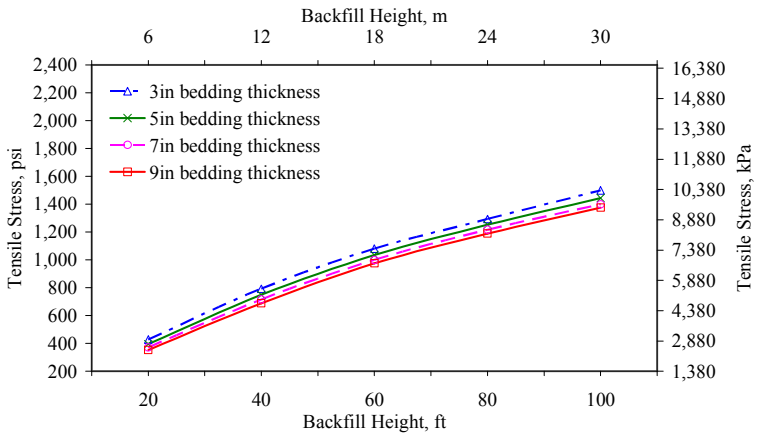

(c)

Figure A.25 Comparison of tensile stresses of 84in-dia pipe versus backfill heights (Si90 for inside bedding); (a) At invert, (b) At crown, and (c) At springline

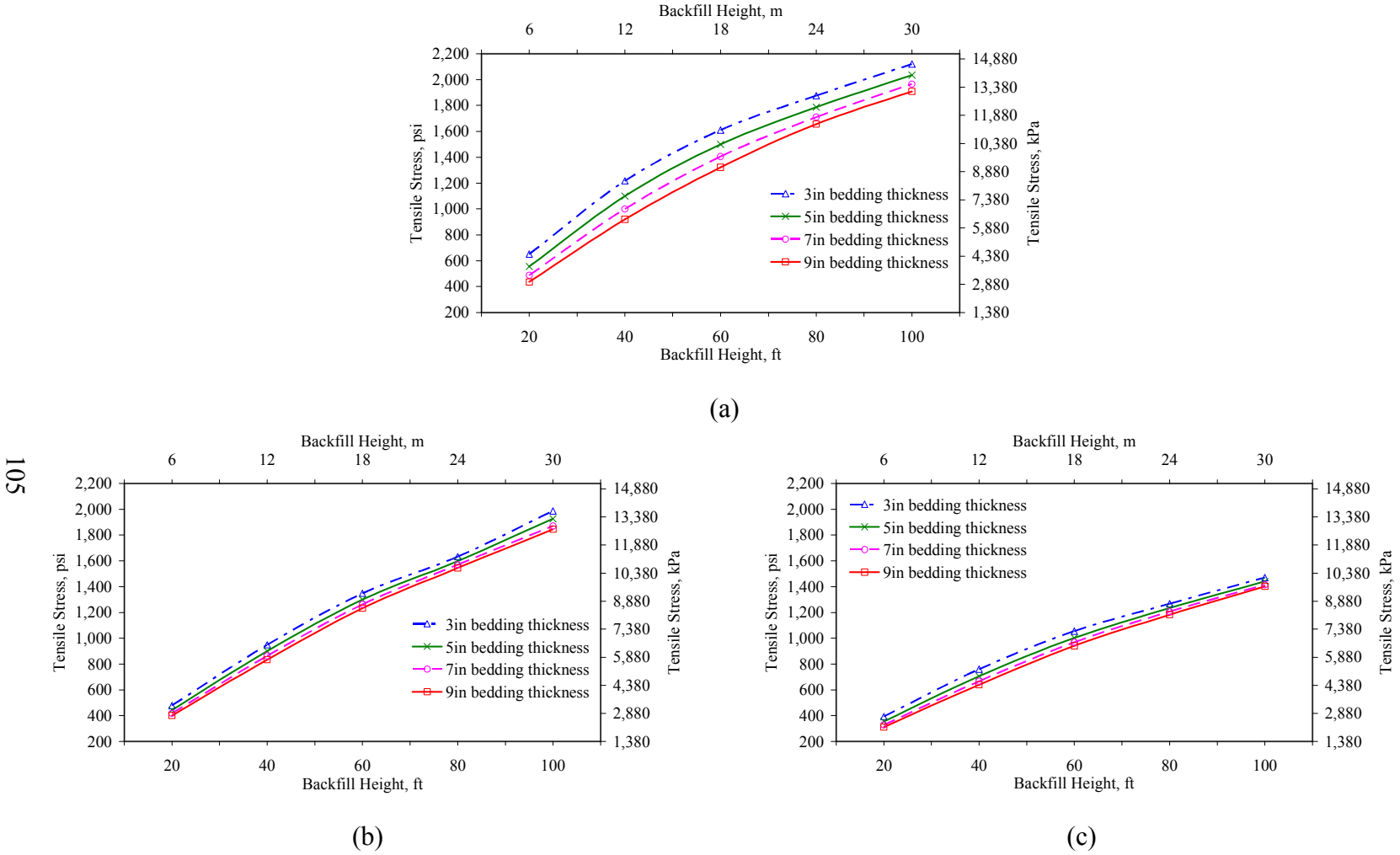

Figure A.26 Comparison of tensile stresses of 84in-dia pipe versus backfill heights (Sn85 for inside bedding); (a) At invert, (b) At crown, and (c) At springline

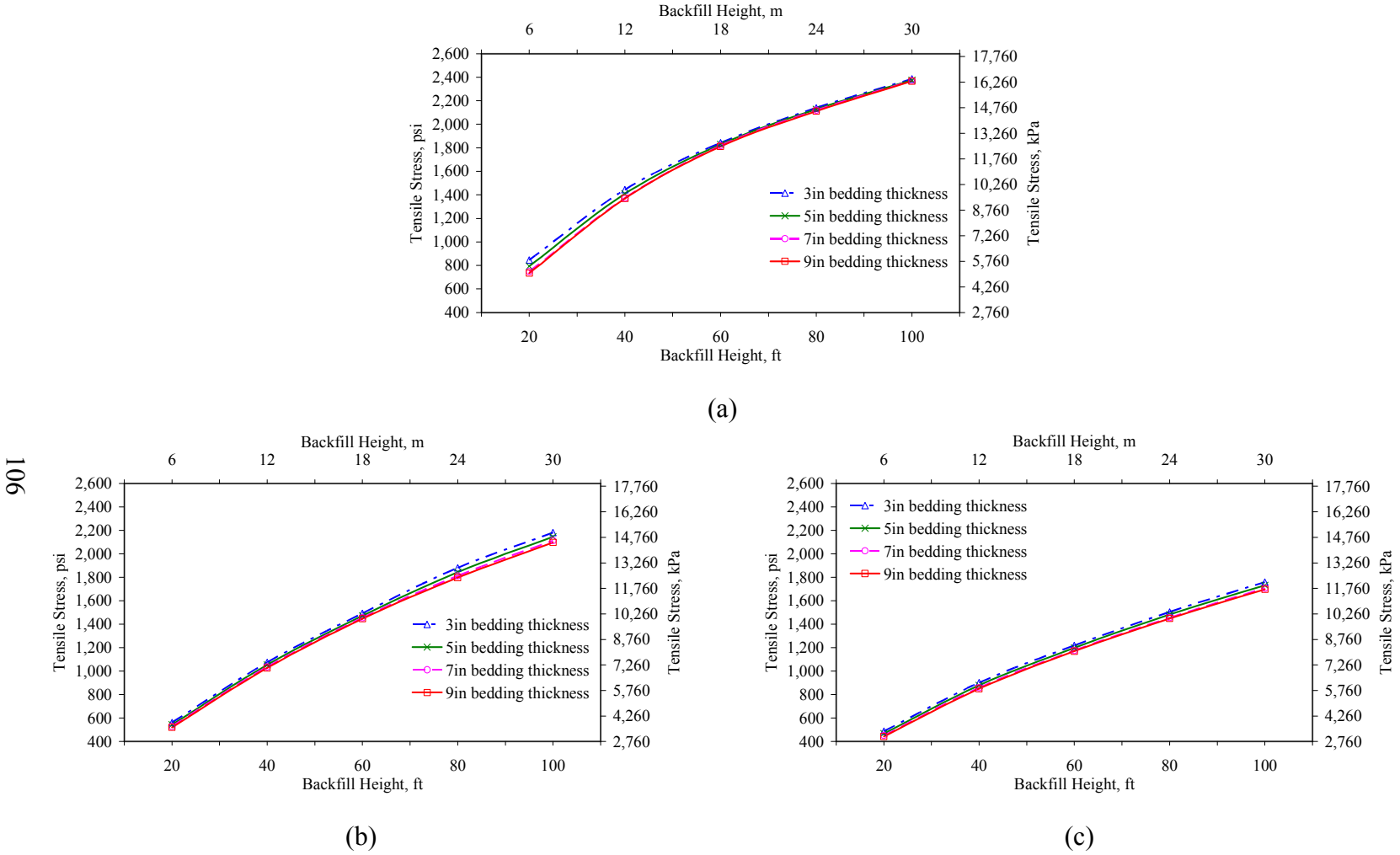

Figure A.27 Comparison of tensile stresses of 84in-dia pipe versus backfill heights (Sn90 for inside bedding); (a) At invert, (b) At crown, and (c) At springline

REFERENCES

American Association of State Highway and Transportation Officials (2005), "AASHTO M 145: *The Classification of Soils-Aggregate Mixtures for Highway Construction Purposes, Standard Specifications for Transportation Materials and Methods of Sampling and Testing,*" Part I, Washington, DC.

American Association of State Highway and Transportation Officials (2005), "AASHTO T 99: *Standard Methods of Test for The Moisture-Density Relations of Soils and Soil-Aggregate Mixtures Using 5.5-lb (2.5-kg) Rammer and 12-in (305-mm) Drop,*" Washington, DC.

American Association of State Highway and Transportation Officials (2005), "AASHTO T 180: *Standard Methods of Test for The Moisture-Density Relations of Soils and Soil-Aggregate Mixtures Using 10-lb (4.5-kg) Rammer and 18-in (457-mm) Drop,*" Washington, DC.

American Association of State Highway and Transportation Officials (2004), "*AASHTO LRFD Bridge Design Specifications*," 3rd Edition.

American Society for Testing Materials (2005), "ASTM D 698: *Testing Methods for Moisture-Density Relations of Soils and Soil-Aggregate Mixtures Using 5.5-lb (2.5-kg) Rammer and 12-in (305 mm) Drop,*" Philadelphia, PA.

American Society for Testing Materials (2005), "ASTM D 1557: *Testing Methods for Moisture-Density Relations of Soils and Soil-Aggregate Mixtures Using 10-lb (4.5-kg) Rammer and 18-in (457 mm) Drop,*" Philadelphia, PA.

American Society for Testing Materials (2005), "ASTM D 2487: *Standard Test Method for Classification of Soils for Engineering Purposes,*" Philadelphia, PA.

ABAQUS, 2005. "ABAQUS version 6.5," ABAQUS, Inc., Pawtucket, RI.

AMERICAN CONCRETE PIPE ASSCOCIATION (1998), "Concrete Pipe Handbook," Irving, TX.

AMERICAN CONCRETE PIPE ASSCOCIATION (2001), "Concrete Pipe Technology Handbook," Irving, TX.

AMERICAN CONCRETE PIPE ASSCOCIATION (2002), "Concrete Pipe Design Manual," Irving, TX.

Arockiasamy, et al. (2002). Arockiasamy, M., Chaallal, O., Limpeteeprakarn, T., and Wang, N., "Experiment and Analytical Evaluation of Flexible Pipes for Culverts and Storm Sewers," Volume II Laboratory Work and Numerical Analysis, Florida Atlantic University, Boca Raton, FL.

Duncan, J.M., Byrne, Peter, Wong, K.S., and Mabry, Phillip, "Strength, Stress-Strain and Bulk Modulus Parameters for Finite Element Analysis of Stresses and Movements in Soil Masses," University of California, College of Engineering, Berkeley, California, Report No. UCB/GT/80-01, August, 1980.

Johnston BP, Sullivan JM Jr, Kwasnik A., "Automatic conversion of triangular finite element meshes to quadrilateral elements," International Journal for Numerical Methods in Engineering 1991; 31:67–84.

Katona, M.G. (1978), "Analysis of Long Span Culverts by the Finite Element Method, Tolerable Movement of Bridge Foundations, Sand Drains, K-Test, Slopes, and Culverts," Transportation Research Record 678, TRB, Washington, DC. pp. 59-66.

Katona, M.G., and Smith, J.B., "CANDE User Manual," Report No. FHWA-RD-77-6, Federal Highway Administration, Washington, DC., October 1976.

Katona, M.G., and Smith, J.B., "CANDE System Manual," Report No. FHWA-RD-77-7, Federal Highway Administration, Washington, DC., October 1976.

Katona, M.G., Vittes, P.D., Lee, C.G., and Ho, H.T., "CANDE 1980: Box Culverts and Soil Models," Report No. FHWA/RD-80/172, Federal Highway Administration, Washington, DC., May 1981.

Katona, M.G., Vittes, P.D., Lee, C.G., and Ho, H.T., "Pressure Distribution Around a Metal Pipe Under Deep Cover," Report No. FHWA/RD-80/172, Federal Highway Administration, Washington, DC., May 1981.

McGrath, et al. (2002). McGrath, T.J., DelloRusso, S.J., and Boynton, J., "Performance of Thermoplastic Culvert Pipe Under Highway Vehicle Loading," Pipelines 2002, G. Kurz Ed., American Society of Civil Engineers.

McGrath, T.J. (2005), "Performance of Thermoplastic Pipe Under Highway Vehicle Loading," MnRoad Research Facility, Waltham, MA.

McGrath, T.J. (2003), "Protocol for 100 Year Service Life of Corrugated HDPE Part1: Evaluation and Control of Stresses in Buried Corrugated HDPE Drain Pipe," Waltham, MA.

Seed, R.B. and Duncan, J.M., "Soil-Structure Interaction Effects of Compaction Induced Stresses and Deflections," University of California, College of Engineering, Berkeley, California, Report No. UCB/GT/83-06, December, 1983.

Selig, E.T., "Soil Parameters for Design of Buried Pipelines," Proceedings, Pipeline Infrastructure Conference, ASCE, 1988, pp. 99-116.

BIOGRAPHICAL INFORMATION

Anupong Kararam was born June 07, 1980 in Bangkok, the capital city in Thailand. He finished his school level in 1997 with the major courses of mathematics and science. Then, in 2001 he received his bachelor degree in Civil Engineering at the Mahidol University, one of the most famous universities in Thailand. After his graduation, he started working for the company "DKJ construction Co.Ltd." in the area of civil engineering for one and a half year. He worked at the site of construction of 8-storey condominium as a field engineer. His main duties were to control the construction processes, and to make the as-built shop drawings using AutoCAD R14. After that, he worked for "Pyramid Development International Co.Ltd." in the areas of structural analysis and design for one and a half year. He designed reinforced concrete structures for the surveillance tower in Suwannabhumi Airport with his senior structural engineering team. He had abundant of chances to analyze and design structural systems using both hand calculation and computer program, "RISA 3D".

Afterward, he entered the graduate program in Structural and Applied Mechanics at the University of Texas at Arlington (UTA) where he did research under Dr. Ali Abolmaali instruction as a Master of Science in Civil Engineering in finite element method. Anupong Kararam has been accepted to the Ph.D. program as a

graduate research assistant in structural mechanics at UTA, and he is awarded the American Concrete Pipe Association scholarship.